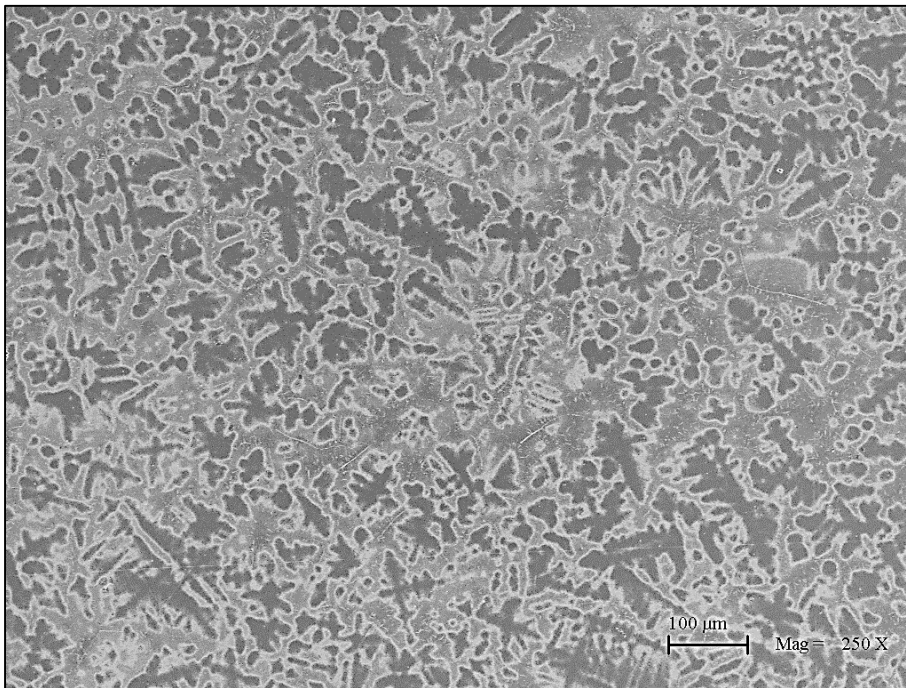


CHALMERS



Ductilizing Refractory High Entropy Alloys

Degree project in the Bachelor of Science in Engineering Program

Mechanical Engineering

THOMAS CHAN HIEN DAM
SARMAD SHABA

Department of Materials and Manufacturing Technology
Division of Advanced Non-destructive Testing
CHALMERS UNIVERSITY OF TECHNOLOGY
Gothenburg, Sweden, 2016 Examiner: Gert Persson Report No. 153/2016

THESIS WORK NO. 153/2016

Ductilizing Refractory High Entropy Alloys

Thesis work for the mechanical engineering program

THOMAS CHAN HIEN DAM

SARMAD SHABA

Department of Materials and Manufacturing Technology

Division of Advanced Non-destructive Testing

CHALMERS UNIVERSITY OF TECHNOLOGY

Gothenburg, Sweden, 2016

Ductilizing Refractory High Entropy Alloys

Thesis work for the mechanical engineering program

THOMAS CHAN HIEN DAM

SARMAD SHABA

© THOMAS CHAN HIEN DAM, SARMAD SHABA, 2016

Thesis work No. 153/2016
Department of Materials and Manufacturing Technology
Division of Advanced Non-destructive Testing
CHALMERS UNIVERSITY OF TECHNOLOGY
SE-412 96 Gothenburg
Sweden
Telephone: + 46 (0)31-772 1000

Cover:

SEM image of the microstructure of refractory HEA $\text{Hf}_{0.5}\text{Nb}_{0.5}\text{Ta}_{0.5}\text{TiZr}$ under 250x magnification. The alloy shows a dendritic microstructure after etching. The dark grey tree-like spots are dendrites and the light grey are interdendrites. There is no sign of secondary phases in the microstructure.

Preface

During the spring of 2016 we carried out our bachelor thesis work at Chalmers University of Technology at Department of Materials and Manufacturing Technology, Gothenburg. This report is our final work at the mechanical engineering program at Chalmers University of Technology.

The authors Thomas Dam and Sarmad would like to thank Sheng Guo at Chalmers University of Technology for giving the opportunity to work with this project and for his supervision. Our other supervisor Saad Sheikh is greatly appreciated for his help during experimental work.

Last but not least, we would like to thank our examiner Gert Persson at Chalmers University of Technology.

Thomas Dam and Sarmad Shaba, Gothenburg, June 2016

Summary

High entropy alloys (HEAs) are a new material group which have recently been focused on by researchers. It is defined as an alloy consisting of 5 or more metallic elements in an equiatomic or a near-equiatomic ratio and having an entropy higher than $\geq 1.5R$, where R being the ideal gas constant, 8.314 J/K mol . HEAs with refractory elements have high yield strength at elevated temperature compared to simpler refractory alloys but are often brittle at room temperature. Current jet engines are usually made of Ni-based alloys which have a limited operating temperature. Finding a new material capable of operating at a higher temperature than Ni-based alloys would improve the efficiency in jet engines as the cooling could be reduced or removed. The aim here is to identify at least one ductile refractory HEA with a single phase solid solution using the electron theory as a strategy, due to the vast amount of combinations possible and also due to the brittleness commonly found in refractory HEAs. In this case, the electron theory applied has been narrowed down to the valence electron concentration (VEC) of the alloy. By controlling the VEC, it is possible to ductilize a refractory HEA. The experimental work was performed in Chalmers University of Technology at Department of Materials and Manufacturing Technology and the available time was limited to three months. A literature review consisting of basic background knowledge of HEAs together with a mapping of current mechanical properties of simpler refractory alloys and refractory HEAs were made. The properties map shows the need for a ductile refractory high entropy due to the current available materials are either too brittle or have low yield strength at elevated temperatures. Four binary alloys with compositions MoTi, Mo_{0.5}Ti, MoNb and Mo_{0.5}Nb were produced by vacuum arc melting. All binary alloys consisted of BCC crystal structure confirmed by x-ray diffraction. A simple bending tests showed that they were brittle, possibly due to their high VEC. A refractory HEA with the composition Hf_{0.5}Nb_{0.5}Ta_{0.5}TiZr was produced in the same fashion. X-ray diffraction and SEM results showed that the alloy was single-phased solid solution with BCC crystal structure. Bending result showed that it was ductile. The ductility was attributed to its low VEC value of 4.29. Lowering the VEC value could be a valid strategy to identify ductile refractory HEAs.

Sammanfattning

Högentropilegeringar (HEAs) är en ny materialgrupp som nyligen fått fokus av forskare. Den är definierad som en multikomponentlegering som består av 5 eller flera metalliska grundämnen där varje komponent har lika eller nästan lika atommängd och ha en entropi högre än $1.5 R$ där R är den ideala gas konstanten, $8,314 \text{ J/K mol}$. Högentropilegeringar som består av värmebeständiga grundämnen har hög sträckgräns i höga temperaturer jämfört med enkla värmebeständiga legeringar men präglas oftast av sprödhet i rumstemperatur. Nuvarande flygplansturbiner är oftast tillverkade i Nickelbaserade legeringar som har en begränsad arbetstemperatur. Genom att hitta ett nytt material som överskrider nuvarande högttemperatursstyrka av dagens Nickelbaserade legeringar kan man öka effektiviteten hos flygplansturbiner genom att minska kylningen eller eliminera det helt. Målet här är att identifiera minst en duktil värmebeständig högentropilegering med enfasig fast lösning med användandet av elektronteori som strategi pga. den stora mängden kombinationer som finns och pga. sprödheten som brukar prägla värmebeständiga högentropilegeringar. I detta fall är elektronteori fokuserad på valenselektronkoncentrationen (VEC) av legeringen. Genom att kontrollera VEC:n så är det möjligt att öka duktiliteten hos en värmebeständig högentropilegering. Det experimentella arbetet utfördes hos Chalmers tekniska högskola på institutionen för material- och tillverkningsteknik och den tillgängliga tiden var begränsad till 3 månader. En litteraturrecension som bestod av grundläggande bakgrund av högentropilegeringar tillsammans med en kartläggning av nuvarande mekaniska egenskaper hos enkla värmebeständiga legeringar och värmebeständiga högentropilegeringar utfördes. Kartläggningen visade ett behov av en duktil värmebeständig högentropilegering då nuvarande material är antingen för spröda eller har för låg styrka vid höga temperaturer. Fyra binära legeringar med sammansättningen MoTi , $\text{Mo}_{0.5}\text{Ti}$, MoNb och $\text{Mo}_{0.5}\text{Nb}$ tillverkades i en ljusbågsugn. Testresultaten från röntgenkristallografin visade för alla binära legeringar att de bestod av BCC kristallstruktur. Ett enkelt böjningstest visade att dem var spröda, möjligen pga. hög valenselektronkoncentration. En värmebeständig högentropilegering med sammansättningen $\text{Hf}_{0.5}\text{Nb}_{0.5}\text{Ta}_{0.5}\text{TiZr}$ tillverkades med samma metod. Röntgenkristallografin och SEM resultatet visade att legeringen var enfasig med BCC kristallstruktur. Böjningstesten visade att legeringen var duktil. Duktiliteten hänfördes till den låga valenselektronkoncentrationen på 4.29. Sänkning av valenselektronkoncentrationen skulle kunna vara en giltig strategi för att identifiera duktila värmebeständig högentropilegeringar.

TABLE OF CONTENTS

1	Introduction.....	1
1.1	Background.....	1
1.2	Limitations.....	1
1.3	Goal	2
1.4	Purpose	2
2	Theoretical frame	3
2.1	Introduction	3
2.2	Earliest report of HEAs	3
2.3	Definition of HEAs.....	3
2.4	Factors behind the properties.....	4
2.4.1	High entropy.....	5
2.4.2	Sluggish diffusion	5
2.4.3	Lattice distortion	6
2.4.4	Cocktail effect	7
2.5	Mechanical properties.....	8
2.5.1	Room temperature properties	8
2.5.2	Elevated temperature strength.....	10
2.6	Refractory alloys.....	13
2.6.1	Simpler refractory alloys	13
2.6.2	Current status on refractory alloys	14
2.6.2.1	High temperature application.....	14
2.6.2.2	Niobium applications	15
2.6.2.3	Molybdenum applications.....	15
2.6.2.4	Tantalum applications	16
2.6.2.5	Tungsten applications	18
2.6.2.6	Rhenium applications.....	18
2.6.2.7	Other refractory alloys and their applications.....	18
2.6.3	Refractory HEAs	18
2.6.3.1	Mechanical properties	18
2.6.3.2	Issues and problems	23
2.6.3.2.1	High density	23
2.6.3.2.2	Brittleness	24
2.7	Strategy.....	24

3	Method	26
3.1	Method for information retrieval	26
3.2	Method for experimental work	26
3.2.1	Binary alloys	26
3.2.2	HEAs	29
3.2.3	Testing methods	36
3.2.3.1	Arc melting	36
3.2.3.2	Weighing	37
3.2.3.3	Cutting	38
3.2.3.4	Grinding and polishing	38
3.2.3.5	Hardness test	38
3.2.3.6	X-ray diffraction	39
3.2.3.7	Bending test	40
3.2.3.8	Metallography analysis	40
3.2.3.9	SEM	40
4	Results	42
4.1	Properties map of refractory alloys	42
4.2	Experimental results	50
4.2.1	Result for binary alloys	50
4.2.2	Result for HEAs	52
5	Conclusion	57
5.1	Conclusions on the literature review and the properties map	57
5.2	Conclusions on the experimental work	57
5.3	Recommendations	59
6	References	60

Appendix

1 INTRODUCTION

The introducing chapter will present the background, the purpose, the limitations and the goals set up for this thesis work.

1.1 Background

High entropy alloys (HEAs) are a new type of material that have only gotten attention by researchers in the past 10 years. HEAs using refractory elements shows promises of material properties suitable for high temperature applications. Due to the vast amount of possible combinations of HEAs, finding suitable compositions using only experimental work is not possible. By applying a suitable strategy, designing alloys would be much easier. Most current refractory HEAs are strong but brittle at room temperature. Finding a strong and ductile refractory HEA would increase the available materials in high temperature applications. According to a study performed by Perepezko, current components made of Ni-based alloys in jet turbines require cooling as it would otherwise melt from the hot gas.[1] Figure 1.1 taken from the same study depicts the specific core power output (kW/(kg/s)) versus the turbine rotor inlet temperature (°C). The green line is the ideal performance which a jet turbine could achieve, while the blue dots below the line are performance data from actual engines. The figure reveals a gap between the current engines and the ideal performance as the required cooling decreases the efficiency. A material capable of operating at a higher temperature than Ni-based alloy would be more efficient as the cooling could be reduced or removed.

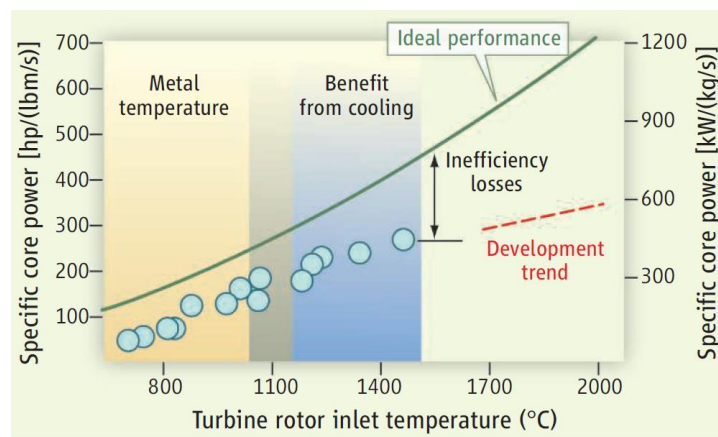


Figure 1.1: Specific core power output (kW/(kg/s)) versus the turbine rotor inlet temperature (°C) showing the development trend of current jet turbines and the possibility of increased efficiency.[1]

1.2 Limitations

Due to the time limit of 3 months and the level of knowledge of the thesis workers, the amount of experimental work will be limited to six alloys within the refractory alloys domain, and at least one of them will be refractory HEA.

The amount of literature review will also be limited to the essential topics related to refractory HEAs and simpler refractory alloys (relative to refractory HEAs, or conventional refractory alloys). These topics are the background knowledge of HEAs and the mechanical properties such as strength (yield strength and fracture strength), ductility (elongation to fracture) and density.

1.3 Goal

Show understanding of HEAs by writing a literature review.

Deliver a properties map (tables and graphs) with at least twenty of the current state of refractory HEAs and simpler refractory alloys. Mainly consisting of their strength (yield strength and fracture strength), ductility (elongation to fracture) and density.

Verify whether the electron theory is a valid strategy to ductilize refractory alloys, with the help of different methods such as x-ray diffraction, hardness test, bending test and metallography analysis. The theory is regarded as valid if one ductile refractory HEA consisting only of single-phase solid solution can be identified.

1.4 Purpose

The purpose behind this thesis work is to verify if the electron theory could be a valid strategy to develop ductile refractory HEAs.

2 THEORETICAL FRAME

The following chapter will act as the literature review for HEAs, the findings for the properties map and reasoning behind the strategy.

2.1 Introduction

Materials have always been a huge asset to the human development. More advanced inventions have put pressure on scientists to discover better materials meeting the ever-increasing requirements. The motivation behind our need to develop can be connected to Maslow's hierarchy of needs, dictating self-actualization as the desire to accomplish everything that one can. [2]

Henry Ford, Gottlieb Daimler and the Wright Brothers were great examples of engineers utilizing available materials to contribute to our society. During the end of the 19th century, the amount of available material was limited to a few hundreds. [3] Today, engineers have over 45 000 different materials in their disposal. Three materials were so important that each corresponding era has been named after them, Stone Age, Bronze Age and Iron Age.

Metals have been used proficiently due to their material properties such as strength and formability. They have been used from making swords to building skyscrapers. From steel, a common alloy created using iron and carbon to the advanced multi-phase TRIP steel with microstructure consisting of ferrite, bainite and retained austenite. [4] This shows how versatile and important of metals and alloying are for developing new materials. As shown above, alloying is a great way to create different materials for different applications. An alloy is defined as a mixture of metals or a metal combined with another element. [5] Steel is a common example of a material utilizing iron as its main component and carbon as an alloying element along with other different elements depending on the steel. An example of a mixture of metals is bronze, a mixture of mainly copper and tin. One of the recent discoveries in alloying is HEAs, showing promising materials properties, especially in high temperature applications.

2.2 Earliest report of HEAs

The concept of HEAs dates back for more than two centuries with the studies of Franz Karl Achard in the late 18th century in Berlin. Achard is most likely the first one to study HEAs, using between five and seven different elements and made more than 900 experiments with 11 metals. In 1788 Achard published a book, unfortunately the book was ignored by other metallurgists and was not focused on until 1963 by Professor Cyril Stanley Smith. [6]

Although no work on the subject has been published until the 80s with the work of Cantor et al.. His work is mostly known as when he, together with his students, made a multicomponent alloy consisting of 20 different elements at 5 at.% each.[7] which is the world record holder of most used elements in an alloy.

2.3 Definition of HEAs

One of the forefathers, Yeh defined the material HEAs as an alloy with at least five metallic elements, and these are mostly in equimolar ratios. But to increase the possible combinations, individual element concentration between 5 to 35 % are also considered as HEAs. [8] The elements between 5 to 35 % are called principal elements and those under the 5 % line are called minor elements. Note that there are HEAs with less than five metallic elements, and these will be shown under the refractory HEAs section.

There is an additional requirement to the definition which contributes to the name. HEAs are defined as having a high configurational entropy.[9] HEAs have to have a configurational entropy higher than 1.5 R at a random-solution state. R is the ideal gas constant, 8.314 J/K mol.

The value of the configurational entropy can be calculated using following formula:

$$\Delta S_{config} = -R \sum_{i=1}^n X_i * \ln(X_i) \quad [\text{J/K}] \quad (1)$$

X_i is the mole fraction of the i th element.

Using an equal amount of atoms of each element in a composition of 4 elements would result in a configurational entropy of 1.386 R. Same principle using 5 elements would give the result 1.609 R. This shows that the additional definition is compatible with the first definition, and 1.5 R is a reasonable limit. Yeh even states that alloys close to these two definitions could be seen as HEAs. In another paper, Yeh defined medium entropy alloys with an interval between 1 R and 1.5 R, and low entropy alloys with a configurational entropy lower than 1 R. [10]

For comparison of alloy systems in a random state, low alloyed steels have an entropy of 0.22 R. Bulk metallic glass such as $Zr_{53}Ti_5Cu_{16}Ni_{10}Al_{16}$ has a configurational entropy of 1.3 R. Even with 5 different metallic elements, it does not constitute as a HEA. This shows how having at least five elements in equiatomic ratios contributes to a higher configurational entropy than other alloys and strengthens the need of the 1.5 R limit.

Later on, the mixing entropy will be used to describe the high entropy effect. The total mixing entropy depends on four factors: configurational, vibrational, magnetic dipole and electronic randomness. [8] The configurational entropy is the major contributor, and that is why for the sake of simplicity, the mixing entropy can be calculated with equation 1.

2.4 Factors behind the properties

There are four core effects affecting the microstructure and the properties of HEAs. [10] These are called the high entropy effect, the sluggish diffusion effect, the severe lattice distortion effect and the cocktail effect. The effects have influence in different areas of physical metallurgy as well. The high entropy effect is important for simplifying the microstructures so the alloys consist of simple solid solution phases with FCC or BCC structures.[11] The sluggish diffusion effect makes alloys develop amorphous and simple crystalline structures. The severe lattice distortion effect plays a huge role in mechanical, physical and chemical properties. The last one called the cocktail effect affects the overall composition, structure and microstructure of the alloy. Yeh illustrates the core effects in their area in the following figure:

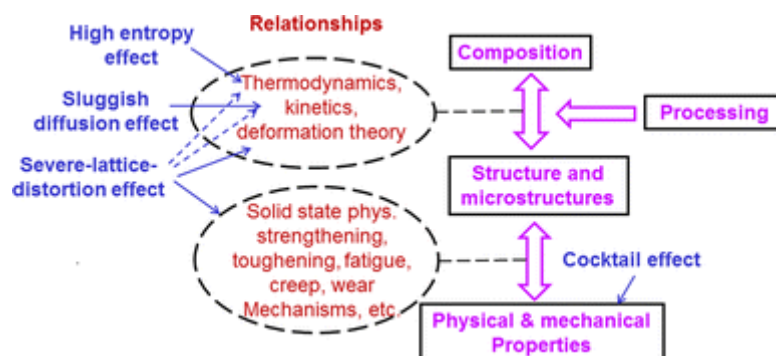


Figure 2.1: Shows the core effects influencing different aspects in physical metallurgy.[10]

2.4.1 High entropy

The high entropy effect enhances the formation of multiple-element solid solution phases. Having an entropy higher than the mixing enthalpy increases the solubility among different elements and prevents phase separation.

The reason behind having high entropy lies in Gibbs free energy defined as:

$$\Delta G_{mix} = \Delta H_{mix} - T * \Delta S_{mix} \quad [\text{kJ}] \quad (2)$$

H is the mixing enthalpy, T is the temperature and S is the mixing entropy. The equilibrium phase of an alloy is decided by the phase with the lowest Gibbs free energy.[4] HEAs with a naturally high mixing entropy would have an advantage of forming multiple-element solid solution phases over phases requiring higher free energy. For HEAs it is important to minimize the number of phases because their microstructure would become complex, which has been observed to create a brittle material because of many intermetallic compounds forming. [8] Cantor et al. have observed through experiments that in multiple-element alloys, the total amount of phases is always below the maximum equilibrium number allowed by the Gibbs phase rule, [7] which is related to having a high mixing entropy.

This effect has not been used for phase prediction in common alloys because their mixing entropy is very low compared with HEAs, which leads to a very small impact on Gibbs free energy.

2.4.2 Sluggish diffusion

It is easy to assume that the diffusion in HEAs is much slower than the diffusion in conventional alloys. Since the HEAs are built with several different elements, an atom diffusing from a spot to another is most likely going to be in a completely different environment than the previous spot. As a result of that it will also have different potential energy. If the new spot has a higher potential energy then it is most possible that the atom will return to its original place, if not then the atom will continue its journey.

The sluggish diffusion effect plays an important role for the high temperature properties of HEAs. It is the main contributor to the high temperature strength, thermal- and chemical stability at high temperatures and the formation of nanostructures. [12][13][14][15]

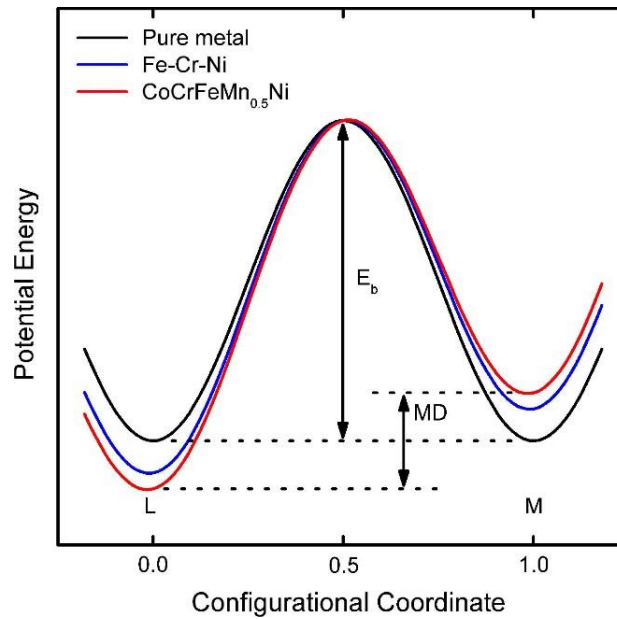


Figure 2.2: A schematic diagram of the variation of LPE and Mean Difference (MD) during the migration of a Ni atom in different matrices. The MD for pure metals is zero, whereas that for HEA is the largest. [8]

Compared to the diffusion of the conventional alloys, the diffusion in HEAs has a much greater variety in the surrounding atoms of the lattice sites of the solid solution phase. [16] This occurs probably because of the low Lattice Potential Energy (LPE) sites who serve as traps and stops the atoms from diffusing, which leads to the sluggish diffusion effect. [6] Tsai et al. [16] showed that for the sluggish diffusion for CoCrFeMnNi, as seen in figure 2.2 the potential energy for a Ni atom between two neighboring sites L and M is different for different matrices. One can see that the mean difference (MD) for a pure metal is zero, whereas the MD for alloys and HEAs is higher.

2.4.3 Lattice distortion

It is known that HEAs consist of multiple elements which has the effect of distorting the lattice of the crystal structure. The crystal structure can be BCC (Body-centered cubic) or FCC (Face-centered cubic) as solid solution phases are commonly found in HEAs.[11] The main reason behind the severe distortions is the difference in atomic size causing lattice strain as the larger atoms pushes on neighboring atoms.

Figure 2.3 shows a BCC (Body-centered cubic) lattice in different configurations. The left one with the same element and the right one with 5 different elements.

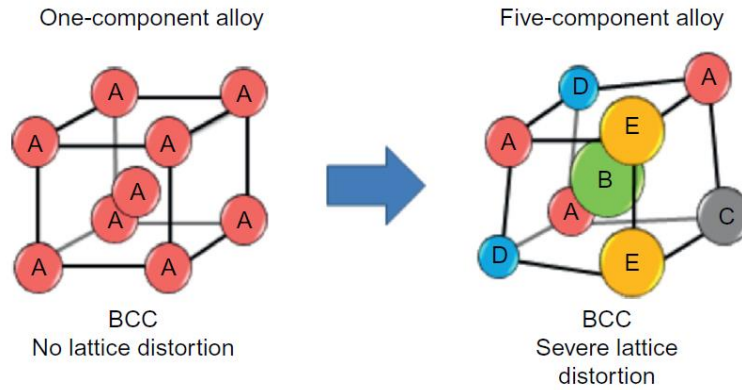


Figure 2.3: The BCC with 5 elements show severe lattice distortion compared to the one with 1 element. [11]

The lattice distortion will make it harder for dislocations to move, causing solid solution hardening in the material. It has been observed that HEA systems developed by Senkov have strength range between 900 to 1,350 MPa.[17] Using the rule of mixture to calculate the strength of the same systems would result a much lower strength. Giving an example in the hardness, MoNbTaVW has a measured hardness of 5,260 MPa, while the rule of mixture calculation would result a hardness of 1,596 MPa. The difference in hardness has been credited to severe lattice distortion caused by the atoms.

2.4.4 Cocktail effect

HEAs can be seen as an atomic-scale composite considering the multi-principal elements are incorporated, therefore they show a combined effect that comes from the basic characteristics and the interaction between all the elements besides the indirect effects of the different elements on the microstructure.[11] This means that if a low density HEA is desired one should use low density elements and so on. It may not always work this way, and there could be some effects on the properties due to the lattice distortion effect.

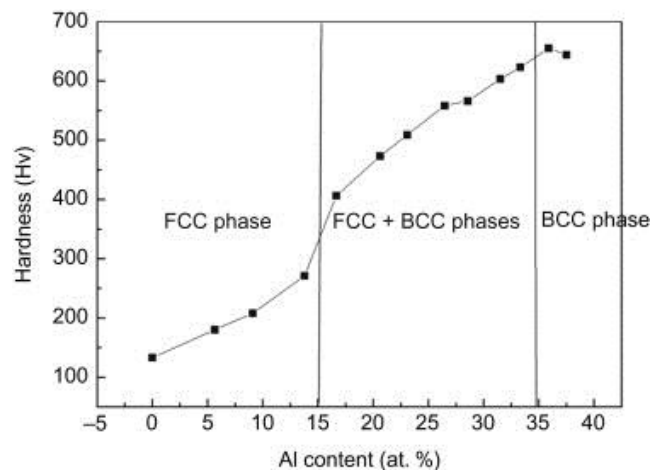


Figure 2.4: Cocktail effect introduced by the interaction of constituent elements in the $Al_xCoCrCuFeAl$ alloy. [6]

Figure 2.4 shows how aluminum has effect on the strength of $Al_xCoCrCuFeNi$ alloy. Aluminum in this alloy system has similar strengthening ability as carbon in steel, even though their strengthening mechanics are different. [11]

2.5 Mechanical properties

In this section, mechanical properties such as hardness, yield strength, fracture strength, ductility and density will be covered and examples from different studies and experiments will be discussed.

Showing the performance (mainly mechanical properties) of HEAs will make it easier to understand the advantages and disadvantages of HEAs over conventional alloys.

2.5.1 Room temperature properties

Tong et al. studied the HEA system $Al_xCoCrCuFeNi$ using different amounts of aluminum, varying from $x=0$ to 3.[18] The hardness increase was credited to the solution hardening mechanism as aluminum atoms are much larger than other principal elements in the alloy system. The lattice distortion effect was believed to have a significant role in strengthening the alloys. A figure from the same authors shows the hardness relating to the amount of aluminum.

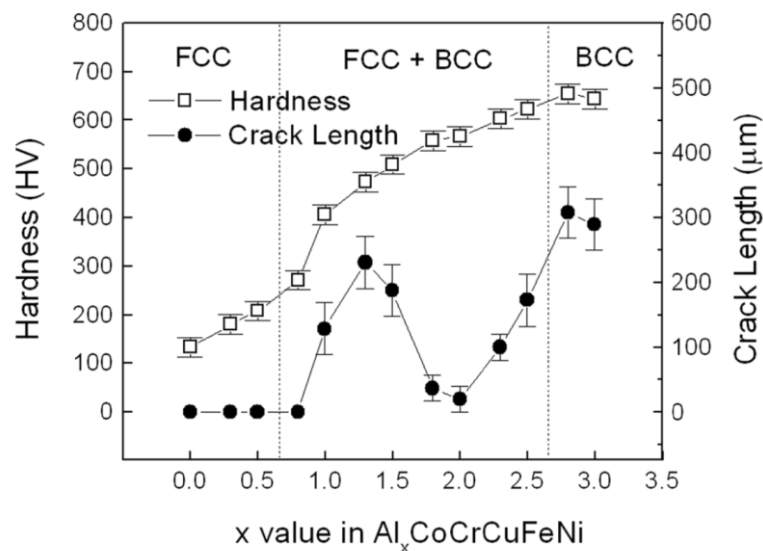


Figure 2.5: Increasing value of aluminum increases the hardness and brittleness.[18]

The Vickers hardness ranged from 133 to 655. Even though increased hardness is a great mechanical property in some applications, the alloy system showed increased crack lengths which indicates brittleness. The increased amount of strong BCC phase when adding more aluminum was the reason behind the increased brittleness.

Li et al. studied 10 different HEA systems with a FeNiCr base and tried adding different elements to the base. [19] The Vickers hardness was measured on these HEAs. The table below shows the systems studied.

Table 2.1: Vickers hardness of the alloys with the structure.[19]

Alloy	Structure	Hardness (HV)
FeNiCrCuCo	FCC	286
FeNiCrCuMo	FCC	263
FeNiCrCuAl	FCC + BCC	342
FeNiCrCuMn	FCC + BCC	296
FeNiCrCoAl	BCC	395
FeNiCrCoAl _{1.5}	BCC	402
FeNiCrCoAl ₂	BCC	432
FeNiCrCoAl _{2.5}	BCC	487
FeNiCrCoAl ₃	BCC	506
FeNiCrCuZr	BCC + compounds	566

The alloys with aluminum showed increased hardness as the aluminum content increased. The hardest alloy contained Zr, the reason behind the strengthening is due to Zr forming compounds with the other elements which causes precipitation hardening. The table shows alloys with BCC structures having a higher hardness than those with FCC structures.

Zhou et al. studied the alloy system AlCoCrFeNiTi_x with different titanium ratios at 0, 0.5, 1 and 1.5. [20] The alloys contained mostly of BCC phase except the Ti_{1.5} system showing a mix of BCC and Laves phase. Nonetheless, these alloys showed excellent mechanical properties during compression, especially the Ti_{0.5} system with a yield strength of 2.26 GPa, a fracture strength of 3.14 GPa and a plastic strain of 23.3 %. According to the authors, these values are greater than most high strength alloys such as BMGs (bulk metallic glasses).

Salishchev et al. experimented with the effects of Mn and V on CoCrFeNi systems. These systems showed varying hardness, tensile strength, yield strength and elongation depending on the alloying elements. [21] They also studied the effect of annealing on the alloys. The table below shows the Vickers hardness for the tested alloy systems.

Table 2.2: Vickers hardness on CoCrFeNi based systems before and after annealing.[21]

Alloy	As-solidified	Annealed
CoCrFeNi	160 ± 4	134 ± 4
CoCrFeNiMn	170 ± 4	135 ± 2
CoCrFeNiV	524 ± 15	587 ± 17
CoCrFeNiMnV	650 ± 27	636 ± 23

V has a huge impact on the hardness of the alloy, and the hardness are threefolded on systems alloyed with V. Annealing the alloys with V has a different result with CoCrFeNiV increasing hardness and CoCrFeNiMnV decreasing hardness. The strength of these systems also showed different result as the intermetallic compounds containing V were brittle, especially CoCrFeNiMnV which fractured at stress values between 62 and 90 MPa. The softer alloys,

CoCrFeNi and CoCrFeNiMn, showed capability of strain hardening and overall ductility, and these were both before and after annealing.

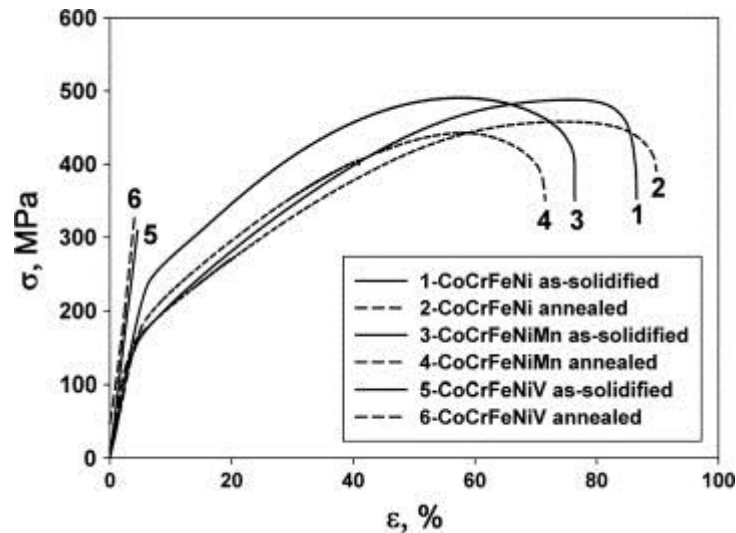


Figure 2.6: Stress-strain curves after tensile tests with CoCrFeNi, CoCrFeNiMn and CoCrFeNiV.[21]

CoCrFeNi before annealing had the greatest elongation to fracture value at 83 %, with a yield strength at 140 MPa and tensile strength at 488 MPa. The HEA CoCrFeNiMn had a lower elongation to fracture value at 71 % but a higher yield strength at 215 MPa and a nearly the same tensile strength at 491 MPa. CoCrFeNiV and CoCrFeNiMnV had two-phase crystal structures which contributed to the brittleness. Meanwhile, the CoCrFeNi and CoCrFeNiMn alloys consisted only of single phase FCC structure which is known for being soft and ductile.

To summarize, increased amounts of BCC structures will result in a harder alloy but also more brittle alloys. Having multiple phases will also lead to the same result. FCC alloys shows ductility but lower hardness and strength.

2.5.2 Elevated temperature strength

Going back to the $Al_xCoCrCuFeNi$ HEA systems studied by Tong et al..[18] Experiments showed that $Al_{0.5}CoCrCuFeNi$ sustained high yield and tensile strength up to 800 °C before softening at 900 °C. Thanks to the FCC structure, it showed extended ductility at elevated temperatures. The increasing strength while the strain increased is sign of work hardening. Systems with higher aluminum content had higher yield strength with $Al_{2.0}CoCrCuFeNi$ showing up to 1600 MPa but these alloys were also more brittle because of the increased amount of BCC structures.

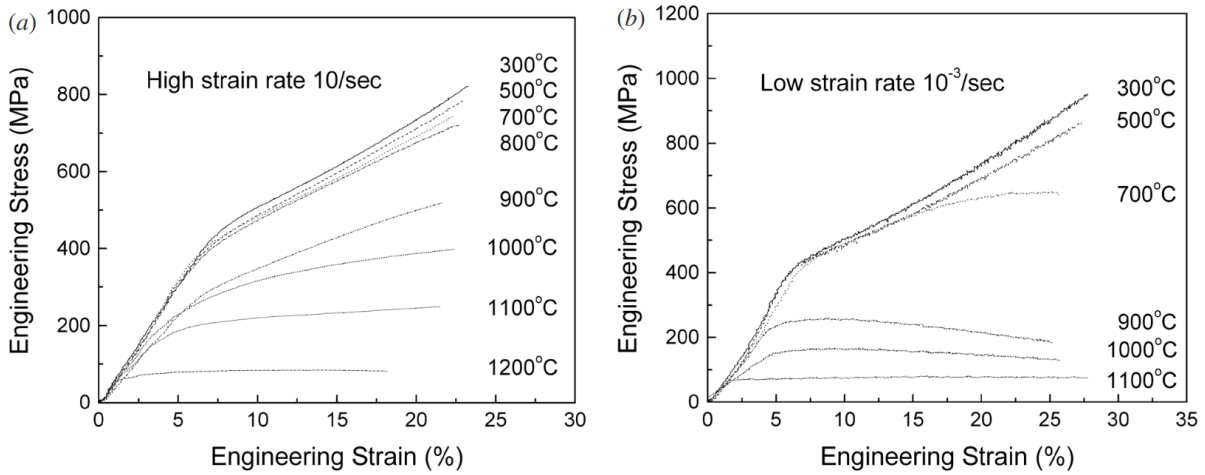


Figure 2.7: Stress-strain curve after compression test of $Al_{0.5}CoCrCuFeNi$ under different temperatures and strain rates a) 10/s b) $10^{-3}/s$. [18]

These figures show how consistent the stress stayed at different temperatures before dropping off at 900 °C.

Hsu et al. investigated $AlCo_xCrFeMo_{0.5}Ni$ with varying Co contents with x ranging from 0.5 to 2.0. [22] The Vickers hardness at the elevated temperature of 1273 K was Hv 340 for Co-0.5 and Co-1.0 alloys. These HEAs have superior hardness compared with the nickel based super alloys In 718 and In 718 H which only had a hardness of Hv 127 at the same temperature.

Kuznetsov et al. studied $AlCoCrCuFeNi$ with near-equiatomic ratio at elevated temperatures. [23] This alloy presented superplastic behavior between the temperatures of 800 to 1000 °C. At 800 °C, the alloy had an elongation till fracture value of 400 % and at increased temperature of 1000 °C, the value increased to 864 %. Even increasing the strain rate from 10^{-4} to $10^{-2}/s$ at 1000 °C did not change the ductility of the alloy. The yield strength were not so impressive, with 63 MPa at 700 °C, 22 MPa at 800 °C and 14 MPa at 900 °C. Note that these alloys were prepared with multi-directional isothermal forging at 950 °C. This method gave the alloys a fine-grain structure with the average grain size of 1.5 μm .

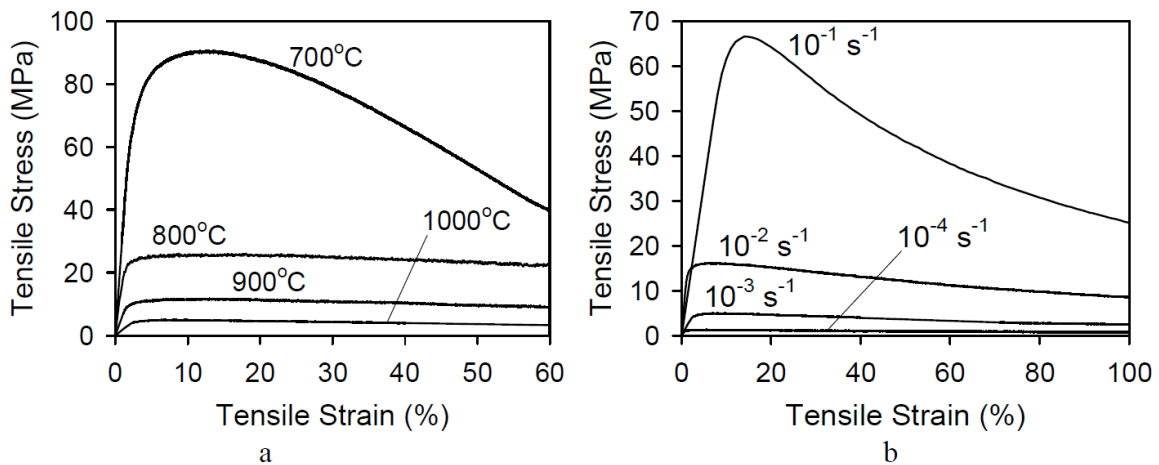


Figure 2.8: Stress-strain curves from tensile tests. a) Different temperatures b) Different strain rates at 1000 °C. [23]

The figure shows a) decreased strength with increased temperature and b) increased strength with increased strain rate.

HEAs seems also to have excellent anneal softening resistance. Table 2.3 shows the hardness for different as-cast alloys after annealing at 1000 °C for 12 h. This implies that the hardness remains almost the same even after annealing the alloys. [8]

Table 2.3: Hardness of as-cast and fully annealed high-entropy alloys and commercial alloys.[8]

Alloys	Hardness, HV as-cast	Hardness, HV annealed
CuTiVFeNiZr	590	600
AlTiVFeNiZr	800	790
MoTiVFeNiZr	740	760
CuTiVFeNiZrCo	630	620
AlTiVFeNiZrCo	790	800
MoTiVFeNiZrCo	790	790
CuTiVFeNiZrCoCr	680	680
AlTiVFeNiZrCoCr	780	890
MoTiVFeNiZrCoCr	850	850
316 Stainless Steel	189	155
17-4 PH Stainless Steel	410	362
Hastelloy C	236	280
Stellite 6	413	494
Ti-6Al-4V	412	341

Some HEAs with FCC structure have also the benefit of extended ductility and sustained high strength at raised temperatures. For example, the yield strength of the CuCoNiCrAl_{0.5}Fe alloy remained the same from room temperature up to 800 °C as seen in figure 2.9. [8]

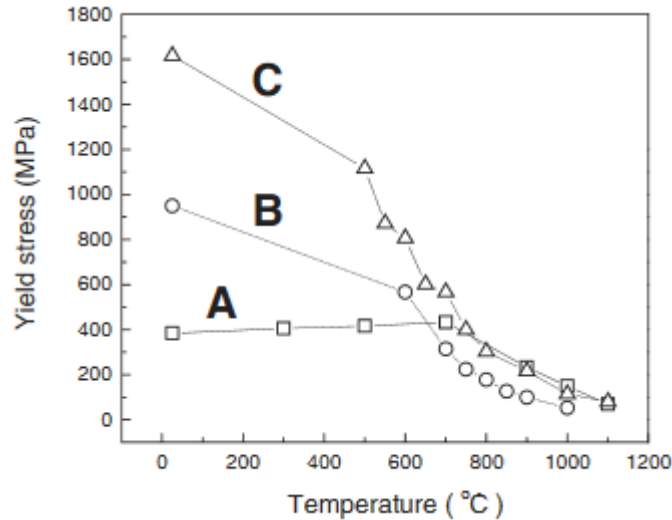


Figure 2.9: Compressive yield strengths of CuCoNiCrAl_xFe alloy system tested at different temperatures: A) CuCoNiCrAl_{0.5}Fe, B) CuCoNiCrAl_{1.0}Fe, C) CuCoNiCrAl_{2.0}Fe alloys.[8]

This only shows some examples of the mechanical properties of HEAs at elevated temperatures. Al_{0.5}CoCrCuFeNi possesses high strength and ductility, and shows superplastic behavior. AlCo_{0.5}CrFeMo_{0.5}Ni and AlCo_{1.0}CrFeMo_{0.5}Ni even beat Ni-based superalloys on high temperature hardness.

2.6 Refractory alloys

This section covers the information for current simpler refractory alloys and refractory HEAs.

2.6.1 Simpler refractory alloys

Refractory metals or simpler refractory alloys are known for their high melting points, which is at least at 4000 °F (2204 °C). [24] These metals/alloys are used in demanding applications which require high-temperature strength and high corrosion resistance. As seen in Table 2.4 the five most used metals are Niobium (Nb), Molybdenum (Mo), Tantalum (Ta), Tungsten (W) and Rhenium (Re). Even though these five metals have high melting points, they have to be mix with other elements to gain corrosion resistance and more ductility. There is also a wider definition including 9 other elements which is shown in figure 2.10. These elements all have relatively high melting points.

Table 2.4: Properties of the refractory metals.[25]

Element	Melting point °C	Density g·cm ⁻³
Niobium, Nb	2468	8.57
Molybdenum, Mo	2610	10.22
Tantalum, Ta	2996	16.6
Tungsten, W	3410	19.3
Rhenium, Re	3186	21.02

1																	18
H	2											13	14	15	16	17	He
Li	Be											B	C	N	O	F	Ne
Na	Mg	3	4	5	6	7	8	9	10	11	12	Al	Si	P	S	Cl	Ar
K	Ca	Sc	Ti	V	Cr	Mn	Fe	Co	Ni	Cu	Zn	Ga	Ge	As	Se	Br	Kr
Rb	Sr	Y	Zr	Nb	Mo	Tc	Ru	Rh	Pd	Ag	Cd	In	Sn	Sb	Te	I	Xe
Cs	Ba	*	Hf	Ta	W	Re	Os	Ir	Pt	Au	Hg	Tl	Pb	Bi	Po	At	Rn
Fr	Ra	**	Rf	Db	Sg	Bh	Hs	Mt	Ds	Rg	Cn	Uut	Fl	Uup	Lv	Uus	Uuo
			3	4	5	6	7	8	9	10	11	12	13	14	15	16	17
			* La Ce Pr Nd Pm Sm Eu Gd Tb Dy Ho Er Tm Yb Lu														
			** Ac Th Pa U Np Pu Am Cm Bk Cf Es Fm Md No Lr														

Figure 2.10: Periodic table with the refractory metals highlighted including the wider definition.

2.6.2 Current status on refractory alloys

HEAs are still in the early research phase, especially refractory HEAs. This section will present mechanical properties data of refractory HEAs and simpler refractory alloys. The main properties to be covered are mechanical properties such as hardness, yield strength, fracture strength, ductility and density. The properties data will point out pros and cons for HEAs and simpler alloys in high temperature applications.

2.6.2.1 High temperature application

As mentioned above, the refractory alloys have a high melting point which gives us the possibility to use them in high-temperature-environments. On the negative side there is the high density problem among the refractory alloys which could be a restriction in some areas, therefore the solid refractory metal need to be alloyed with other refractory metals in order to reduce the density or gain more ductility. Due to the high density and melting point of the refractory alloys, they are rarely fabricated by casting. The most common processing is powder metallurgy where powders of the metals are compacted, and sintered to form dense bulk alloys.

Furthermore, an inspection of the application of each refractory metal and some of its alloys will be done below.

2.6.2.2 Niobium applications

As a pure metal the production of niobium is estimated to be between 60 000-84 000 tons/year, and the consumption of niobium has been at this rate for about 10 years. [26] The largest use of niobium is in the production of uranium (6% Niobium). Other than that, one can find Nb as electrical components in sodium vapor lamps and in x-ray tubes working as the target material of the x-ray beam. [27]

Niobium has many uses together with the other refractory metals. It is the least dense of the refractory metals and can be annealed to achieve a wide range of elasticity and strength. Alloyed niobium is mostly used in the aircraft industry due to its relatively low density as seen in table 2.4 above and high corrosion temperature at 400⁰ C. [28] An alloy of niobium is used in the main engine of the Apollo Lunar Modules, the C103 alloy, which is an alloy containing 89% Nb, 10% Hf and 1% Ti. [29][30]

Another space related alloy can be found on the nozzle of the Apollo CSM which is made from Nb-Ti alloy. Even though having the high corrosion resistance, this alloy had to be coated to prevent the alloy becoming brittle. [29]

Table 2.5 shows two different Nb-Hf alloys, NC-184 and NC-250 both containing 5 wt.% Hf. The difference between these alloys is that the NC-250 alloy was prepared using a niobium powder containing more oxygen than the NC-184 alloy.

Table 2.5: Mechanical properties of Nb-5Hf and Nb-5Hf + O₂[31]

Specimen	Nominal composition (wt.%)	Analysis (wt.%)	Test temp. (°C)	0.2% YS (MPa)	UTS (MPa)	Elongation (%)	Red. area (%)
NC-184	Nb-5Hf	< 0.04 O ₂	25	228.20	348.19	25.2	58.4
NC-184	Nb-5Hf	<0.04 C	1095	126.86	175.82	14.4	57.8
		-					
NC-250	Nb-5Hf + O ₂	-	-196	762.56	983.88*	12.4	17.0
NC-250	Nb-5Hf + O ₂	0.067 O ₂	25	332.33	438.16	24.3	46.0
NC-250	Nb-5Hf + O ₂	0.028 C	1095	326.12	339.20	18.6	42.5
NC-250	Nb-5Hf + O ₂	-	1205	244.76	248.20	9.2	64.2

* True stress at fracture

2.6.2.3 Molybdenum applications

Molybdenum is the most common refractory metals and is mostly used as an alloying element in different iron and steel materials. [32]Molybdenum is also used as reflective heat shields and different furnace hardware due to its ability to perform well under these circumstances. [33]

The most used molybdenum based alloys is TZM which contains only 0.5% titanium and 0.08% zirconium and the rest is molybdenum. [33]This specific alloy has a significant difference in material properties than pure Mo as seen in figure 2.11 together with MHC which is another Mo-based alloy consisting of 1.2% hafnium and 0.1% carbon.

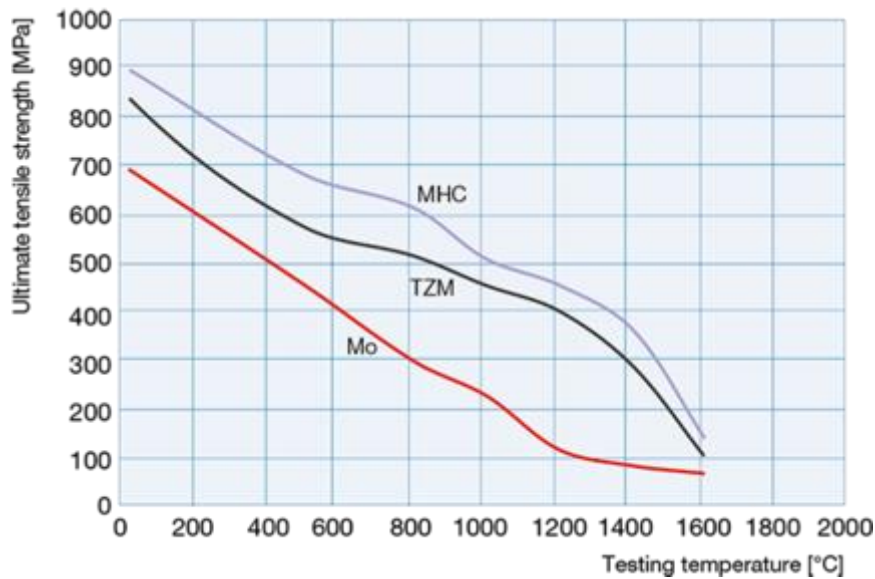


Figure 2.11: Ultimate tensile strength comparison between Mo, TZM and MHC. [34]

Similar to the TZM alloy there is the Molybdenum TZC alloy with the composition of Mo-1Ti-0.3Zr. [35] This alloy behaves very similar to the TZM alloy but with a slightly different mechanical properties. A test made by Tietz et al. at Stanford University shows that TZM has better strength between 1800 and 2400 °F (982- 1316 °C) and at room temperature whilst the TZC have better strength between 2500 and 3500 °F (1371-1927 °C). The strength of the alloys can be seen as equal at 2500 °F (1371 °C). [36]

Molybdenum may also be combined with rhenium. For example there is the Mo-47.5Re alloy, which has been applied in nuclear and aerospace application due to its excellent mechanical properties at both high and low temperatures.[37] [38]

2.6.2.4 Tantalum applications

Tantalum is often found together with niobium therefore both elements have related names as Niobe being the daughter of the mythical Greek king Tantalus.

The main usage area of tantalum today is in the electronic business and mainly in automotive electronics, personal computers and mobile phones. Tantalum oxide and carbide are used in glass lenses and cutting tools respectively. [39] Tantalum is one of the most corrosion resistant substance available and is used as a cheaper substitute for platinum in medical surgeries due to its chemical properties.

A tantalum based alloy called T-111 with the composition of Ta-8%W-2%Hf was developed in the early 1960s [40]. The T-111 seems to be a very strong to temperatures around 1100 °C and yet ductile at low temperatures. The alloy is bendable at room temperatures, and has good weldability and good corrosion resistance against alkali metals. In the 1970s it was seen as a good candidate to space power applications. [41]

As seen in figure 2.12, both the ultimate tensile strength and the yield strength seem to be relatively high at temperatures around 1200 °C. However both the ultimate tensile strength and the yield strength decrease with increased temperature as seen in almost every alloy. The T-111 alloy shows values close to the TZM alloy showed in figure 2.11.

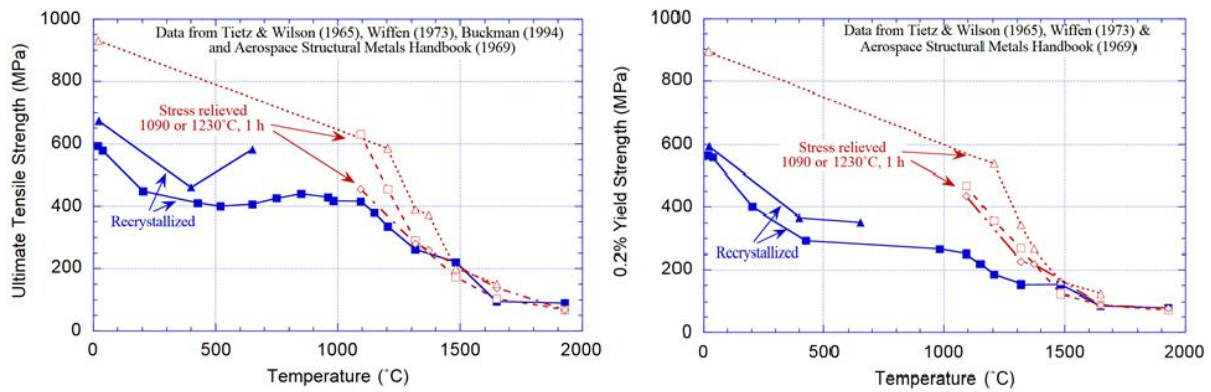


Figure 2.12: Tensile strength-temperature and Yield strength-temperature curves of Ta-8%W-2%Hf. [40]

As mentioned before, the T-111 alloy is ductile as seen in figure 2.13. Unfortunately the figure only shows temperature as low as 0 °C although it seems that the T-111 have good ductility even at temperatures well below 0 °C and even at temperatures as low as at least -196°C. [41]

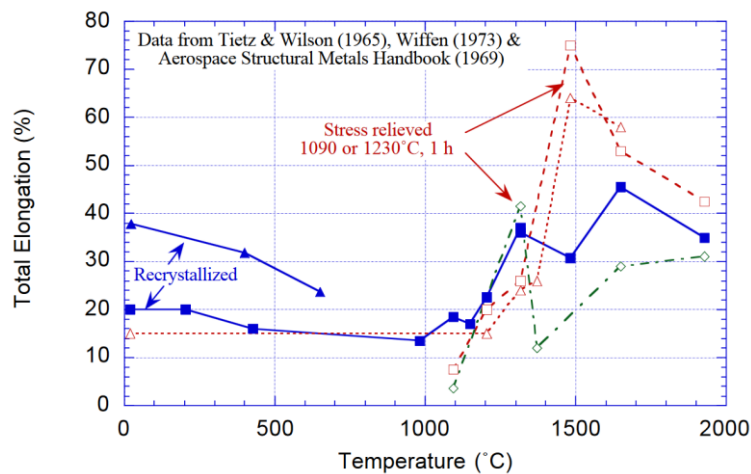


Figure 2.13: Total elongation-temperature curve of Ta-8%W-2%Hf.[40]

In the refractory group of materials we find tungsten as the most alloyed element with tantalum. The three most common tantalum-tungsten alloys are: Ta – 2.5% W, Ta – 7.5% W and Ta – 10% W. [35] These Ta-W alloys have a high level of corrosion resistance, high melting points, high tensile strength and high elastic modulus as seen in table 2.6.

Table 2.6: Material properties of different Ta-W alloys. [42][43][44][45]

Alloy	Density (g/cm ³)	Melting Point (°C)	Tensile Strength (MPa)	Yield Strength (MPa)	Hardness (HV)	Elongation (%)
Ta-2.5%W	16.7	3005	345	230	195	20
Ta-7.5%W	16.8	3030	550	460	205	6-7
Ta-10%W	16.9	3025	1035-1165	875-1005	200	27

2.6.2.5 Tungsten applications

Tungsten is the refractory metal almost everybody has been in contact with since it was used in lightbulbs before the LED and CFL lamps came along.

Tungsten has a very high density but is also the metal with the highest melting point. Therefore tungsten and its alloys are used where high temperature is present and the density is not an issue.[46] Despite the high density, tungsten alloys could even be used in aerospace applications as nozzles for different rocket or missiles. For example, tungsten was used in the nozzle of the UGM-27 Polaris missiles between 1961 and 1996. [47]

Another application area for tungsten is not based on the refractory properties but simply on its high density. Tungsten is widely used as a balance material in airplanes, helicopters and heads of golf clubs. [48][49]

2.6.2.6 Rhenium applications

Rhenium is the latest discovered refractory metal and also the most expensive one, and it is obtained from the ores of other refractory metals and copper. Alloying it with other refractory metals can add ductility and tensile strength to the final product.

Rhenium is commonly used in the jet-engine industry and different turbine applications whereas Ni-based alloys are used, and these Ni-based alloys make for 70% of the rhenium production worldwide. [50] For example, rhenium alloys was used in the F-15, F-16, F-22 and F-35 jet engines. [51][52]

2.6.2.7 Other refractory alloys and their applications

Despite the refractory alloys mentioned above, we have a wider definition of refractory alloys that also include Cr, Hf, Ir, Os, Rh, Ru, Ti, V and Zr. In this section the focus will primarily be on Ti. Titanium is a well-known metal with a wide usage area. Titanium alloys can in most cases be sorted into two groups. The corrosion resistant alloys, based on mainly Ti-Pd, and the Ti-V-Al (or Mn) group with its good mechanical properties.

The second group is the most common and can be found in different airplane and jet engine parts for example there is the ATI 64-MIL™ alloy which has the composition of Ti-6Al-4V. The ATI 45Nb™ Alloy is a Ti based alloy containing 45% Nb. This alloy is a good material choice for the rivets that secure aluminum panels in the aircraft industry, especially those areas being exposed to high temperatures. [53]

2.6.3 Refractory HEAs

The definition for refractory HEAs are basically HEAs consisting of refractory metals and those included by the wider definition, and the alloy may contain non-refractory metal as long as the alloys show high heat resistance. The refractory metals are highlighted with dark blue in figure 2.10 and the light blue are the wider definition of refractory metals.

2.6.3.1 Mechanical properties

Two refractory HEAs were researched by Senkov et al. [54], and the compositions were $\text{Nb}_{25}\text{Mo}_{25}\text{Ta}_{25}\text{W}_{25}$ and $\text{V}_{20}\text{Nb}_{20}\text{Mo}_{20}\text{Ta}_{20}\text{W}_{20}$, respectively. Note that the first alloy does not consist of five elements or more but is still regarded as a HEA because of the high mixing entropy. These alloys showed promising Vickers hardness of 4.46 GPa and 5.42 GPa in the previous research. [55] The first alloy achieved following compression properties.

Table 2.7: Compression properties of $Nb_{25}Mo_{25}Ta_{25}W_{25}$. [54]

Temperature (°C)	Yield stress (MPa)	Peak stress (MPa)	Peak strain (%)	Stress at 25%
23	1058	1211	1.5	1135*
600	561	-	-	1140
800	552	-	-	1283
1000	548	1008	16	763
1200	506	803	12	725
1400	421	467	9	331
1600	405	600	27	597

The alloys shows high yield strength but fractured at an elongation of 2.6 % at room temperature. At higher temperature, the yield strength decreased but the elongation increased to over 20 %. This density for this composition is $\rho = 13.75 \text{ g/cm}^3$.

Table 2.8: Compression properties of $V_{20}Nb_{20}Mo_{20}Ta_{20}W_{20}$. [54]

Temperature (°C)	Yield stress (MPa)	Peak stress (MPa)	Peak strain (%)	Fracture stress (MPa)	Fracture strain %
23	1246	1270	0.5	1087	1.7
600	862	1597	13	1597	13
800	846	1536	16	1509	17
1000	842	1454	14	1370	19
1200	735	943	4.2	802	7.5
1400	656	707	1.6	-	-
1600	477	479	0.95	-	-

The alloy consisting of 5 elements shows greater yield strength at room temperature and at elevated temperature. As expected, higher yield strength usually results in poor ductility, $V_{20}Nb_{20}Mo_{20}Ta_{20}W_{20}$ had a lower fracture strain, with 19 % at 1000 °C as its best. The density is $\rho = 12.36 \text{ g/cm}^3$. Both alloys shows high compression yield strength and moderate ductility at $T = 600 \text{ °C} - 1600 \text{ °C}$. The high strength and brittleness at room temperature can be related to the high melting point that both these compositions have.

Another refractory HEA with the equiatomic composition $MoNbHfZrTi$ was tested by Guo. [56] The alloy shows a high compressive yield strength at 1719 MPa at room temperature and good overall yield strength at elevated temperatures. The table below shows the yield strength, maximum strength and fracture strain at different temperatures for the alloy.

Table 2.9: Compression properties of MoNbHfZrTi at different temperatures.[56]

T (K)	296-C	296-H	1073	1173	1273	1373	1473
σ_p (MPa)	1803	1640	1095	938	654	399	194
$\sigma_{0.2}$ (MPa)	1719	1575	825	728	635	397	187
δ (%)	10.12	9.08	>60	>60	>60	>60	>60

296-C stands for As-cast state and 296-H stands for As-homogenized. As-cast shows greater strength and elongation than after homogenization. This alloy consists of single phase disordered BCC crystal structure and have a calculated density of 8.64 g/cm³. Senkov et al. tested four refractory HEAs NbTiVZr, NbTiV₂Zr, CrNbTiZr and CrNbTiVZr. [57] These alloy systems have one shared property which is their low densities, being 6.52 g/cm³, 6.34 g/cm³, 6.67 g/cm³, and 6.57 g/cm³, respectively. Table 2.10 shows the mechanical properties during a compression test. All alloys decreased in yield strength at higher temperatures and showed strain softening above 873 K. Notice the big difference in strength between T=873 K and T=1073 K for all alloys.

Table 2.10: Compression properties of four refractory HEAs at different temperatures.[57]

Alloy/properties		NbTiVZr	NbTiV ₂ Zr	CrNbTiZr	CrNbTiVZr
T=298 K	$\sigma_{0.2}$ (MPa)	1105	918	1260	1298
	σ_{10} (MPa)	1430	1300	-	-
	σ_{20} (MPa)	1732	1635	-	-
	ϵ_t (%)	>50	>50	6	3
T=873 K	$\sigma_{0.2}$ (MPa)	834	571	1035	1230
	σ_{10} (MPa)	884	701	1130	1360
	σ_{20} (MPa)	767	716	1030	-
	ϵ_t (%)	>50	>50	>50	>10
T=1073 K	$\sigma_{0.2}$ (MPa)	187	240	300	615
	σ_{10} (MPa)	178	228	455	601
	σ_{20} (MPa)	174	185	435	512
	ϵ_t (%)	>50	>50	>50	>50
T=1273 K	$\sigma_{0.2}$ (MPa)	58	72	115	259
	σ_{10} (MPa)	68	60	138	205
	σ_{20} (MPa)	77	53	136	183
	ϵ_t (%)	>50	>50	>50	>50

Among these four alloys, CrNbTiVZr had the best mechanical properties in form of a high yield strength at 1298 MPa at room temperature and 615 MPa at T= 1073 K while the other alloys did not reach half of the yield strength at that specific temperature. Even though it was brittle compared to other alloys at room temperature, the ductility increased with increased temperature. The alloy consisted of BCC phase and Laves phase, and the author recommended controlling the amount of Laves phase to increase the ductility at room temperature.

Senkov et al. experimented with a refractory high entropy with the composition HfNbTaTiZr showing promising compression strength and ductility at room temperature. [58] The material has a yield strength at 928 MPa, a fracture strain over 50 % and a density of 9.94 g/cm³. It has a Vickers hardness at 3826 MPa. HfNbTaTiZr consisted of single phase BCC crystal structure and the high strength was attributed to solid-solution strengthening. The alloy even showed strain hardening as shown in figure 2.14, where the stress increases with increasing strain.

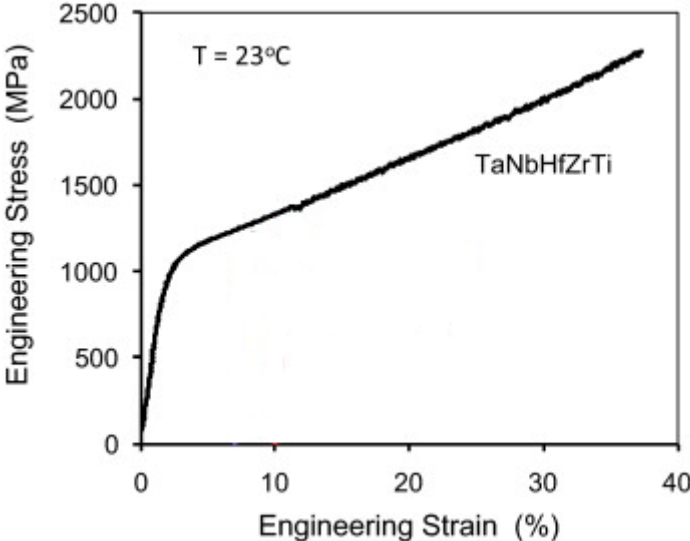


Figure 2.14: Engineering stress vs. engineering strain compression curves of the TaNbHfZrTi at room temperature.[58]

In search for ductile refractory HEAs, Juan et al. modified a ductile alloy with the composition of HfNbTaTiZr and modified it to create HfMoTaTiZr and HfMoNbTaTiZr. [59] Both of these alloys have simple BCC crystal structure with the presence of secondary phases and the densities of 10.24 g/cm³ and 9.97 g/cm³, respectively. Table 2.11 shows the yield strength and fracture strain at different temperatures.

Table 2.11: Compression properties of HfMoTaTiZr, HfMoNbTaTiZr and HfNbTaTiZr. [58] [59] [60]

Test Temperature (°C)	HfMoTaTiZr		HfMoNbTaTiZr		HfNbTaTiZr	
	Yield strength $\sigma_{0.2}$ (MPa)	Fracture strain ϵ_f (%)	Yield strength $\sigma_{0.2}$ (MPa)	Fracture strain ϵ_f (%)	Yield strength $\sigma_{0.2}$ (MPa)	Fracture strain ϵ_f (%)
25	1600	4	1512	12	928	>50
800	1045	19	1007	23	535	
1000	855	>30	814	>30	295	
1200	404	>30	556	>30	92	

Both alloys have high yield strength at room temperature and at elevated temperatures. With HfMoNbTaTiZr excelling in ductility and having greater strength at T= 1200 °C. Compared with the reference composition HfNbTaTiZr, the yield strength of HfMoNbTaTiZr is more than six times at T=1200 °C.

Wu et al. experimented with an equiatomic HEA with the composition HfNbTiZr. The alloy consists of a single phase solid solution with a BCC crystal structure. It exhibited a yield strength of 896 MPa, an ultimate tensile strength of 969 MPa and a fracture strain of 14.9 %. No high temperature test has been performed for this alloy. The alloy has a low VEC value of 4.25. [61] The density has been calculated to 8.22 g/cm³.

Chen et al. investigated NbMoCrTiAl in an equiatomic composition.[62] Table 2.12 shows the yield strength, maximum strength and fracture strain of the alloy at different temperatures. The alloy has a high yield strength at elevated temperatures before plummeting at T=1200 °C.

Table 2.12: Compression properties of NbMoCrTiAl.[62]

Testing temperature °C	$\sigma_{0.2}$ (MPa)	σ_{max} (MPa)	ϵ_p (%)
25*	-	1010	-
400*	1080	1100	2.0
600	1060	1170	>2.5
800*	860 ± 110	1000 ± 195	>2.0
1000	594 ± 5	630 ± 16	>15.0
1200	105 ± 14	116 ± 8	>24.0

* Fracture occurred during the experiment.

The density of the alloy has been calculated to 6.17 g/cm³, which is light compared with other refractory HEAs. Like other alloys, the ductility increases with increasing temperature.

Another low density refractory HEA has been experimented by Stepanov et al. which had the composition of AlNbTiV.[63] The alloy had coarse-grained single BCC crystal structure with density of 5.59 g/cm³. Table 2.13 shows the yield strength, maximum strength and fracture strain during compression tests. The alloy showed brittle fracture at room temperature but showed increased ductility at elevated temperatures. Compression test for T=800 °C and T=1000 °C does not show maximum strength and fracture strain as the strength increased with increasing elongation and the tests were stopped after reaching 50 % elongation. The author credited Al for the increased compression strength at 800 °C.

Table 2.13: Compression properties of AlNbTiV.[63]

T(°C)	$\sigma_{0.2}$ (MPa)	σ_p (MPa)	ϵ (%)
20	1020	1318	5
600	810	1050	12
800	685	-	-
1000	158	-	-

Senkov et al. tested two different refractory HEAs with the composition $\text{AlMo}_{0.5}\text{NbTa}_{0.5}\text{TiZr}$ and $\text{Al}_{0.4}\text{Hf}_{0.6}\text{NbTaTiZr}$. [64] The first alloy has the density of 7.40 g/cm^3 and the second one is a bit heavier with a density of 9.05 g/cm^3 . Both consisted mainly of BCC crystal structure and both showed high strength at room temperature.

Table 2.14: Compression properties of $\text{AlMo}_{0.5}\text{NbTa}_{0.5}\text{TiZr}$. [64]

T (K)	$\sigma_{0.2}$ (MPa)	σ_p (MPa)	E (GPa)	δ (%)
296	2000	2368	178.6	10
1073	1597	1810	80	11
1273	745	772	36	>50
1473	250	275	27	>50

Table 2.15: Compression properties of $\text{Al}_{0.4}\text{Hf}_{0.6}\text{NbTaTiZr}$. [64]

T (K)	$\sigma_{0.2}$ (MPa)	σ_p (MPa)	E (GPa)	δ (%)
296	1841	2269	78.1	10
1073	796	834	48.8	>50
1273	298	455	23.3	>50
1473	89	135	-	>50

Table 2.14 and 2.15 show the yield strength, maximum strength, elastic modulus E and fracture strain at different temperatures. $\text{AlMo}_{0.5}\text{NbTa}_{0.5}\text{TiZr}$ has much higher strength than $\text{Al}_{0.4}\text{Hf}_{0.6}\text{NbTaTiZr}$ at all temperatures. Similar for both alloys, the strength decreases and the ductility increases with increasing temperature. The author reported Al additions as an effective way to increase yield strength, increase ductility at tested temperatures and decrease density compared with $\text{CrMo}_{0.5}\text{NbTa}_{0.5}\text{TiZr}$.

Zhang et al. synthesized $\text{HfNbTiVSi}_{0.5}$ showing high compression yield strength and fracture strain at room temperature and at high temperatures. [65] The values are 1399 MPa for yield strength and 10.9 % fracture strain at room temperature. At $T=800 \text{ }^\circ\text{C}$ and $T=1000 \text{ }^\circ\text{C}$, the yield strength were measured to 875 MPa and 240 MPa with elongation over 50 % for both. The density for this composition is 8.60 g/cm^3 . The increased strength at high temperatures was credited to the addition of silicon which resulted in the formation of silicide. The alloy consisting of BCC crystal structure was strengthened by the silicide.

2.6.3.2 Issues and problems

This section expands on the common problems found in refractory alloys.

2.6.3.2.1 High density

There are refractory HEAs with low density, shown by our properties map, but these do not possess high strength at elevated temperatures. An exception was NbMoCrTiAl showing a yield strength of 600 MPa at $T=1000 \text{ }^\circ\text{C}$ but this alloy proved to be very brittle at room temperature, fracturing before a yield strength could be measured.

The reason for high density can be traced to the elements used by the different compositions. Refractory metals have great high temperature properties but most of them also have high

density with a few exceptions such as titanium with a density of 4.506 g/cm^3 . The rule of mixture applies roughly in refractory HEAs, and alloying elements with high melting point usually results in alloys with great high temperature properties. A refractory HEA with a density lower than steel's density of 7.86 g/cm^3 would be regarded as low density. [24] Aiming for a density lower than aluminum is unrealistic as there is no refractory element with a density lower than aluminum's density.

2.6.3.2.2 Brittleness

One of the main factors behind the crystalline structures and physical properties are the interatomic bond in metals and alloys. There are four different types of bonds are called metallic, ionic, covalent and van der Waals bond. There is a strong relation between the strength of the interatomic bond and interatomic distance. Metallic elements with the smallest atomic dimensions have the highest interatomic strength which has a profound effect on the melting point. Among the transition metals, group 6 has the lowest value on the coefficient of linear expansion and the interatomic distance, and that is why they possess high melting points. Refractory metals have a high melting temperature thanks to the strong covalent bond holding the atoms together. As the covalent bond is the strongest bond among those four types, the covalent bond contributes to a higher strength and higher hardness, which makes refractory metals brittle by nature. Tungsten for example has a very high melting point and hardness, but it is very brittle. [66]

Alloys tend to become more ductile with increased temperature as the amount of metallic bonds are increased with increasing temperature as the covalent bonds are "destroyed" by the thermal vibration. Metallic bonds are not as strong as covalent bonds.

2.7 Strategy

This section will cover the reasoning behind the strategy to identify ductile refractory HEAs. The strategy is based on the free electron theory which explains the behavior of valence electrons in solid metallic elements. The free electron theory is complicated for our level of education, so multiple examples from studies will be covered to prove the legibility of our strategy.

As an example of valence electron concentration (VEC) affecting ductility, Li et al. developed four refractory HEAs with the compositions, ZrNbHf, ZrVTiNb, ZrTiNbHf and ZrVTiNbHf. [67] These alloys consist of elements from group four and group five. Group four elements have 4 valence electrons and group five elements have 5 valence electrons, these are the electron configurations in the ground state. Figure 2.15 shows a section of the periodic table with the group number and VEC listed above the elements. Considering only refractory elements, group four consists of Ti, Zr, Hf and group five consists of V, Nb and Ta. They found that the ideal tensile strength correlated with the composition ratio from the two groups. The strongest alloy ZrVTiNb had a ratio of 2:2 consisting of 2 elements from group four and 2 elements from group five. The alloy with the composition ZrVTiNbHf had a lower ideal tensile strength with a ratio of 3:2. The alloy with the lowest strength had the composition ZrTiNbHf and a ratio was 3:1. The author suggest that a lower composition ratio between those two groups would increase the ideal tensile strength.

	3	4	5	6	7	8	9
Sc	Ti	V	Cr	Mn	Fe	Co	
Y	Zr	Nb	Mo	Tc	Ru	Rh	
*	Hf	Ta	W	Re	Os	Ir	

Figure 2.15: Section of the periodic table containing refractory elements. The group number also stands for the VEC for each column.

Qi and Chrzan studied Mo and W based alloys, finding that the metals becomes intrinsically ductile if the average valence electron numbers are decreased. [68] Intrinsic ductility focuses on the crystal structure of the material which in this case are BCC crystal structures. Their calculations suggests that the alloys tested could be more ductile than pure Mo, as pure Mo are intrinsically brittle.

In a study regarding W-based alloys using first-principle calculations, Hu et al. [69] found that the shear modulus G is correlated with the alloying elements' amount of valence electrons. The composition tested was $W_{53}X$, with X being the alloying element. All alloying elements decreased the shear modulus of BCC W, but Cr and Mo which had the same number of valence electrons did not affect the shear modulus significantly. Using elements with less or more valence electrons than W has a pronounced effect on decreasing the shear modulus.

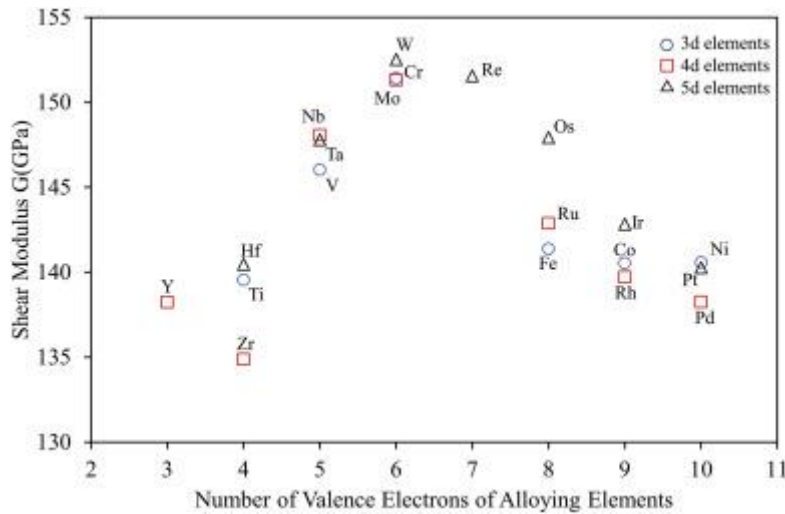


Figure 2.16: Shear moduli of the $W_{53}X$ alloys versus number of valence electrons used in the alloying elements.[69]

By observation, figure 2.16 shows that increasing number of valence electrons of the alloying elements decreases the shear modulus further more. The same conclusion can be drawn for decreasing number of valence electrons of the alloying elements. Alloying W with Y, Zr and Pd have the strongest effect on the shear modulus. This latter result will be the base for the binary refractory alloy research using Mo-X instead of W-X.

3 METHOD

The method sections covers the procedure used for the literature review, the properties map and the experimental work.

3.1 Method for information retrieval

Chalmers Library and Google search engine were the main tools used for collecting information about the basics of HEAs, studies of valence electron concentration related to refractory alloys, properties data of refractory HEAs and simpler refractory alloys. Missing properties data were calculated using the rule of mixtures for properties such as density, melting temperature or hardness value. The hardness value has been taken from a handbook.[70] The mathematical definition is formulated below. The data point is x_i of element i and the weight of each data point is w_i . The data point can be either the density, melting point or hardness value of each element. \bar{x} stands for the mixed value of a calculated property for an alloy.

$$\bar{x} = \frac{\sum_{i=1}^n w_i x_i}{\sum_{i=1}^n w_i} \quad [-] \quad (3)$$

Useful information were collected and cited using Mendeley for easier management during the writing process. The sources were processed through Copyright Clearance Center to receive the rights to use the material.

3.2 Method for experimental work

The method applied during the experimental work are split into three sections: Binary alloys, HEAs and Testing methods, where a more detailed description of the testing procedures will be covered.

3.2.1 Binary alloys

Mo-based binary alloys has been chosen to be experimented with as Mo have a high melting temperature, relatively low density compared with W. Mo belongs to group 6 elements and they are known for being hard to ductilize because of the strong bonds which leads to a high melting temperature. [9] The combinations to be tested will be based on their phase diagrams which gives a clue if the alloys consist of single phase solid solution or not. It is important to find a single phase solid solution in a binary alloy for the desired element which is Mo in this case before experimenting with HEAs. If single phase solid solution cannot be found in the binary alloy's case then it is highly unlikely to find single phase solid solution in the HEA.

Experiments regarding the Mo-based binary alloys will also use the study regarding W-based alloys using first-principle calculations by Hu et al. [69] The result from the study indicates that using Ti and Nb as an alloying element for W-based alloys would decrease the shear modulus which hopefully would increase the ductility. Mo and W belongs to group 6 and elements belonging to the same group usually behave the same. According to the study mentioned earlier, using Y, Zr or Hf as the alloying element would decrease the shear modulus even more than using Ti and Nb but there are other problems to consider. Zr or Hf alloyed with Mo would likely contain secondary phases. The argument is shown in figure 3.1 and 3.2. Both phase diagrams show multiple phases for Mo-Zr and Mo-Hf. Y is highly reactive and unstable at high temperatures which would make it difficult and dangerous to work with. Multiple elements

suggested by the study has be disregarded for experimental work as those elements are unfeasible for usage as they are either expensive, have a high density or not a refractory element.

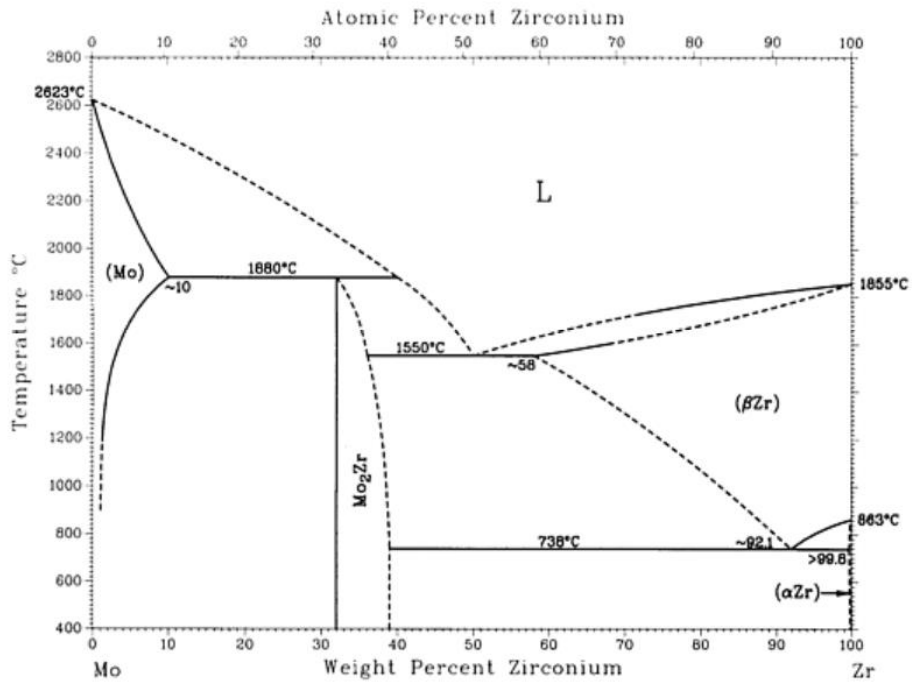


Figure 3.1: Phase diagram of Mo-Zr.[42]

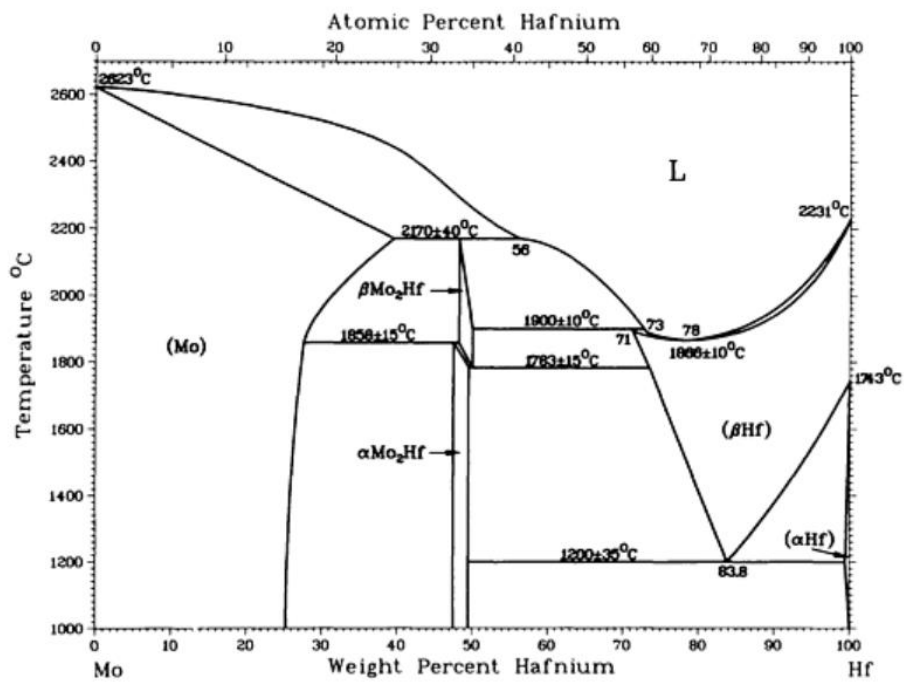


Figure 3.2: Phase diagram of Mo-Hf.[42]

Phase diagrams for Mo-Ti and Mo-Nb are shown in figure 3.3 and 3.4. Both of them indicate single phase solid solution at elevated temperature. Mo-Ti has a miscibility gap which could contain multiple phases when the temperature is lowered but it should mostly consist of β-

phase. It is uncertain if the Mo-Nb will remain single-phased at room temperature as lowest temperature provided in the phase diagram is 2400 °C.

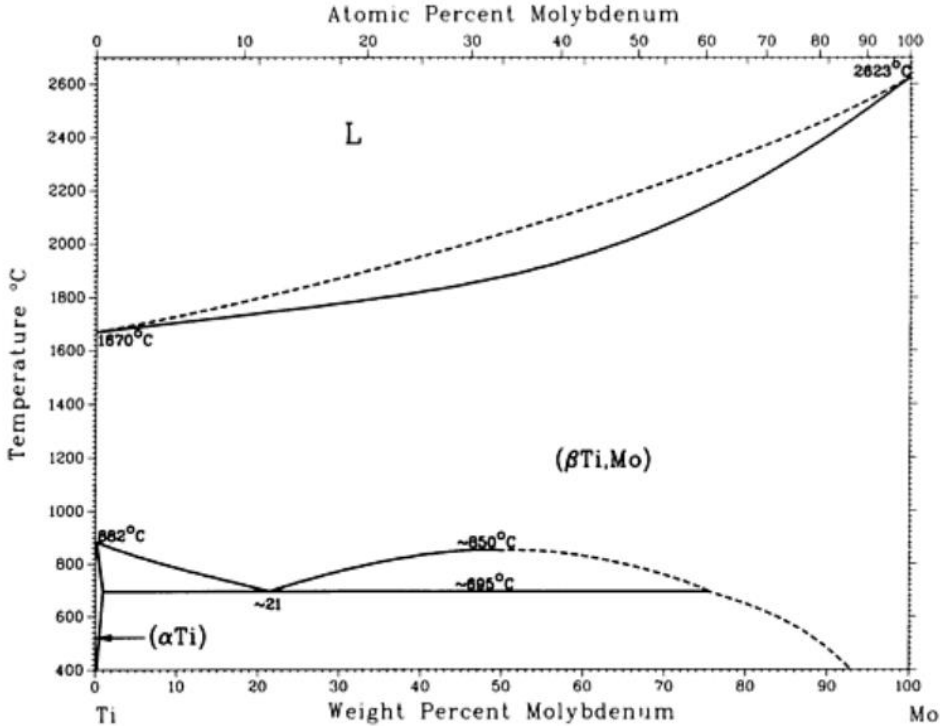


Figure 3.3: Phase diagram of Mo-Ti.[42]

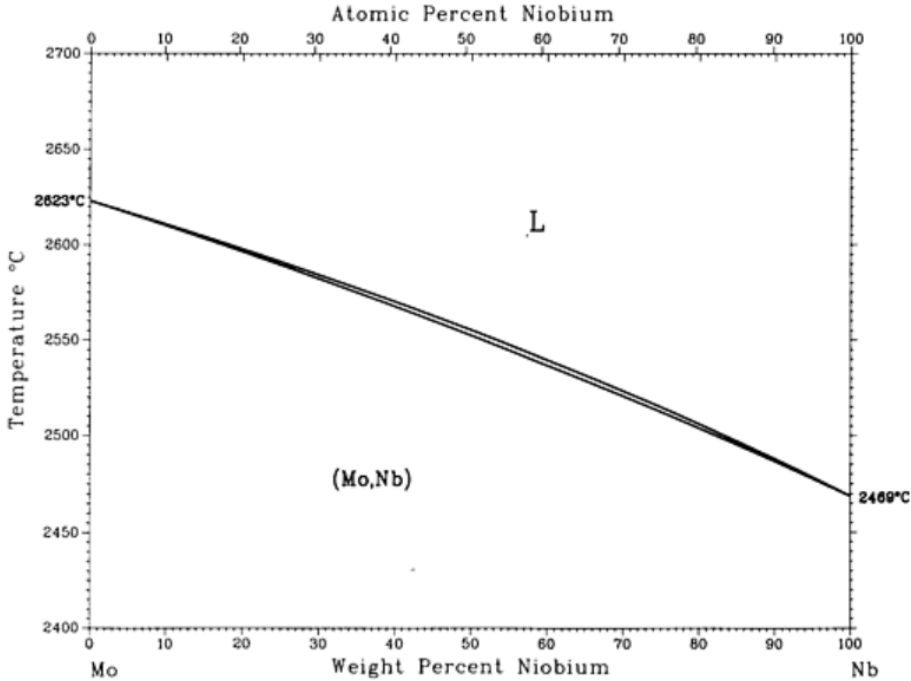


Figure 3.4: Phase diagram of Mo-Nb.[42]

Combinations to be tested are MoTi, Mo_{0.5}Ti, MoNb and Mo_{0.5}Nb. These samples were analyzed with hardness tests to check if the hardness values are in reasonable range (< 400 HV). If the hardness is way too high than the rule of mixture value, then it would indicate the presence

of secondary phases, which in turn possibly make the alloy brittle. All samples were analyzed using XRD to check the phase constitution. Bending tests were performed to roughly estimate the ductility. The result from the binary alloy experiment will help determine the strategy for the refractory HEA.

The chemical compositions with the atomic percent of each element for the four binary alloys are listed below in table 3.1. The calculated weight for each element in each alloy used for the cast samples is also specified in the same table.

Table 3.1: Chemical composition in at.%/gram in of four binary refractory alloys.

Alloy ID/Element	Mo	Nb	Ti
MoTi	50.0/16.679	-	50.0/8.321
Mo_{0.5}Ti	33.3/12.513	-	66.7/12.487
MoNb	50.0/10.161	50.0/9.839	-
Mo_{0.5}Nb	33.3/6.810	66.7/13.190	-

3.2.2 HEAs

Due to the result from the binary alloys experiments with Mo-Nb and Mo-Ti together with Mo-Hf and Mo-Zr phase diagrams, a conclusion has been drawn that a Mo-containing HEA would most likely be brittle due to high VEC or contain secondary phases. Two different HEAs were prepared to show those effects, one for the brittleness and other one for the secondary phases.

HfMoTiVZr in equiatomic ratio with a VEC value of 4.6 was prepared to show that a Mo-containing refractory HEA forms secondary phases with other refractory elements, which affects the ductility of the material. The phase diagrams for Mo-Zr and Mo-Hf shown in figure 3.1 and 3.2 suggests that secondary phases will be formed. The phase identification will be done using x-ray diffraction.

MoNbTaVW was prepared to show that a Mo-containing HEA with single phase BCC is brittle due to not low enough VEC, with the VEC value of 5.4. The neutron diffraction figures indicates that MoNbTaVW is a single phase solution and the result from the compression test suggest that MoNbTaVW should be brittle. [54] The alloy was melted and cut into suitable size for a bending test to show the fracture surface.

Hf_{0.5}Nb_{0.5}Ta_{0.5}TiZr was the refractory HEA to validate the electron theory. With a low VEC of 4.29, it has the possibility of being ductile. The alloy was melted, polished and tested using x-ray diffraction, bending test and Vickers hardness test. The elements used for this alloy does not have a huge atomic radii difference which makes the lattice distortion effect weak. No elements from group 6 is in this composition as they have been proven to form secondary phases with other elements quite easily. A larger part of Ti and Zr were proposed because of their low VEC, a lesser amount of Hf and Ta because their high density. A small part of Nb was also used as the aim is to lower the VEC. The close proximity of these elements on the periodic table helps with lowering the heat of mixing. A more negative heat of mixing between two elements would most likely form compounds.

The phase diagrams for the binary alloys Hf-Nb, Hf-Ta, Hf-Ti, Hf-Zr, Nb-Ta, Nb-Ti, Nb-Zr, Ta-Ti, Ta-Zr and Ti-Zr are shown in figure 3.5, 3.6, 3.7, 3.8, 3.9, 3.10, 3.11, 3.12, 3.13 and 3.14. The ten phase diagrams show all the possible binary combinations among the elements in $\text{Hf}_{0.5}\text{Nb}_{0.5}\text{Ta}_{0.5}\text{TiZr}$. Almost all the phase diagrams indicate a possibility of single phase solid solution between respective elements listed above, but it is very dependent on the composition ratio. Almost half of the binary combinations has the possibility of having multiple phases depending on the ratio. It is also important to note that the high testing temperature in all the phase diagrams, therefore it is uncertain if the alloy will remain a single phase solid solution at room temperature. Even though secondary phases might form for the binary alloys' cases, the high entropy effect may be able to suppress the formation of secondary phases for $\text{Hf}_{0.5}\text{Nb}_{0.5}\text{Ta}_{0.5}\text{TiZr}$. The high entropy effect increases the chance of $\text{Hf}_{0.5}\text{Nb}_{0.5}\text{Ta}_{0.5}\text{TiZr}$ having a single phase solid solution even though the binary phase diagrams might say otherwise.

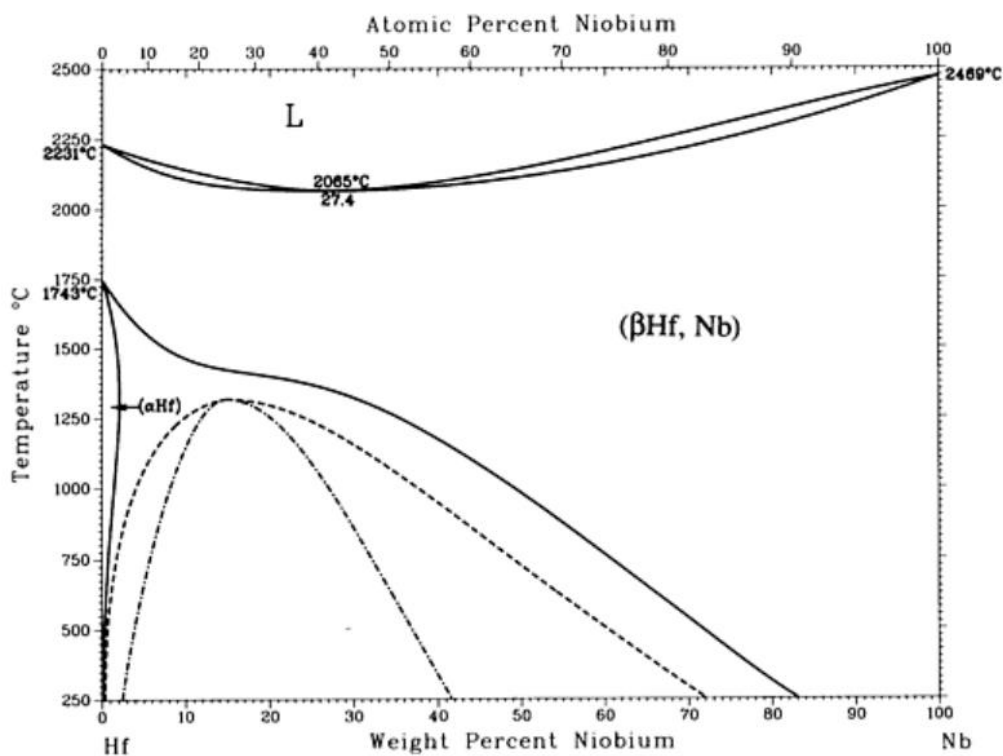


Figure 3.5: Phase diagram of Hf-Nb.[42]

Figure 3.5 shows the phase diagram for the binary alloy Hf-Nb in different composition ratios. The alloy can consist of α -phase, β -phase or with a possibility of a multiple phases depending the amount of Nb.

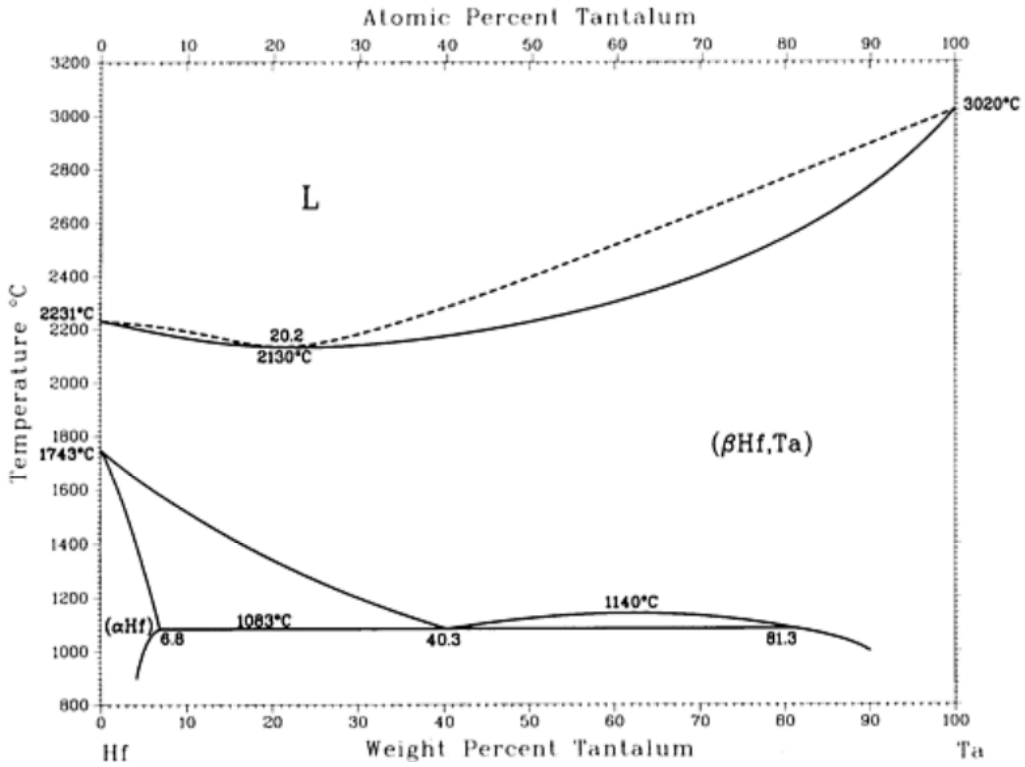


Figure 3.6: Phase diagram of Hf-Ta.[42]

Figure 3.6 shows the phase diagram for the binary alloy Hf-Ta in different composition ratios. The alloy can consist of α -phase, β -phase or multiple phases depending the amount of Ta. The testing temperature is above 800 °C. Result may vary at room temperature.

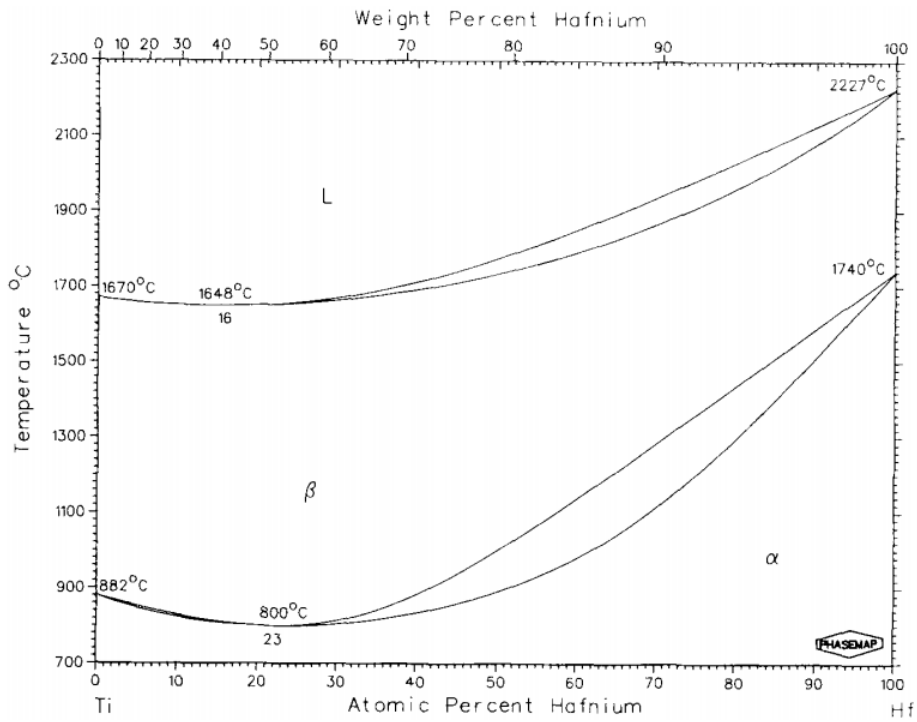


Figure 3.7: Phase diagram of Hf-Ti.[71]

Figure 3.7 shows the phase diagram for the binary alloy Hf-Ti in different composition ratios. The lower part indicates a single phase solid solution consisting of α -phase at an elevated temperature independent of the composition ratio.

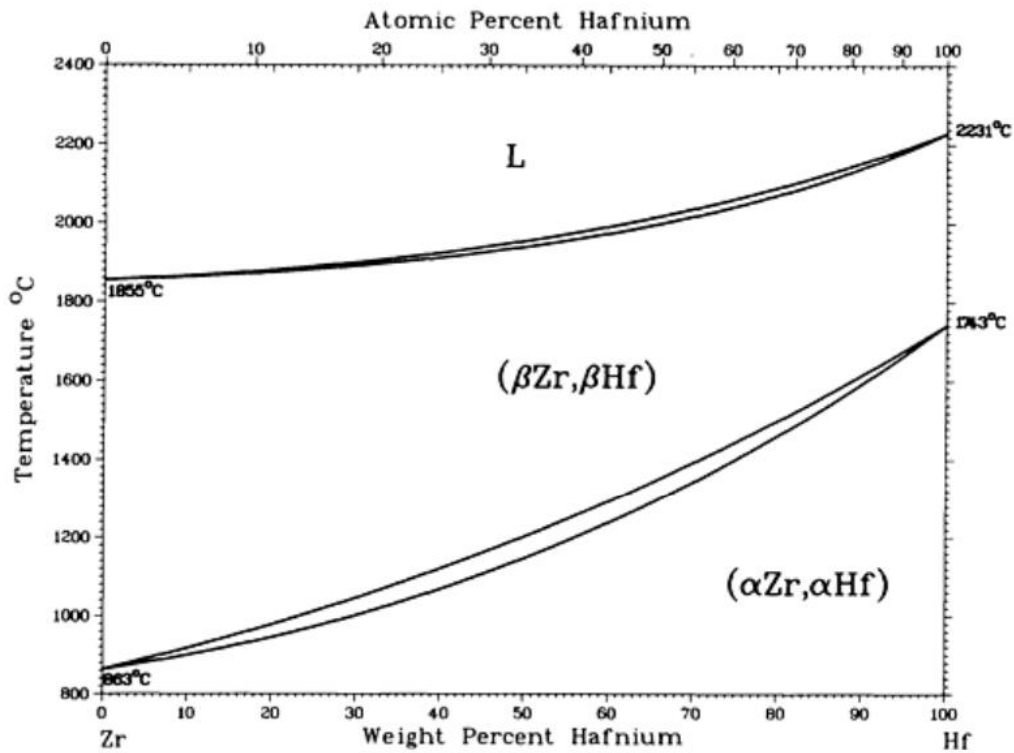


Figure 3.8: Phase diagram of Hf-Zr.[42]

Figure 3.8 shows the phase diagram for the binary alloy Hf-Zr in different composition ratios. The lower part indicates a single phase solid solution consisting of α -phase at an elevated temperature independent of the composition ratio.

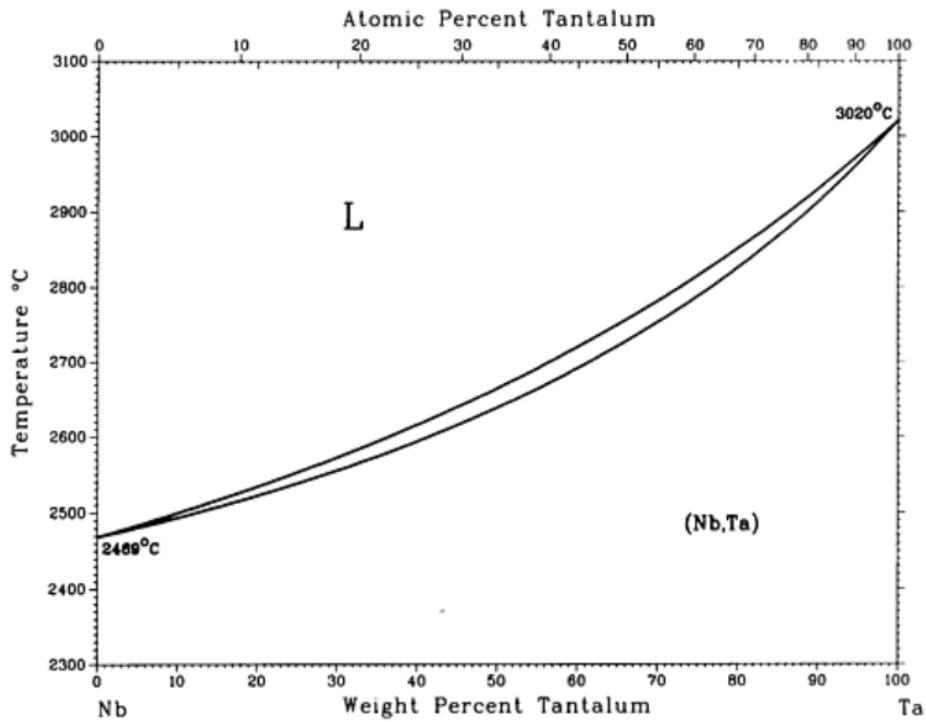


Figure 3.9: Phase diagram of Nb-Ta. [42]

Figure 3.9 shows the phase diagram for the binary alloy Nb-Ta in different composition ratios. The lower part indicates a single phase solid solution at an elevated temperature independent of the composition ratio. Note the high temperature, it is uncertain if the alloy will remain a single phase solid solution at room temperature.

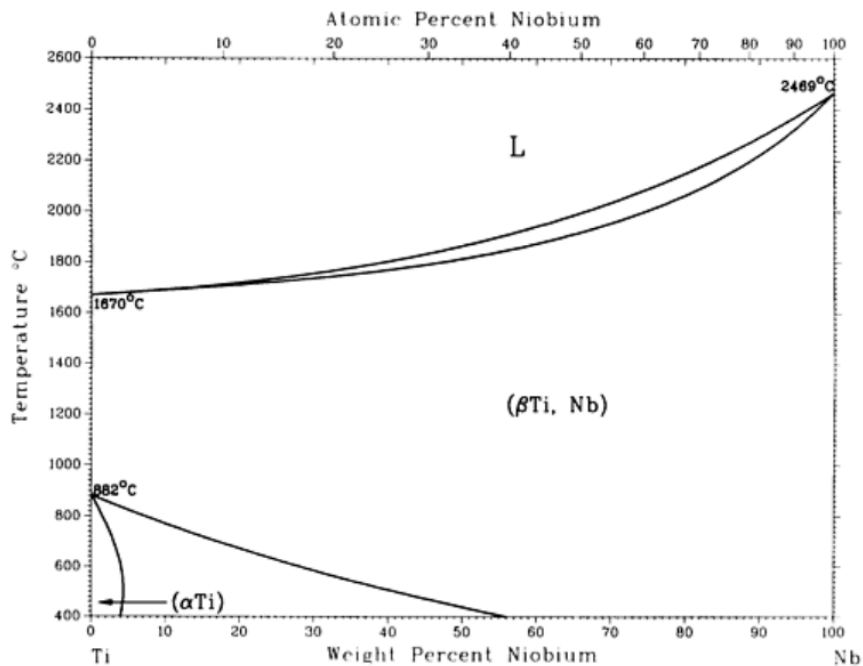


Figure 3.10: Phase diagram of Nb-Ti. [42]

Figure 3.10 shows the phase diagram for the binary alloy Nb-Ti in different composition ratios. The diagram indicates single phase solution that depends on the composition ratio. The phase changes from α -phase to β -phase depending on the ratio.

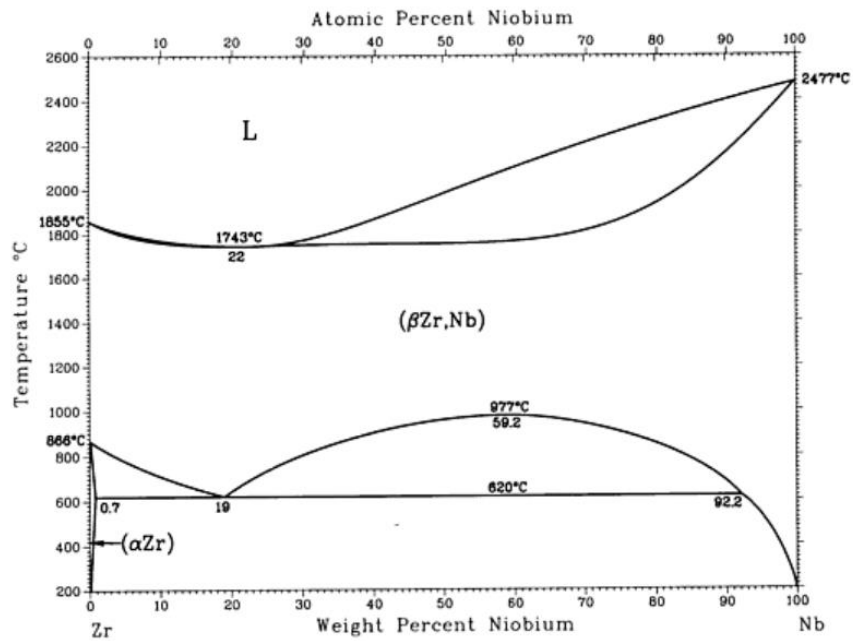


Figure 3.11: Phase diagram of Nb-Zr. [42]

Figure 3.11 shows the phase diagram for the binary alloy Nb-Zr in different composition ratios. The alloy consists mainly of β -phase at elevated temperature. There is a miscibility gap in the β -phase which may introduce multiple phases.

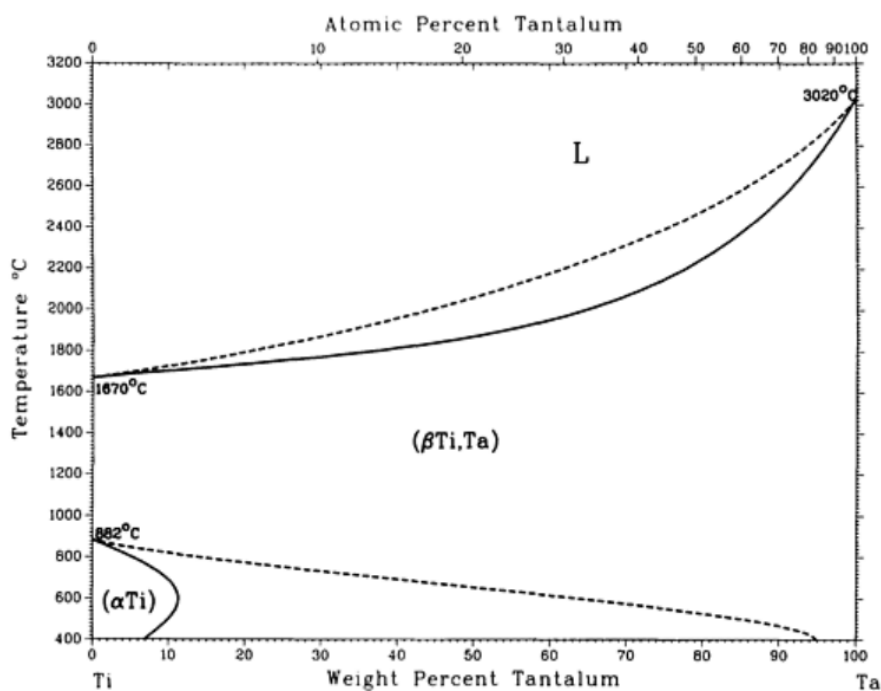


Figure 3.12: Phase diagram of Ta-Ti. [42]

Figure 3.12 shows the phase diagram for the binary alloy Ta-Ti in different composition ratios. The diagram indicates single phase solution that depends on the composition ratio. The phase changes from α -phase to β -phase depending on the ratio.

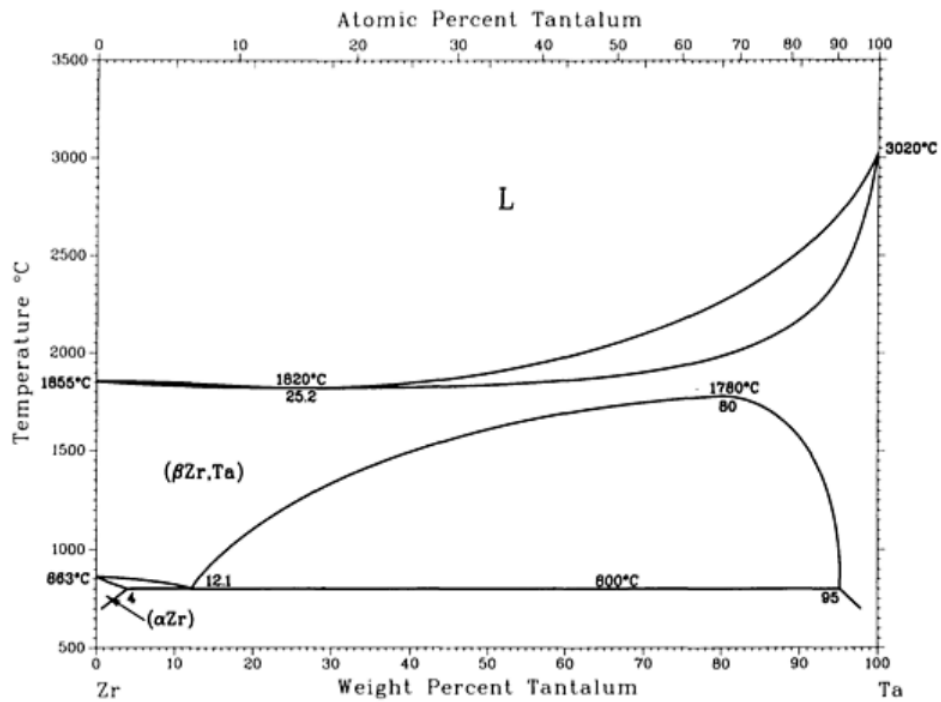


Figure 3.13: Phase diagram of Ta-Zr.[42]

Figure 3.13 shows the phase diagram for the binary alloy Ta-Zr in different composition ratios. There are three stable phases in the Ta-Zr system, liquid, β -phase and α -phase. The β -phase area forms a miscibility gap at temperature below 1780 °C.

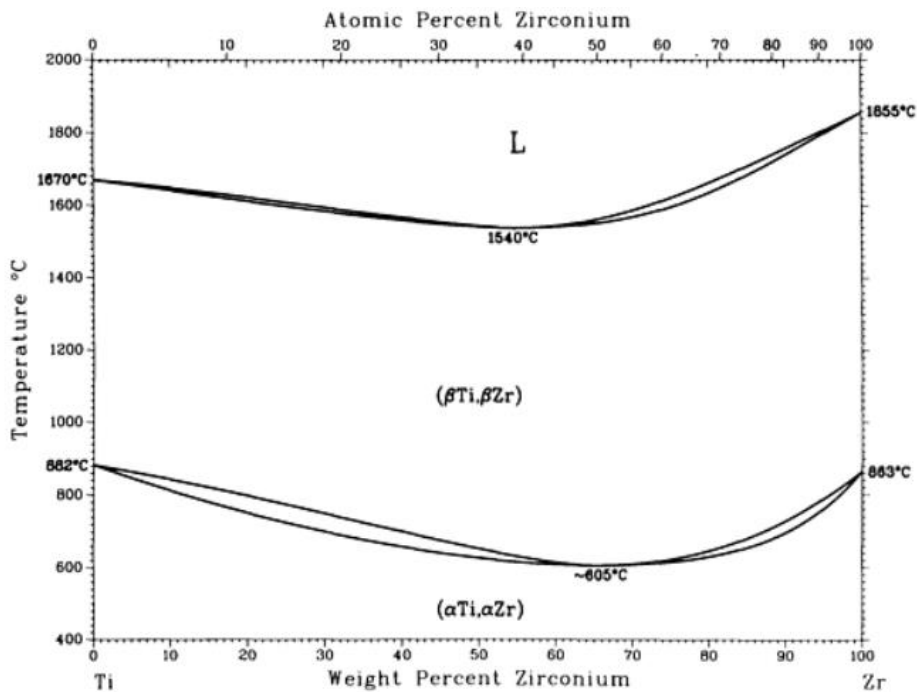


Figure 3.14: Phase diagram of Ti-Zr.[42]

Figure 3.14 shows the phase diagram for the binary alloy Ti-Zr with different composition ratios. The lower part indicates a single phase solid solution consisting of α -phase at a temperature above 400 °C independent of the composition ratio.

Chemical composition for these three refractory HEAs are listed in table 3.2. The calculated weight for each element in each alloy used for the samples is also specified in the same table.

Table 3.2: Chemical composition in at.%/gram in of three refractory HEAs.

Alloy ID/Element	Hf	Mo	Nb	Ta	Ti	V	W	Zr
HfMoTiVZr	20.0/ 13.450	20.0/ 7.230	-	-	20.0/ 3.607	20.0/ 3.839	-	20.0/ 6.874
MoNbTaVW	-	20.0/ 3.967	20.0/ 3.842	20.0/ 7.482	-	20.0/2. 106	20.0/ 7.602	-
Hf_{0.5}Nb_{0.5}Ta_{0.5}TiZr	14.3/ 8.552	-	14.3/ 4.451	14.3/ 8.669	28.6/ 4.587	-	-	28.6/ 8.741

3.2.3 Testing methods

This section covers the procedures used in the different testing, and equipments used during the experiment work.

3.2.3.1 Arc melting

A vacuum arc melting equipment with model Arc Melter AM supplied by Edmund Bühler GmbH is used to melt and mix the elements together. It utilizes a non-consumable tungsten electrode to create an electric arc that passes through the raw material in an evacuated chamber backfilled with argon gas. The arc will heat up the gas and plasma will be created to heat up the material put in a crucible plate. Two different pumps are used for creating vacuum, a rotary pump capable of a pressure of 10^{-2} mbar and a diffusion pump capable of a pressure of 10^{-5} mbar. The vacuum effect cleans the container of debris and removes the air which reduces the risk for oxidation. The mold and plates are made out of copper because of the material's ability to transfer heat quickly, seen in figure 3.15. The copper mold used for this project has got a cross section of 10 by 10 millimeter. The chamber, the crucible plate and the tungsten electrode are water-cooled by an external chiller to prevent them from getting overheated by the heat generated during the melting process.

Conventional melting technologies such as residential furnaces will not work as the melting temperature for refractory metals are very high. Arc Melter AM has the capability to melt samples up to 200 g at temperatures up to 3500 °C. Titanium got a high affinity with oxygen which is why there is a titanium ball in the crucible plate, as seen in figure 3.15. It is melted before melting the target alloys, to getter oxygen in the chamber.



Figure 3.15: Copper mold (left side) used for arc melting and copper plate (right side) with mold inserted, elements added and a titanium ball for oxygen collection.

3.2.3.2 Weighing

It is important to have the right amount of each element to get the desired alloy composition, therefore each element should be weighted carefully before mixing together. Each element has the tolerance of 0.005 gram and the weighting is done using the OHAUS PA214C scale. Although the weighting is carefully done, the elements are not 100% pure and may have a slight amount of impurities. This does not affect the final mixture due to the purity levels are “good enough”. The purity of the element vary from 99.95 % to 99.995 % whereas the most common level of purity is 99.95 %. The pure elements come in different size and shape, and the most common forms are rod and plate. As a result of the original shape, cutting of the element in smaller pieces is necessary in order to get the desired weight of the element. The cutting is done with a manual metal shear.

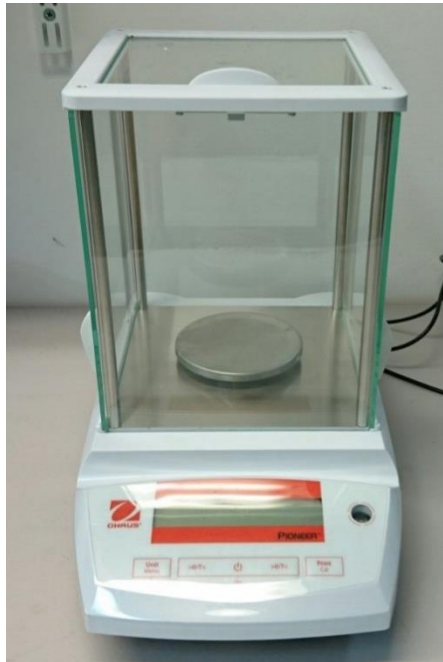


Figure 3.16: Picture of OHAUS PA214C scale.

3.2.3.3 Cutting

The alloy cast in the Arc melting furnace will be bar-shaped. The shape makes it easier to cut the alloy into smaller pieces using the Struers Discotom-2 machine. The reason to cut the sample is to be able to use the same sample for different tests.

The cutting machine has different saw blades to be used depending on the base element of each sample. Since HEAs do not have any base element, this makes the cutting part a bit difficult and leads heat generated the sample. The heat could even destroy the sample and make it unusable as the crystal structure could change because of the heat.

3.2.3.4 Grinding and polishing

Every cut sample was attached to a PolyFast cylinder to ease up the grinding and polishing work. These cylinders are made through adding 20ml of PolyFast powder together with the cut sample into the Struers CitoPress-20 machine. The machine melts the powder and makes a PolyFast cylinder with the sample in it.

Every piece was grinded and polished since a flat and shiny surface is required for further testing. This operation will be done using the Struers Tegrapol-31 machine with used force of 30-40 N for the grinding and 20-30 N for the polishing. Each run will take about 4-5 minutes and the rotating direction is changed between the runs. SiC grinding papers are used for the grinding part. The roughness of the grinding papers has the grit size of ISO P240, P500, P800, P1200, and P2000. For the final polishing, discs with the different particle size of 9 μ m, 3 μ m and 1 μ m was used together with DiaPro which is an abrasive solution to get a finely polished surface.

3.2.3.5 Hardness test

Wolpert DIA Testor 2RC was used to test the Vickers hardness of the alloys. The weight used will be 1 kg held for 15 seconds and the indenter was a pyramidal diamond. A total of 7 or 8 indents was done for each sample. These indents were analyzed through a microscope called Leica Leitz DMRX. The Vickers hardness values were measured and calculated with

AxioVision V 4.8.2.0 and Microsoft Excel. The Vickers hardness was determined by the simplified equation (4).[72] HV is the Vickers hardness, F (N) is the force (Kg) from the indenter, A is the area of the indenter and lastly d (mm) is the average length of the diagonals of the indentation.

$$HV = \frac{F}{A} \approx \frac{0.01819F}{d^2} \quad (4)$$

All samples were ground and polished before the hardness test, and the method was described in the previous section.



Figure 3.17: Picture of Wolpert DIA Testor 2RC.

3.2.3.6 X-ray diffraction

Supervisor Saad Shiekh operated the x-ray diffraction machine called Bruker AXS D8 Advance to analyze the crystal structure of the tested alloys. XRD machines projects a beam of x-ray radiation at a rotating object in which the object's atoms will scatter the incoming waves of x-ray which is called elastic scattering. The object will diffract if the beam's wavelength λ , angle θ and the distance between the lattice planes d fulfills Bragg's law, given in equation (5).

$$2d\sin\theta = n\lambda \quad [-] \quad (5)$$

The diffraction pattern helps with phase identification which can be used to identify the crystal structure, such as FCC crystal structure, BCC crystal structure and other different phases. The diffraction patterns were analyzed through a database to help determine the crystal structure. The result was presented in form of a graph with the y axis as "a.u." and the x axis as 2θ . "a.u." stands for arbitrary unit which is a relative unit of measurement to show the ratio of intensity which in this case is counts per second (CPS), as it counts the number of pulses that happens when the sample diffracts.



Figure 3.18: Picture of Bruker AXS D8 Advance.

3.2.3.7 Bending test

A bending test was conducted by hand. Bending a thin part of the sample could roughly tell if the sample is brittle or ductile depending on if it breaks off or bends to some degree. The fracture surface will also tell if it is brittle fracture or a ductile fracture.

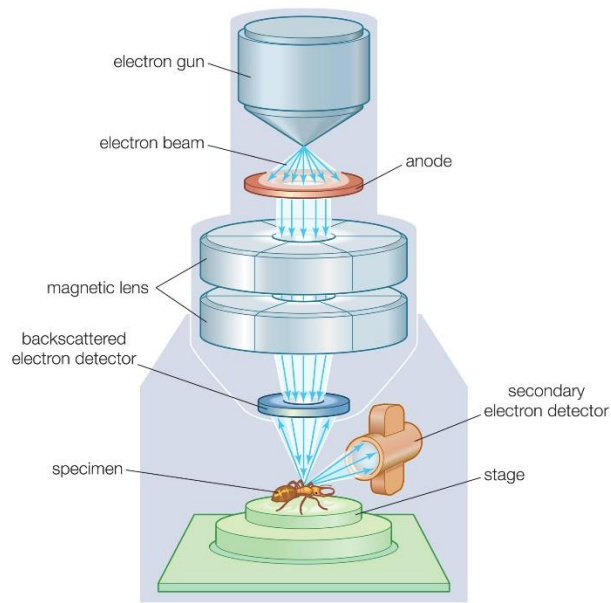
To analyze the ductility furthermore a small rectangular piece is cut from the sample using the Buehler Isomet 2000 machine and bent in the same way as mentioned above. This rectangular sample makes it easier to see the fracture surface.

3.2.3.8 Metallography analysis

Before performing the metallography analysis, the samples need to be prepared by grinding and polishing described in section 3.2.3.4. This method was used for identifying the microstructure of the samples. Etchant used consists of 45 parts of H_2O , 5 parts of Hf and 1.5 parts of HNO_3 , and the exact etchant used depends on the chemical composition of the sample. By controlling the time the sample spends in the etchant, it is possible to reveal the boundaries and the structure, which are visible through a normal microscopy.

3.2.3.9 SEM

As a few samples showed to be brittle, further analysis of the fracture area had to be done using the scanning electron microscope (SEM). The SEM is as the name says an electron microscope that uses electrons instead of light. The electrons sent by the SEM on the sample interact with its surface and reflects back and creates a picture of the sample on a TV or display. The main reason to use SEM over a traditional microscope is that SEM allows more parts of the sample to be in focus at once due to its large field of depth, and this also leads to a better resolution of the image of the sample. The better resolution compared with traditional microscope is due the much shorter wavelength of electrons, than that of the visible light. The SEM allows the operator to have more control of the magnifying scale, focus, brightness, contrast etc. These advantages makes the SEM the primary choice for a clear picture of the sample. [73]



© 2012 Encyclopædia Britannica, Inc.

Figure 3.19: The construction of a SEM[73]

4 RESULTS

The results section covers the properties for refractory HEAs and simpler refractory alloys found during the research phase and the testing data achieved during the experimental work.

4.1 Properties map of refractory alloys

Mapping out the current status of refractory alloys showed that there is still a need for ductile refractory HEAs. The figures and the interpretation of them will strengthen the reason to identify ductile refractory HEAs.

Following figure shows the yield strength (MPa) versus the fracture strain (%) at room temperature for all the collected materials. The circular markers represent refractory HEAs while the square markers represent simpler refractory alloys, and these markers have their own color which corresponds to a specific alloy. Note that there is one HEAs missing yield strength data as it was too brittle at room temperature, more precisely, NbMoCrTiAl. All refractory HEAs collected were tested through compression while simpler refractory alloys were tensile tested. The figure illustrates clearly that simpler refractory alloys have a higher fracture strain than refractory HEAs, even though tensile tests usually results in a lower fracture strain than through compression testing. There are three outliers for refractory HEAs which are NbTiVZr, NbTiV₂Zr and HfNbTaTiZr. One of them are masked in by another in the figure as their yield strength are very close to each other. NbTiVZr and NbTiV₂Zr have a mutual problem, as they become relatively weak at high temperatures, with a yield strength of 187 MPa respectively 240 MPa at 800 °C. HfNbTaTiZr has moderate high temperature strength when compared with other refractory HEAs. The compression yield strength is 535 MPa at 800 °C, 295 MPa at 1000 °C and drops down to 92 MPa at 1200 °C.

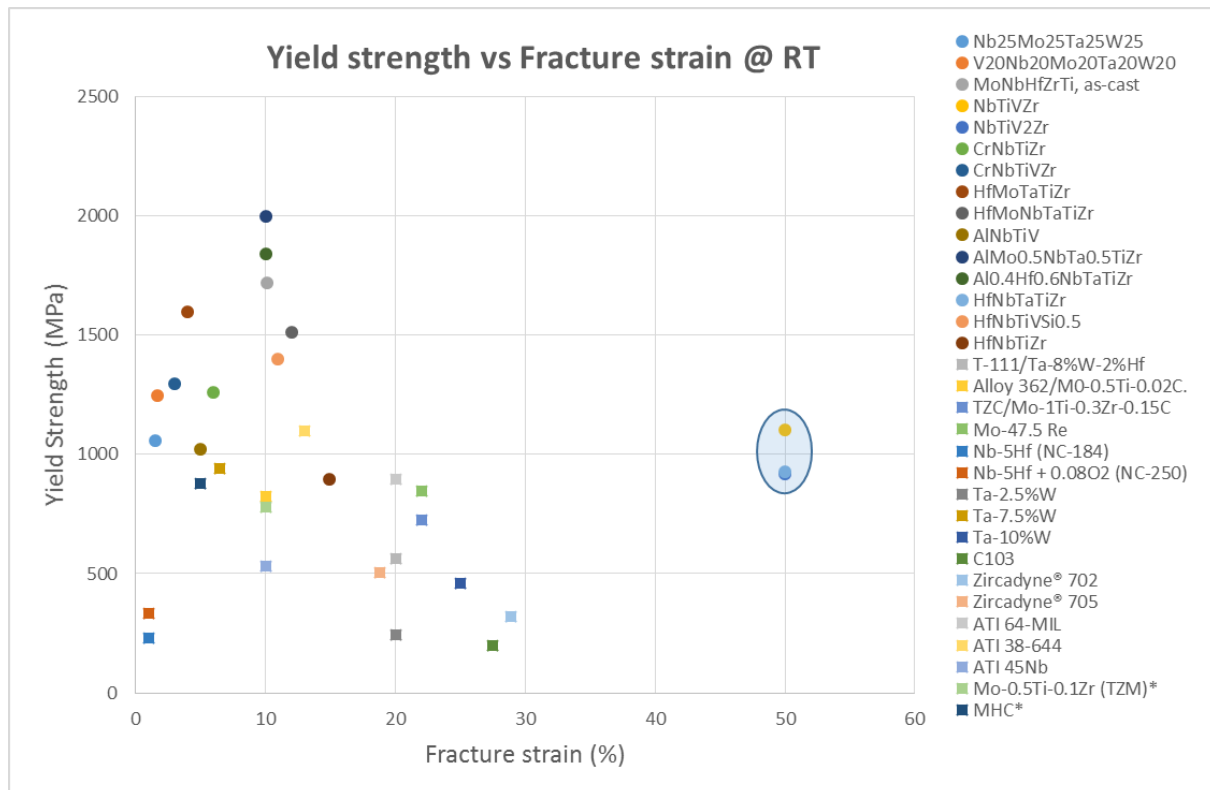


Figure 4.1: Yield strength versus Fracture strain for the collected materials.

To analyze the melting temperature versus the density of simpler refractory alloys and refractory HEAs, a table of the properties was made. These values were later used in the making of a comparison graph to further understand the connection between the density and the melting point for different refractory alloys.

The density measured in (g/cm^3) were gathered on the table and they are mostly taken directly from the source of each alloy where it was reported, although some of the gathered alloys had to be calculated separately due to no data was presented from the source. The melting point temperatures however were calculated using the rule of mixture in Kelvin for all alloys presented on table 4.1.

Table 4.1: Density and melting points values for collected refractory alloys.

Alloy/properties	Density (g/cm ³)	Melting point (K)
Alloy 362/Mo-0.5Ti-0.02C.	10.2 [35]	2883
ATI 38-644	4.82 [74]	1875
ATI 45Nb	5.7[53]	2173
ATI 64-MIL	4.47[75]	1866
C103	8.85[30]	2623
MHC*	9.1[34]	2892
Mo-0.5Ti-0.1Zr (TZM)*	10.16[34]	2893
Mo-47.5 Re	13.5[37]	2723
Nb-5Hf (NC-184)	8.7*	2737
Nb-5Hf + 0.08O ₂ (NC-250)	8.7*	2737
T-111/Ta-8%W-2%Hf	16.83*	3284
Ta-10%W	16.9*	3308
Ta-2.5%W	16.7[44]	3269
Ta-7.5%W	16.8*	3297
TZC/Mo-1Ti-0.3Zr-0.15C	10.1[35]	2873
Zircadyne® 702	6.51[76]	2125
Zircadyne® 705	6.64[76]	2112
Al _{0.4} Hf _{0.6} NbTaTiZr	9.05[64]	2397
AlMo _{0.5} NbTa _{0.5} TiZr	7.4[64]	1982
AlNbTiV	5.59[63]	1920
CrNbTiVZr	6.57[57]	2232
CrNbTiZr	6.67[57]	2262
HfMoNbTaTiZr	9.97[59]	2582
HfMoTaTiZr	10.24[59]	2548
HfNbTaTiZr	9.94[58]	2523
HfNbTiVSi _{0.5}	8.6[65]	2266
HfNbTiZr	8.22*	2058
MoNbHfZrTi, as-cast	8.64*	2444
Nb ₂₅ Mo ₂₅ Ta ₂₅ W ₂₅	13.75*	3177
NbMoCrTiAl	6.17*	2089
NbTiV ₂ Zr	6.32[57]	2245
NbTiVZr	6.52[57]	2258
V ₂₀ Nb ₂₀ Mo ₂₀ Ta ₂₀ W ₂₀	12.36*	2946

*Calculated values using rule of mixture, otherwise specified by source.

Figure 4.2 shows the melting temperature (K) and the density (g/cm³) for each alloy. The data were taken from table 4.1. The circular markers represent refractory HEAs while the square markers represent simpler refractory alloys, and these markers have their own color which corresponds to a specific alloy. A higher density correlated with a higher melting temperature. Thus, making an alloy with great high temperature properties would usually result in a heavy alloy. Steel is commonly used in structural applications, and a refractory alloy with a density lower than steel's density of around 7.85 g/cm³ would be considered as a low density alloy.[24] A comparison with another common structural material such as aluminum would be unrealistic for refractory alloys as no refractory elements are close to aluminum's low density of 2.7 g/cm³.

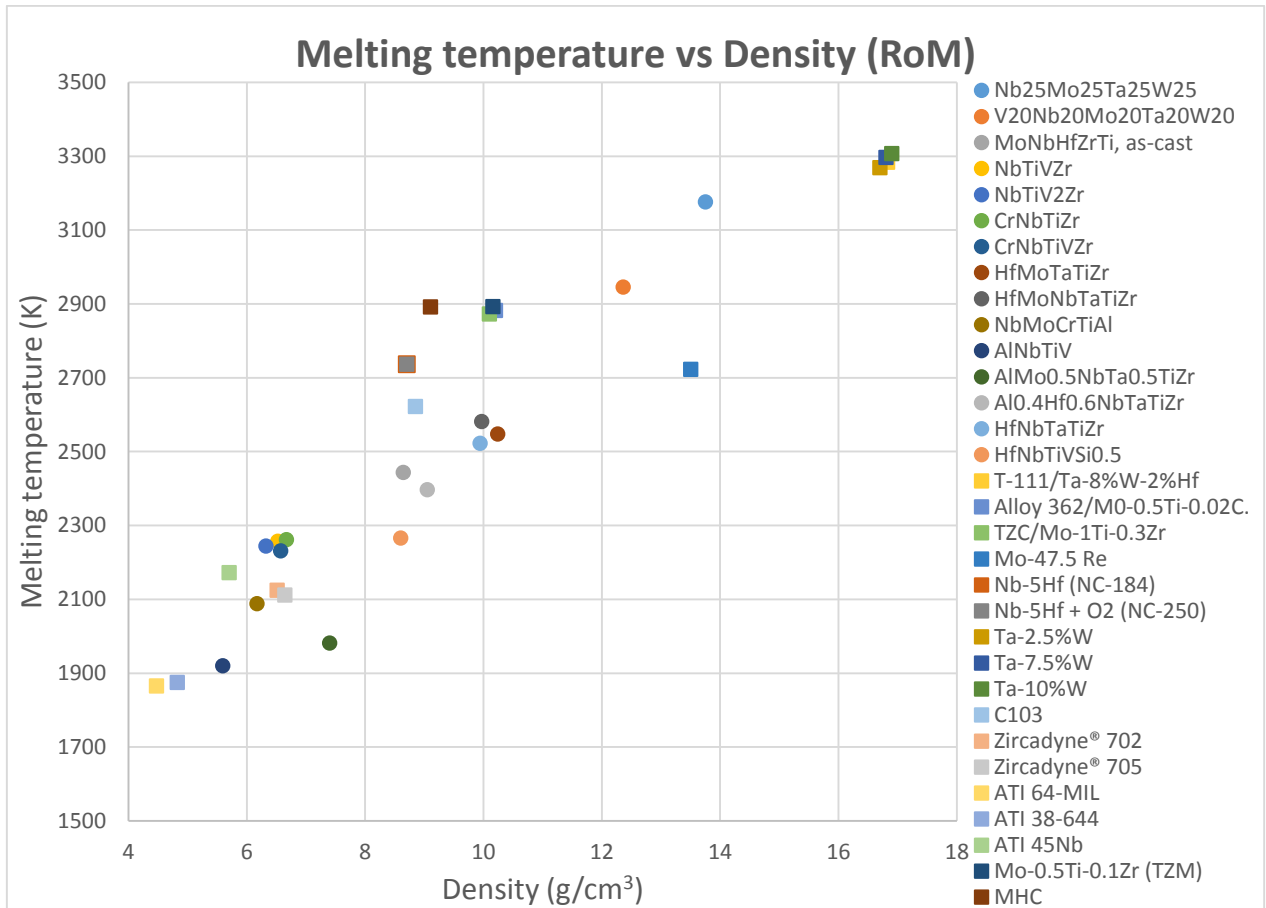


Figure 4.2: Melting temperature versus Density for the collected materials.

The most common testing temperatures found among the research papers for refractory HEAs were room temperature, 800 °C and 1000 °C. That is why figure 4.3 and figure 4.4 show the yield strength versus fracture strain at 800 °C respectively 1000 °C. While simpler refractory alloys had different testing temperatures because of different testing standards or Fahrenheit based testing temperatures were used. For example, 1000 °F translates to roughly 538 °C.

Figure 4.3 shows the yield strength (MPa) vs fracture strain (%) graph with a higher testing temperature of 800 °C for simpler refractory alloys and refractory HEAs. The circular markers represent refractory HEAs while the square markers represent simpler refractory alloys, and these markers have their own color which corresponds to a specific alloy. One simpler refractory alloy, C103, is tensile tested around 800 °C, and the rest of the simpler refractory alloys have missing data regarding fracture strain above room temperature and most of them are not even tested at higher temperatures. C103 has a much lower yield strength than rest of the materials shown. It illustrates that refractory HEAs soften at high temperatures and become ductile, but still maintain higher strength compared with simpler refractory alloys. A majority of them have a reported fracture strain of 50 %, as most researchers tend to stop the test at that point.

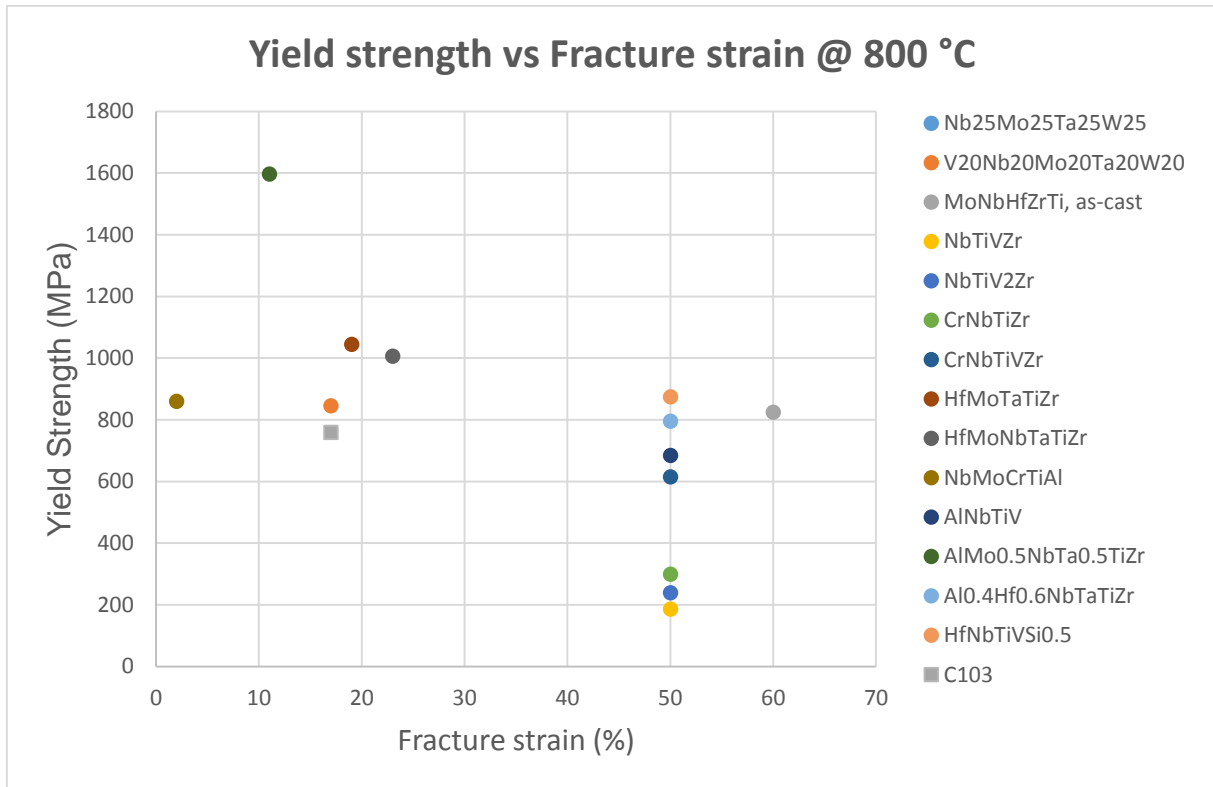


Figure 4.3: Yield strength versus Fracture strain at 800 °C for the collected materials.

Figure 4.4 shows the yield strength (MPa) vs fracture strain (%) graph with a higher testing temperature of 1000 °C for simpler refractory alloys and refractory HEAs. The circular markers represent refractory HEAs while the square markers represents simpler refractory alloys, and these markers have their own color which corresponds to a specific alloy. Once again, it is just one simpler refractory alloy visible, T-111/Ta-8%W-2%Hf. T-111 possess much lower yield strength and fracture strain compared with the refractory HEAs tested at the same temperature. A few simpler refractory alloys are missing from the figure as the fracture strain data for this specific temperature is missing. As before, most of the refractory HEAs have a reported fracture strain of 50 % as most researchers tend to stop the test at that point. There is a clear trend of increasing fracture strain and decreasing yield strength when the temperature is increased.

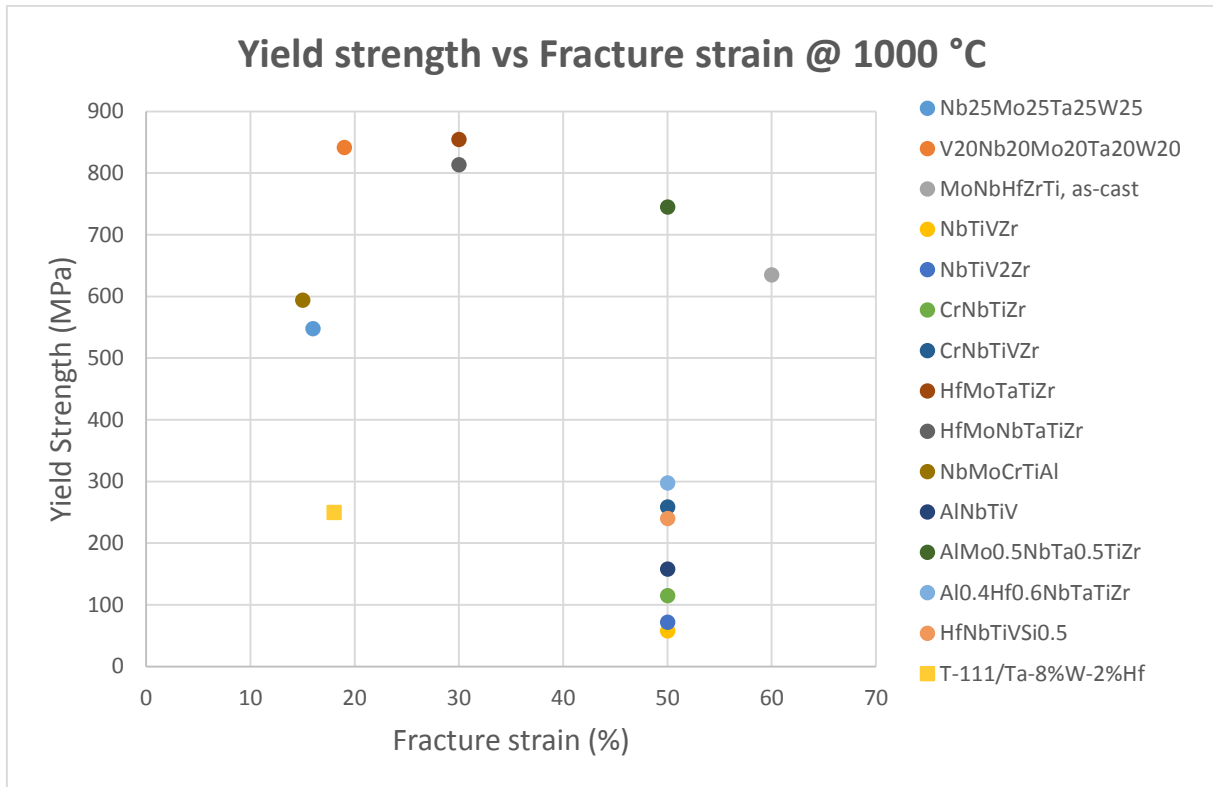
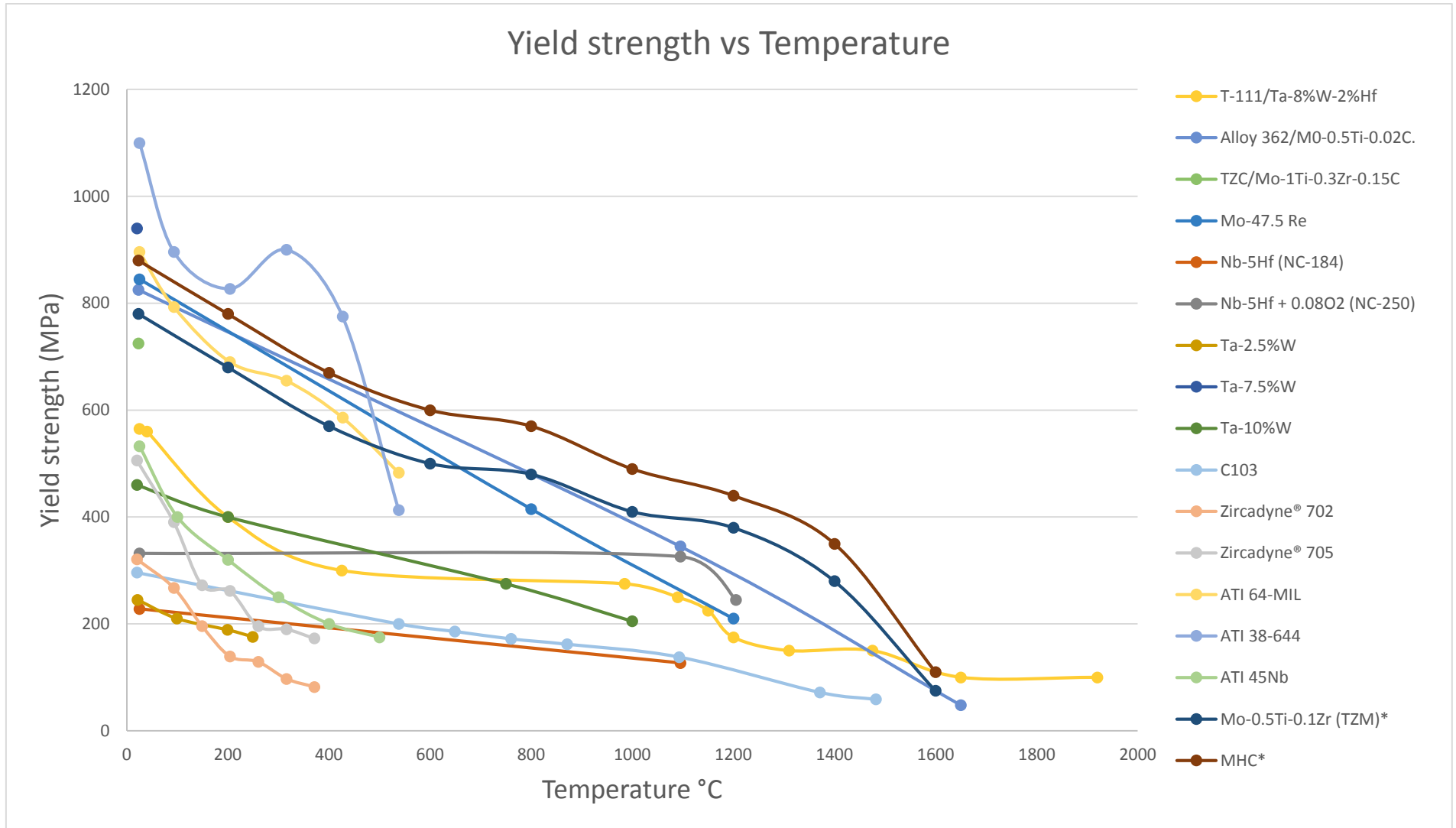


Figure 4.4: Yield strength versus Fracture strain at 1000 °C for the collected materials.

Figure 4.5 and 4.6 show yield strength versus temperature for simpler refractory alloys and HEAs respectively. In a comparison between these two groups it is easy to observe that HEAs as a group is much stronger than simpler refractory alloys at high temperatures, although in some cases two groups overlap with each other, as some of the simpler refractory alloys could reach yield strength values above 400 MPa at temperatures around 1000 °C like the TZM and the MHC alloys. For the HEAs as a group, yield strength values well above 500 MPa at 1000 °C could be seen as something usual and not something that stands out as for the case of the TZM and MHC alloys. At room temperatures, HEAs are clearly the better group and the obvious choice although there is one good competitor from the simpler refractory alloys which is the ATI 38-644, a Ti based alloy with yield strength value of 1100 MPa at room temperature. At temperatures higher than 1000 °C most of the simpler refractory alloys drop their strength whilst the HEAs keep have yield strength above 400 MPa even at as high temperatures as 1600 °C whilst the earlier mentioned alloys, TZM and MHC drops to 75 and 110 MPa respectively. The T-111 alloy from the simpler refractory group however seems to have yield strength of 100 MPa at temperatures as high as 1920 °C, which could be seen as an excellent property for the alloy.

The data presented in the figures of this section are collected from the theoretical frame section and put together on a big table which can be found in Appendix 1.



*0.2 proof stress

Figure 4.5: Yield strength versus Temperature for simpler refractory alloys.

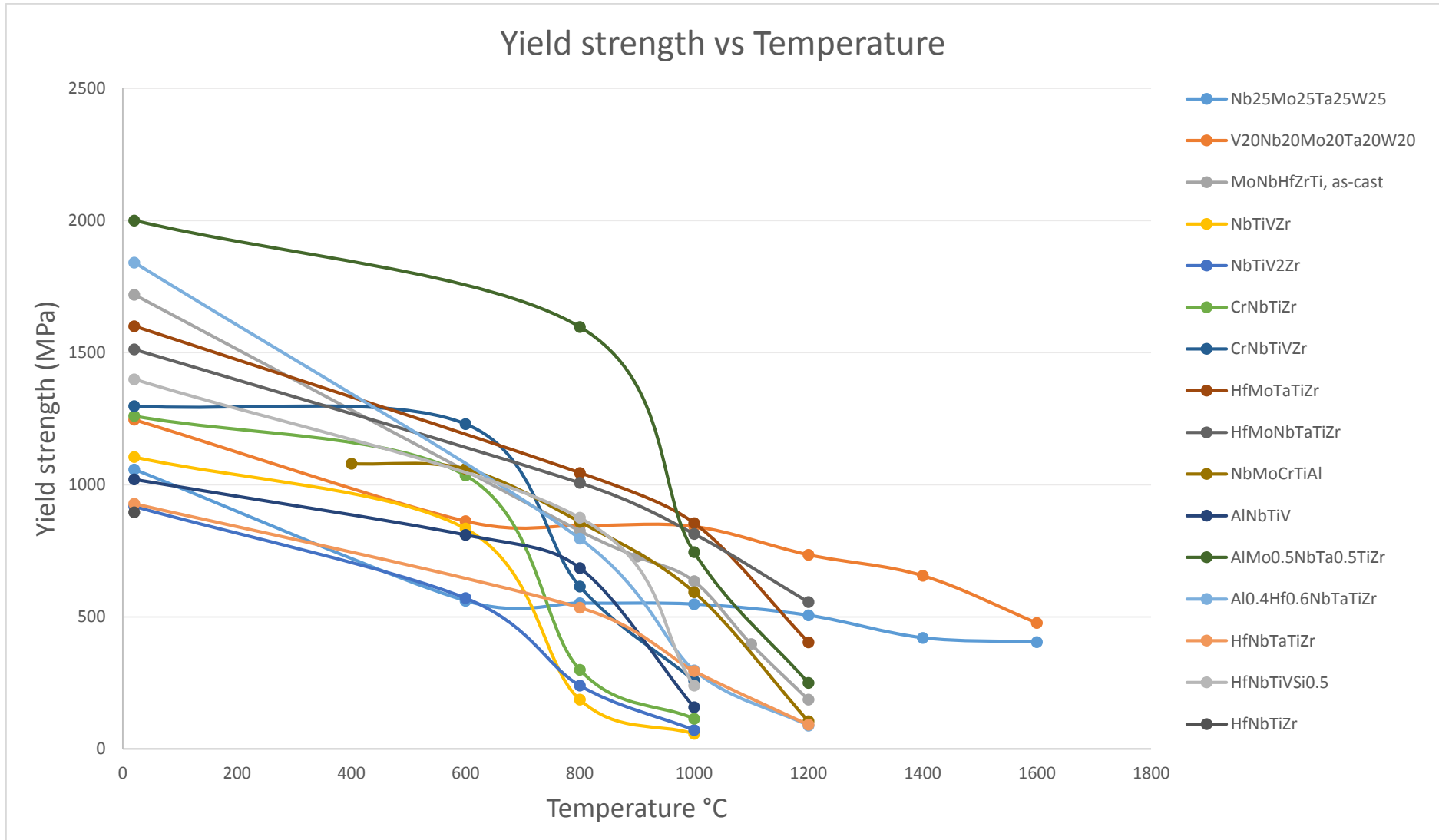


Figure 4.6: Yield strength versus temperature for refractory HEAs.

4.2 Experimental results

The testing results from the experimental work are divided into two sections, the binary alloys section and the HEAs section.

4.2.1 Result for binary alloys

Four different Mo-based binary alloys were prepared, and the tested Vickers hardness values are listed below on table 4.3. The individual hardness measurements are listed in table 4.2. Seven to eight indents were made for each sample. The Vickers hardness values are the mean value taken from the individual measured hardness values.

Table 4.2: Individual measurements of Vickers hardness values of MoTi, Mo_{0.5}Ti and MoNb, Mo_{0.5}Nb.

Composition	Individual measurements (HV)							
Mo _{0.5} Nb	439	421	435	416	431	408	420	
MoNb	493	513	502	484	509	498	521	
MoTi	356	361	359	361	355	377	373	369
Mo _{0.5} Ti	310	317	300	316	302	311	301	302

Table 4.3: Vickers hardness values, calculated Vickers hardness, standard deviation and VEC values of MoTi, Mo_{0.5}Ti, MoNb and Mo_{0.5}Nb.

Composition	VEC	RoM hardness (HV)	Vickers hardness (HV)	Standard deviation
Mo _{0.5} Nb	5.33	142	424	10,2
MoNb	5.5	146	503	11,5
MoTi	5	128	364	7,6
Mo _{0.5} Ti	4.67	118	307	6,5

Mo_{0.5}Nb and MoNb have Vickers hardness values of 424 and 503. These values are very high compared with the calculated Vickers hardness of 142 and 146. The increased hardness from alloying can be attributed to the strong bonds made by Mo and Nb. It also could indicate presence of secondary phases on both alloys. The x-ray diffraction analysis shown in figure 4.7 depicts Mo_{0.5}Nb in red and MoNb in black. For Mo_{0.5}Nb, the last peak at 2theta around 120 degree has a shoulder which is an indication of secondary phases in the alloy. Each peak is a fulfillment of Bragg's law, as given in equation 5. The intensity (a.u.) is on the y axis and the angle 2θ is on the x axis which describes the angle between the incident rays and the surface of the sample. The characteristics of a BCC crystal structure is marked with *I* on top of the three peaks in the figure. The small peak present in both Mo-Nb alloys at 2theta around 55 degree is identified as k-beta emission line. Both Mo_{0.5}Nb and MoNb alloys have a BCC crystal structure with indications of secondary phases.

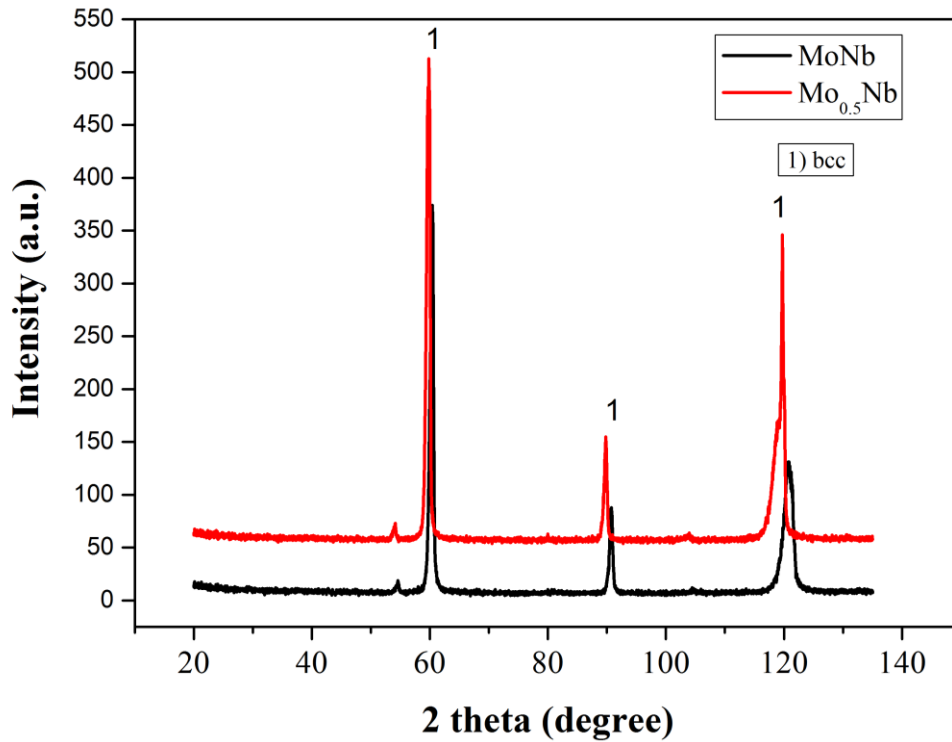


Figure 4.7: X-ray diffraction for Mo_{0.5}Nb and MoNb.

MoTi and Mo_{0.5}Ti have reasonable Vickers hardness values of 364 and 307 as the calculated hardness is 118 and 128. The results from x-ray diffraction shown in figure 4.8 verified that both compositions consists of BCC crystal structure. Mo_{0.5}Ti is the red line and MoTi is the black line. MoTi has a small at 2theta around 55 degree, also identified as k-beta emission line. The characteristics of a BCC crystal structure is marked with 1 in the figure.

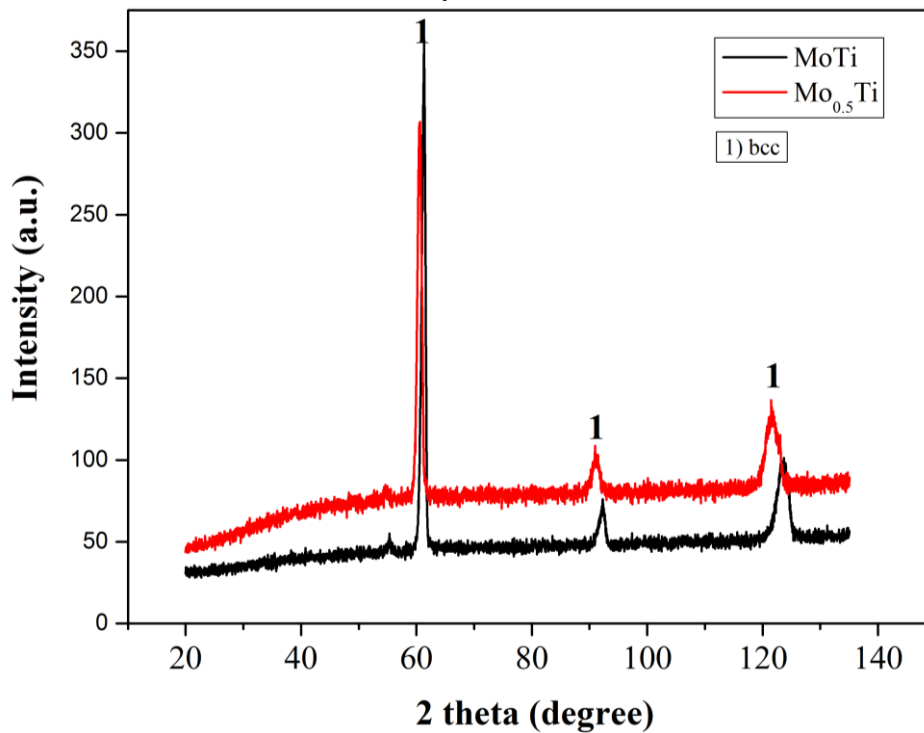


Figure 4.8: X-ray diffraction for Mo_{0.5}Ti and MoTi.

The bending results for MoTi and MoNb are shown in figure 4.9 and 4.10. Both alloys fractured immediately after slight bending. No sign of ductility is shown. $\text{Mo}_{0.5}\text{Ti}$ and $\text{Mo}_{0.5}\text{Nb}$ were not tested and SEM tests were not performed on any binary alloy samples because of the clear bending results. Both alloys shows no sign of plastic deformation.

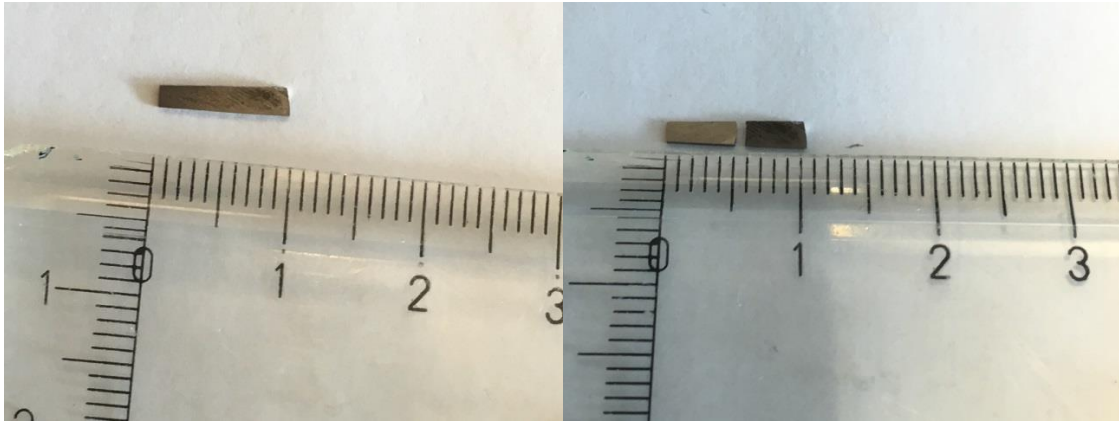


Figure 4.9: MoTi before (left) and after (right) the bending test.

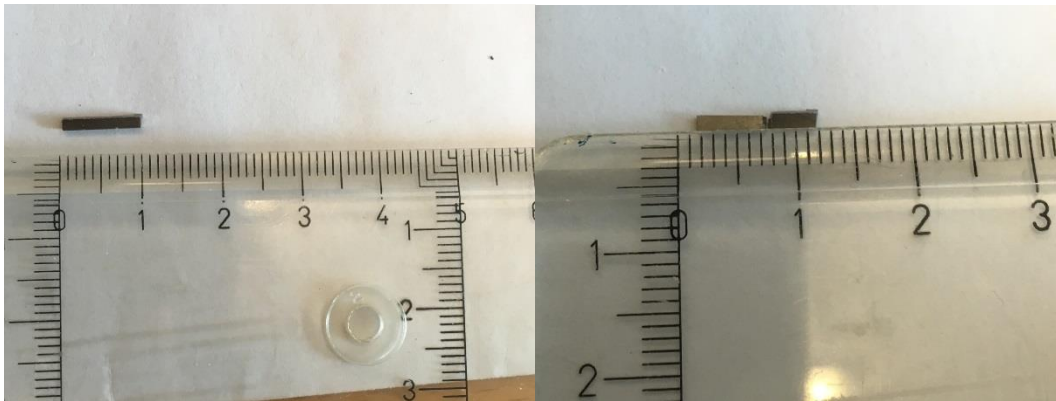


Figure 4.10: MoNb before (left) and after (right) the bending test.

4.2.2 Result for HEAs

The x-ray diffraction result for equiatomic HfMoTiVZr is shown in figure 4.11. The XRD shows that HfMoTiVZr contains a mix of FCC and BCC phases. Peaks marked with 1 in the figure are for the FCC phase and 2 are for the BCC phase. The FCC phase corresponds to $\text{Mo}_2\text{Zr}_{0.9}$, and the BCC phase corresponds to $\text{Hf}_{0.6}\text{Mo}_{0.4}$. Hardness measurement and bending test for this refractory HEA was not performed as the sample broke into multiple pieces already during the cutting process which clearly indicates brittleness.

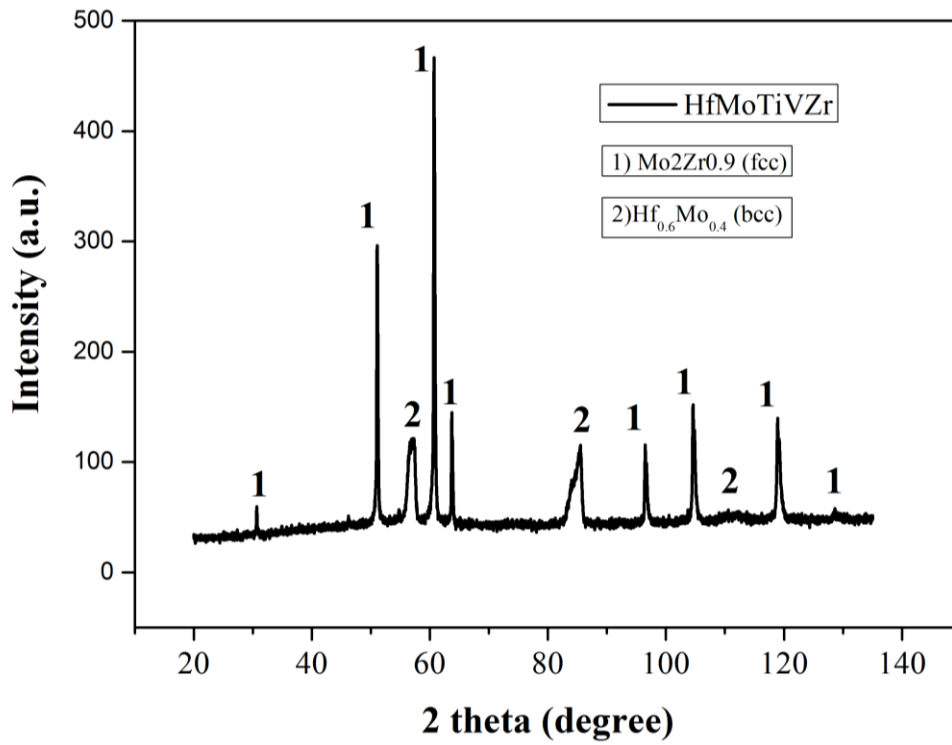


Figure 4.11: X-ray diffraction of refractory HEA HfMoTiVZr.

A bending test was performed for equiatomic refractory HEA MoNbTaVW. The SEM images of the fracture surface in different magnifications are shown in figures 4.12 and 4.13.

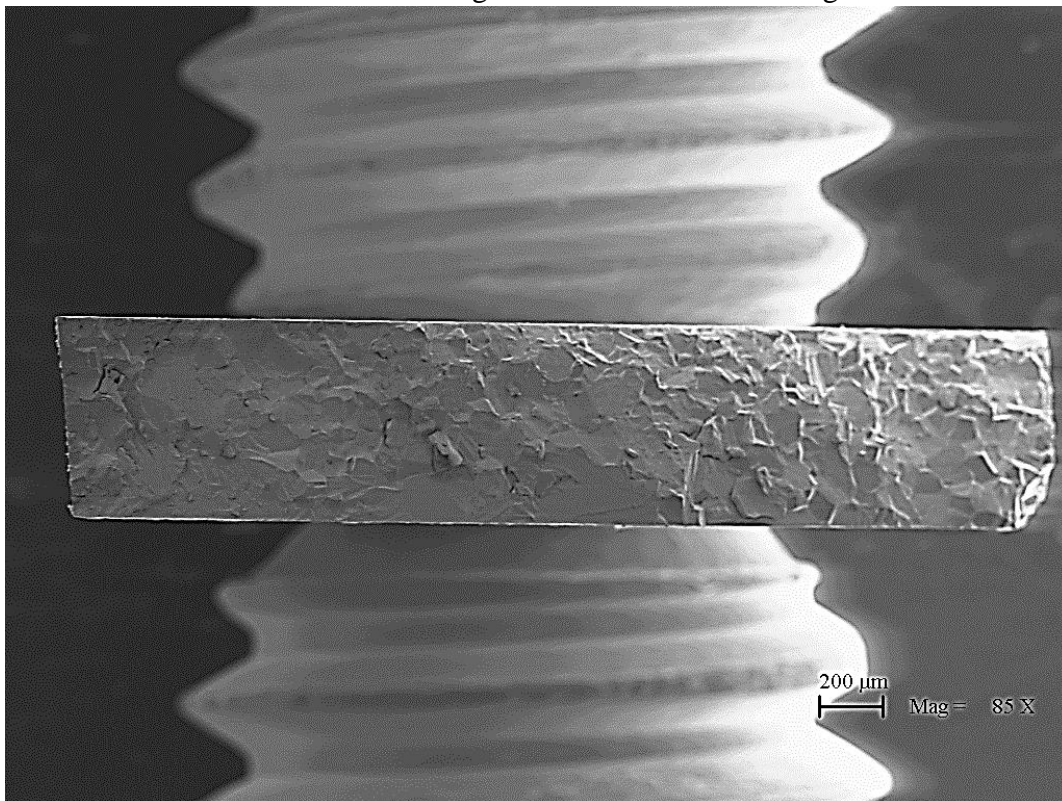


Figure 4.12: SEM image of the fracture surface for MoNbTaVW in 85x magnification.

An overview of the fracture surface for VNbMoTaW can be seen above under 85 times of magnification. The surface shows no sign of “dimples” which would be microvoids that initiate crack formation and indicate a ductile fracture. Instead, there are clear signs of intergranular and cleavage fracture. Intergranular fracture are cracks along grain boundaries and this type of fracture surface can be clearly seen in figure 4.13 under 300 times of magnification. The large flat surfaces on the right side of the fracture area are clear signs of intergranular fracture. Also, no sign of plastic deformation could be observed on the bent sample.

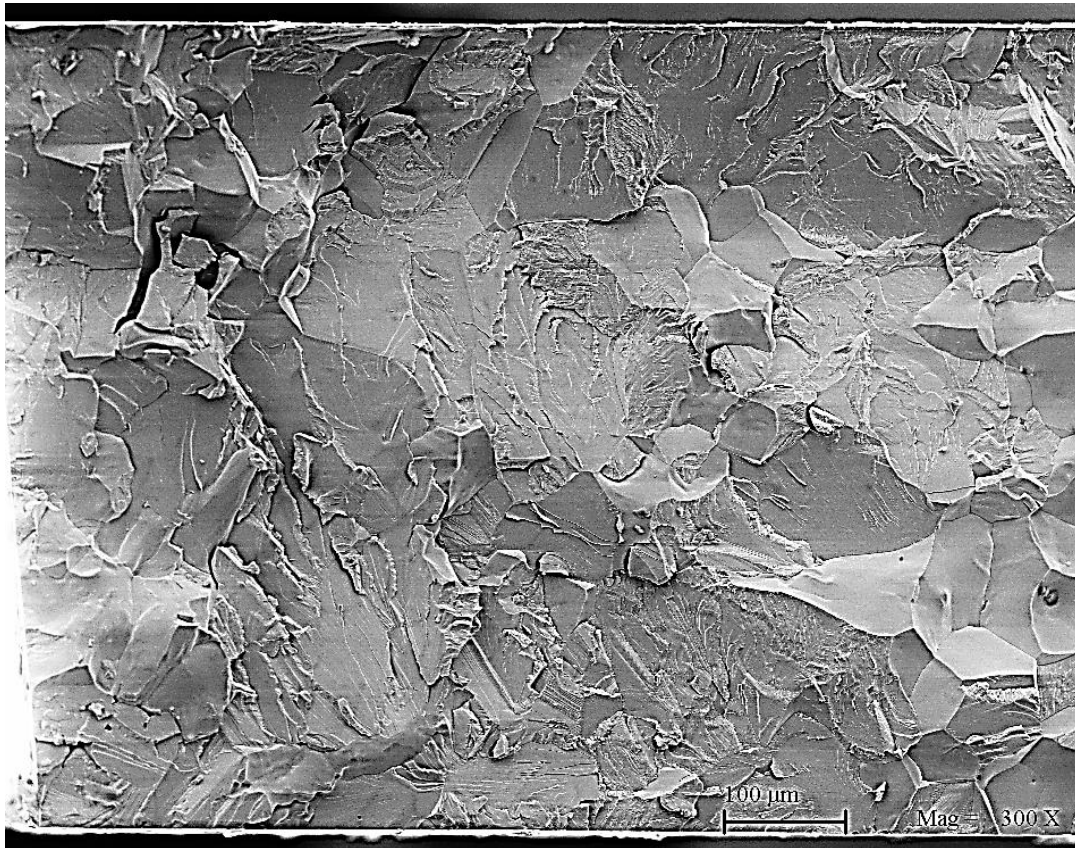


Figure 4.13: SEM image of the fracture surface for MoNbTaVW in 300 x magnification.

However, $\text{Hf}_{0.5}\text{Nb}_{0.5}\text{Ta}_{0.5}\text{TiZr}$ shows signs of ductility. The Vickers hardness values are within reasonable values compared with the values from the tests. The individual hardness measurements for $\text{Hf}_{0.5}\text{Nb}_{0.5}\text{Ta}_{0.5}\text{TiZr}$ are listed in table 4.4. Table 4.5 shows the tested Vickers hardness values for $\text{Hf}_{0.5}\text{Nb}_{0.5}\text{Ta}_{0.5}\text{TiZr}$. In comparison, the hardness value is lower than $\text{Mo}_{0.5}\text{Nb}$ and MoNb . The bending result shown in figure 4.14 depicts a thin sample of the alloy bent to an almost 90° degree angle with an unbent sample for comparison on the left side.

Table 4.4: Individual measurements of Vickers hardness values of $Hf_{0.5}Nb_{0.5}Ta_{0.5}TiZr$.

Composition	Individual measurements (HV)						
$Hf_{0.5}Nb_{0.5}Ta_{0.5}TiZr$	373	373	370	374	385	380	380

Table 4.5: Vickers hardness values, calculated Vickers hardness, standard deviation and VEC values of $Hf_{0.5}Nb_{0.5}Ta_{0.5}TiZr$.

Composition	VEC	RoM hardness (HV)	Vickers hardness (HV)	Standard deviation
$Hf_{0.5}Nb_{0.5}Ta_{0.5}TiZr$	4.29	112.3	376	4.9

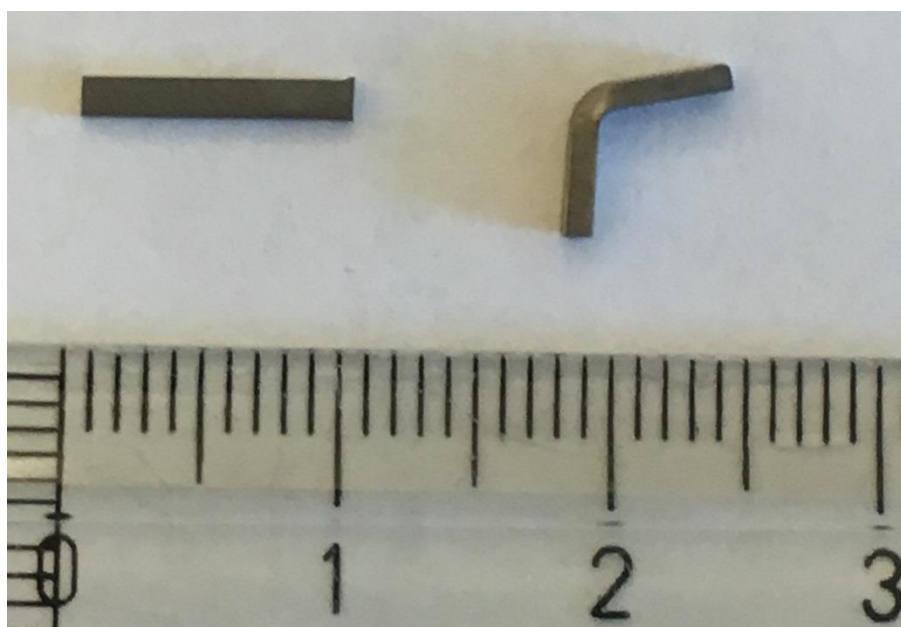


Figure 4.14: Bending result for $Hf_{0.5}Nb_{0.5}Ta_{0.5}TiZr$.

As seen in figure 4.15, the $Hf_{0.5}Nb_{0.5}Ta_{0.5}TiZr$ alloy has the x-ray diffraction pattern with three distinct peaks marked with 1 in the figure. These peaks indicate a single phase solution with BCC structure in the alloy. There is a small peak at 2θ around 55 degree which is also identified as k-beta emission line.

To confirm the x-ray diffraction pattern, and to verify a single phase solution in the mixture, further analysis with a scanning electron microscope had to be done.

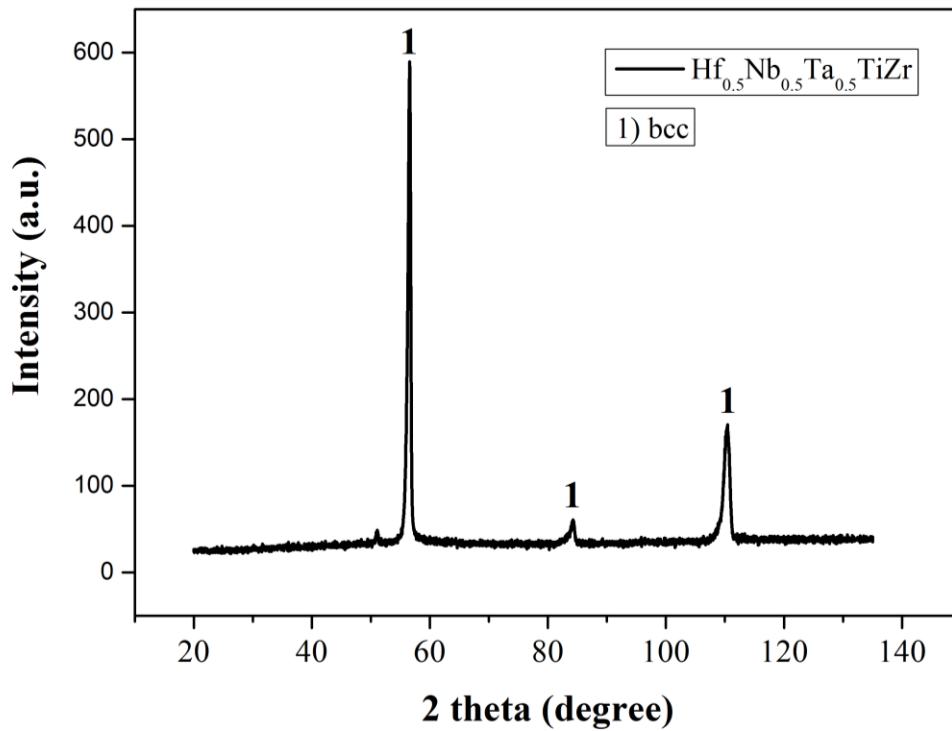


Figure 4.15: X-ray diffraction of refractory HEA $\text{Hf}_{0.5}\text{Nb}_{0.5}\text{Ta}_{0.5}\text{TiZr}$.

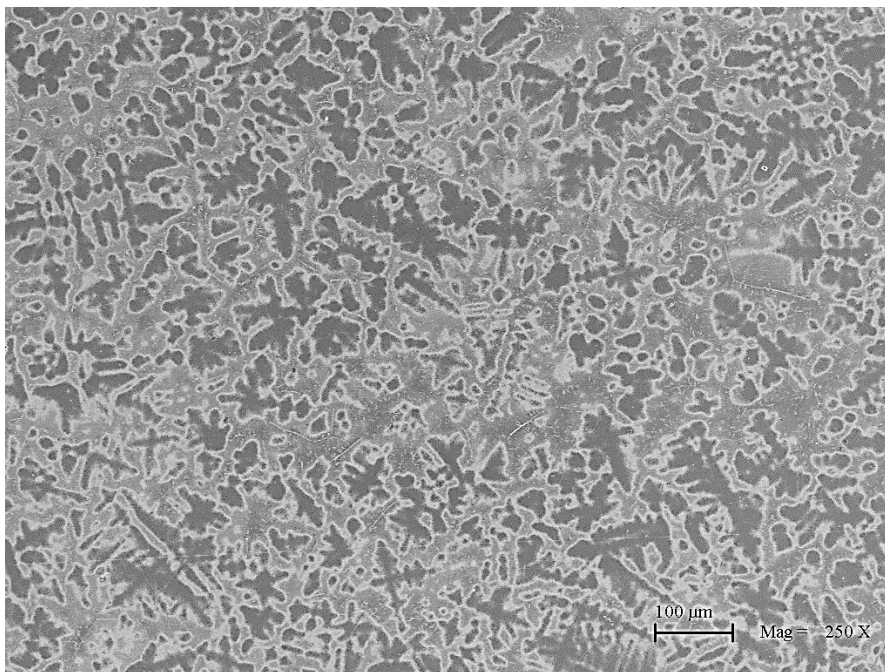


Figure 4.16: Microstructure of $\text{Hf}_{0.5}\text{Nb}_{0.5}\text{Ta}_{0.5}\text{TiZr}$ in 250x magnification.

Figure 4.16 shows an overview of the microstructure from a SEM image under 250x magnification. The alloy shows a dendritic microstructure after etching. The dark grey tree-like spots are dendrites and the light grey are interdendrites. There is no sign of secondary phases which confirms the result from x-ray diffraction about this alloy being a single phase solid solution.

5 CONCLUSION

The conclusion is divided into the literature review and properties map part, experimental work part and the part for recommendations for further research.

5.1 Conclusions on the literature review and the properties map

A short literature review regarding the basic knowledge of HEA has been delivered and written about in the Theoretical Frame section. The scope of the review includes some brief history of HEAs, the definition of HEAs, the four core effects and examples of mechanical properties in HEAs.

By observing the current state of refractory alloys, there is still a need for ductile refractory HEAs. Below are reasons behind the statement.

- Refractory HEAs outperforms most simpler refractory alloys in terms of yield strength at room- and elevated temperatures.
- A majority of refractory HEAs are brittle.
- Efficiency in jet turbines can be increased with materials capable of working at higher temperatures than today's high-temperature materials, such as Ni-based alloys.
- The density is highly dependent on the elements used in the alloy, but it is possible for a refractory HEA to be lighter than simpler refractory alloys.
- The current data of refractory HEAs are results mainly from compressions tests, which means the expected tensile ductility could be much lower than the compression ductility.

There is discrepancy in the properties data because of the different testing temperatures and testing methods, and using compressions tests or tensile tests. Compression tests usually generate higher yield strength and fracture strength. The difference in testing temperatures can be observed in figure 4.5 and 4.6, and refractory HEAs generally have better high temperature strength.

To sum it up, there are sufficient reasons for improving the ductility for refractory HEAs as there is no much ductile refractory HEAs available at the moment, and there is a real world application for these materials.

5.2 Conclusions on the experimental work

The test results for the binary alloys show that MoTi, Mo_{0.5}Ti, MoNb and Mo_{0.5}Nb are brittle, possibly due to their high VEC values. The four alloys did not follow the prediction made by the study regarding W-based alloys Hu et al.. [69] Alloying Mo with Ti or Nb did not improve ductility at all, which suggest that a Mo-containing HEAs would most likely be brittle and therefore does not meet the requirement of the goal. The XRD results for HfMoTiVZr confirmed that it had a BCC crystal structure and presence of a secondary FCC phase, which could contribute to the brittleness observed during the experimental work.

Even if there is no secondary phases in a Mo-containing refractory HEAs, it is not guaranteed that the alloy is ductile. MoNbTaVW is an example of a brittle refractory HEA with single-phase BCC solid solution. The brittleness can be attributed to the high VEC value of 5.4. The clear signs of brittleness of MoNbTaVW can be observed on the intergranular/cleavage fracture surface of the alloy. The binary alloy experiment along with the results from HfMoTiVZr confirms that finding a ductile Mo-containing refractory HEA with a single-phase solid solution is a challenge.

Hf_{0.5}Nb_{0.5}Ta_{0.5}TiZr exhibited signs of ductility, as it was bendable to an almost 90 ° degree. The x-ray diffraction result shows a single-phased BCC crystal structure and the microstructure analysis shows a dendritic structure with no signs of secondary phases. In this case, the high entropy effect helped with suppressing formation of secondary phases. The reasonable Vickers hardness further strengthens the conclusion of no presence of secondary phases. The ductility can be attributed to the low VEC value of 4.29 as other factors are eliminated such as secondary phases. The alloy has a density of 8.66 g/cm³ which unfortunately will not put it among the low density refractory alloys.

Figure 5.1 shows single phased solid solution refractory HEAs arranged by their VEC values with their compositions listed in the legend. Among those alloys, HfNbTaTiZr, Hf_{0.5}Nb_{0.5}Ta_{0.5}TiZr and HfNbTiZr are ductile with their respective VEC values of 4.4, 4.29 and 4.25. The rest of the refractory HEAs listed are brittle and marked with square markers. The common property among those three ductile HEAs, marked with circular markers, is their low VEC value. Their values are under 4.4. MoNbHfZrTi has a VEC value of 4.6 and is reported as brittle. The brittle to ductile transition seem to occur between the VEC values 4.4 and 4.6. The transition zone is the grey area between HfNbTaTiZr and MoNbHfZrTi.

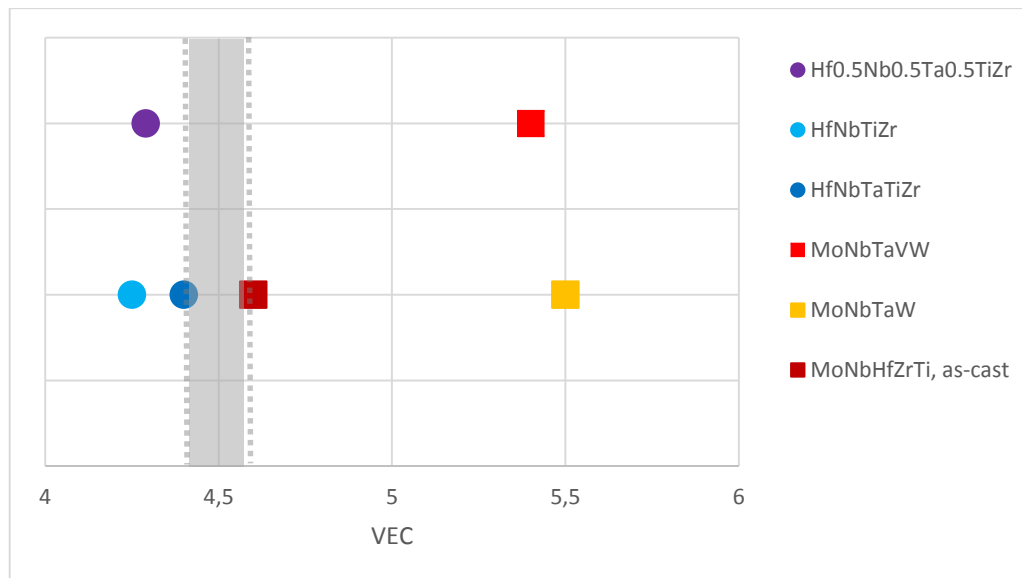


Figure 5.1: VEC chart of six refractory HEAs. The alloys with lower VEC have shown signs of ductility while those with high VEC are brittle.

To sum it up, lowering the VEC value could be a valid strategy to design ductile refractory HEAs, as long as the elements considered in the alloy do not counteract the ductility with secondary phases or intermetallic compounds.

5.3 Recommendations

There are still many tests to perform for the refractory HEA $\text{Hf}_{0.5}\text{Nb}_{0.5}\text{Ta}_{0.5}\text{TiZr}$. For instance, the ductility can only be verified through compression tests and preferably tensile tests. The bendability is merely a sign of ductility. The yield strength in elevated temperature can also only be verified through compression tests or tensile tests. Before doing that, fine tuning the composition ratio might net a more ductile alloy.

Moreover, creating a new mixture could also be beneficial and a step forward in the right direction. A suggestion is to try and create a mixture containing at least one of the group 6 elements at low quantity, preferably tungsten or molybdenum, together with 2 or 3 group 4 elements and maybe one from group 5 at low quantity. This composition should have a low VEC value. It is still uncertain if a composition with a VEC value between 4.4 and 4.6 is ductile or brittle, and therefore one should aim to pass that transition area.

While choosing the elements for the mixture, it is suggested to check the phase diagrams between those elements in order to increasing the chance of getting single phase solid solution in the final mixture. Even though some elements do not have any single phase solid solution with each other, there is a possibility that they create a single phase solid solution while being mixed with other elements, due to the high entropy effect in the mixture.

If tungsten is chosen as the group 6 element, the melting of the tungsten should be done carefully and thorough to avoid unmelted tungsten particles remain in the final mixture.

6 REFERENCES

- [1] J. H. Perepezko, "The Hotter the Engine, the Better," *Science* (80-.), vol. 326, no. 5956, pp. 1068–1069, 2009.
- [2] A. H. Maslow, "A Theory of Human Motivation," *Psychol. Rev.*, vol. 50, pp. 370–396, 1943.
- [3] M. Ashby, H. Shercliff, and D. Cebon, *Materials Engineering, Science, Processing and Design*, 3rd ed. Oxford, UK: Butterworth-Heinemann, 2014.
- [4] J. Kliber, B. Mašek, O. Zacek, and H. Staňková, "Transformation Induced Plasticity (TRIP) Effect Used in Forming of Carbon CMnSi Steel ," *Mater. Sci. Forum*, vol. 500–501, pp. 461–470, 2005.
- [5] W. D. Callister and D. G. Rethwisch, *Materials Science and Engineering An Introduction*, 9th ed. John Wiley & Sons, 2014.
- [6] B. S. Murty, J. W. Yeh, and S. Ranganathan, *High Entropy Alloys*. Elsevier, 2014.
- [7] B. Cantor, I. T. H. Chang, P. Knight, and A. J. B. Vincent, "Microstructural development in equiatomic multicomponent alloys," *Mater. Sci. Eng. A*, vol. 375–377, pp. 213–218, Jul. 2004.
- [8] J.-W. Yeh, S.-K. Chen, S.-J. Lin, J.-Y. Gan, T.-S. Chin, T.-T. Shun, C.-H. Tsau, and S.-Y. Chang, "Nanostructured High-Entropy Alloys with Multiple Principal Elements: Novel Alloy Design Concepts and Outcomes," *Adv. Eng. Mater.*, vol. 6, no. 5, pp. 299–303, 2004.
- [9] J.-W. Yeh, "Physical Metallurgy of High-Entropy Alloys," *JOM*, vol. 67, no. 10, pp. 2254–2261, 2015.
- [10] J.-W. Yeh, "Alloy Design Strategies and Future Trends in High-Entropy Alloys," *JOM*, vol. 65, no. 12, pp. 1759–1771, 2013.
- [11] J. W. Yeh, "Recent progress in high-entropy alloys," *Ann. Chim. Sci. des Mater.*, vol. 31, no. no.6, pp. 633–648, 2006.
- [12] C.-Y. Hsu, C.-C. Juan, W.-R. Wang, T.-S. Sheu, J.-W. Yeh, and S.-K. Chen, "On the superior hot hardness and softening resistance of AlCoCrFeMo0.5Ni high-entropy alloys," *Mater. Sci. Eng. A*, vol. 528, no. 10–11, pp. 3581–3588, Apr. 2011.
- [13] M.-H. Tsai, C.-W. Wang, C.-W. Tsai, W.-J. Shen, J.-W. Yeh, J.-Y. Gan, and W.-W. Wu, "Thermal Stability and Performance of NbSiTaTiZr High-Entropy Alloy Barrier for Copper Metallization," *J. Electrochem. Soc.*, vol. 158, no. 11, pp. H1161–H1165, 2011.
- [14] M.-H. Tsai, J.-W. Yeh, and J.-Y. Gan, "Diffusion barrier properties of AlMoNbSiTaTiVZr high-entropy alloy layer between copper and silicon," *Thin Solid Films*, vol. 516, no. 16, pp. 5527–5530, Jun. 2008.
- [15] T.-T. Shun, C.-H. Hung, and C.-F. Lee, "Formation of ordered/disordered nanoparticles in FCC high entropy alloys," *J. Alloys Compd.*, vol. 493, no. 1–2, pp. 105–109, Mar. 2010.
- [16] K. Y. Tsai, M. H. Tsai, and J. W. Yeh, "Sluggish diffusion in Co-Cr-Fe-Mn-Ni high-entropy alloys," *Acta Mater.*, vol. 61, no. 13, pp. 4887–4897, 2013.

- [17] M.-H. Tsai and J.-W. Yeh, "High-Entropy Alloys: A Critical Review," *Mater. Res. Lett.*, vol. 2, no. 3, pp. 107–123, 2014.
- [18] C.-J. Tong, M.-R. Chen, J.-W. Yeh, S.-J. Lin, S.-K. Chen, T.-T. Shun, and S.-Y. Chang, "Mechanical performance of the Al_xCoCrCuFeNi high-entropy alloy system with multiprincipal elements," *Metall. Mater. Trans. A*, vol. 36, no. 5, pp. 1263–1271.
- [19] C. Li, J. C. Li, M. Zhao, and Q. Jiang, "Effect of alloying elements on microstructure and properties of multiprincipal elements high-entropy alloys," *J. Alloys Compd.*, vol. 475, no. 1–2, pp. 752–757, May 2009.
- [20] Y. J. Zhou, Y. Zhang, Y. L. Wang, and G. L. Chen, "Solid solution alloys of AlCoCrFeNiTi_[sub x] with excellent room-temperature mechanical properties," *Appl. Phys. Lett.*, vol. 90, no. 18, p. 181904, 2007.
- [21] G. A. Salishchev, M. A. Tikhonovsky, D. G. Shaysultanov, N. D. Stepanov, A. V. Kuznetsov, I. V. Kolodiy, A. S. Tortika, and O. N. Senkov, "Effect of Mn and V on structure and mechanical properties of high-entropy alloys based on CoCrFeNi system," *J. Alloys Compd.*, vol. 591, pp. 11–21, Apr. 2014.
- [22] C.-Y. Hsu, W.-R. Wang, W.-Y. Tang, S.-K. Chen, and J.-W. Yeh, "Microstructure and Mechanical Properties of New AlCo_xCrFeMo_{0.5}Ni High-Entropy Alloys," *Adv. Eng. Mater.*, vol. 12, no. 1–2, pp. 44–49, 2010.
- [23] A. V. Kuznetsov, D. G. Shaisultanov, N. D. Stepanov, G. a. Salishchev, and O. N. Senkov, "Superplasticity of AlCoCrCuFeNi High Entropy Alloy," *Mater. Sci. Forum*, vol. 735, no. January, pp. 146–151, 2012.
- [24] M. Baucio and A. S. Metals, *ASM Metals Reference Book, 3rd Edition*: ASM International, 1993.
- [25] H. E. J. McCoy, R. L. Stephenson, and J. R. J. Weir, *MECHANICAL PROPERTIES OF SOME REFRACTORY METALS AND THEIR ALLOYS*. 1964.
- [26] John F. Papp, "Commodity Summaries 2015: Niobium," 2015.
- [27] J. Eckert, "Niobium compounds and alloys," *Int. J. Refract. Met. Hard Mater.*, vol. 12, no. 6, pp. 335–340, Jan. 1993.
- [28] C. K. Gupta and A. K. Suri, *Extractive Metallurgy of Niobium*. Taylor & Francis, 1993.
- [29] J. Hebda, "Niobium Alloys High Temperature Application," 2001.
- [30] W. Chang, "C-103 Niobium Properties and Products," pp. 1–27, 2010.
- [31] R. T. Begley, W. N. Platte, A. I. Lewis, and R. L. Ammon, *DEVELOPMENT OF NIOBIUM-BASE ALLOYS*. 1961.
- [32] M. J. Magyar, "Commodity Summaries 2009: Molybdenum," 2015.
- [33] R. E. Smallwood, A. C. B.-10 on Reactive, R. Metals, and Alloys, *Refractory Metals and Their Industrial Applications: A Symposium*, no. nr. 849. ASTM, 1984.
- [34] "Molybdenum | Plansee," 2016. [Online]. Available: <http://www.plansee.com/en/materials/molybdenum.html>. [Accessed: 13-Apr-2016].

- [35] A. I. H. Committee, *ASM Handbook, Volume 02 - Properties and Selection: Nonferrous Alloys and Special-Purpose Materials*. ASM International, 1990.
- [36] B. O. Metals, T. E. Tietz, and J. W. Wilson, *Behavior and Properties of Refractory Metals*. Stanford University Press, 1965.
- [37] Rhenium Alloys Inc, "Molybdenum-Rhenium Alloy, Annealed."
- [38] J. C. Carlen, "Molybdenum-rhenium alloy." Google Patents, 1995.
- [39] John F. Papp, "Commodity Summaries 2016: Tantalum," 2016.
- [40] S. J. Zinkle, "Thermophysical and Mechanical Properties for Ta-8%W-2%Hf (6/30/98 draft for APEX)," 1998.
- [41] P. E. Moorhead and P. L. Stone, "Survey of Properties of T111," 1970.
- [42] H. Baker and H. Okamoto, *ASM Handbook, Volume 03 - Alloy Phase Diagrams*. ASM International, 1992.
- [43] B. W. Gosser, *Modern Materials: Advances in Development and Applications*. Elsevier Science, 1965.
- [44] H.C. Starck, "H.C. Starck Ultra 76 Alloy (Ta 2.5%W)." [Online]. Available: <http://www.matweb.com/search/datasheettext.aspx?matguid=66c848e4804a45728b27fab92a240467>. [Accessed: 13-Apr-2016].
- [45] J. R. Davis and A. S. M. I. H. Committee, *ASM Specialty Handbook: Heat-Resistant Materials*. ASM International, 1997.
- [46] N. R. C. (U. S.). C. on Technical Aspects of Critical and S. M. P. on Trends in Usage of Tungsten, *Trends in Usage of Tungsten: Report*. National Research Council, National Academy of Sciences-National Academy of Engineering, 1973.
- [47] P. Ramakrishanan, *Powder Metallurgy*. New Age International (P) Limited, 2007.
- [48] A. Arora, "Tungsten Heavy Alloy For Defence Applications," *Mater. Technol.*, vol. 19, no. 4, pp. 210–216, 2004.
- [49] V. S. Moxson and F. H. (Sam) Froes, "Fabricating sports equipment components via powder metallurgy," *JOM*, vol. 53, no. 4, pp. 39–41, 2001.
- [50] A. V Naumov, "Rhythms of rhenium," *Russ. J. Non-Ferrous Met.*, vol. 48, no. 6, pp. 418–423, 2007.
- [51] Désirée E. Polyak, "2009 Minerals Yearbook," *USGS Miner. Yearb.*, no. September, 2011.
- [52] B. Cantor, H. Assender, and P. Grant, *Aerospace Materials*. CRC Press, 2001.
- [53] Allegheny Technologies Inc., "ATI 45Nb™ Alloy," www.ATImetals.com, 2012. [Online]. Available: https://www.atimetals.com/Documents/ti-45nb_tds_en_v1.pdf. [Accessed: 13-Apr-2016].
- [54] O. N. Senkov, G. B. Wilks, J. M. Scott, and D. B. Miracle, "Mechanical properties of Nb₂₅Mo₂₅Ta₂₅W₂₅ and V₂₀Nb₂₀Mo₂₀Ta₂₀W₂₀ refractory high entropy alloys," *Intermetallics*, vol. 19, no. 5, pp. 698–706, May 2011.

- [55] O. N. Senkov, G. B. Wilks, D. B. Miracle, C. P. Chuang, and P. K. Liaw, "Refractory high-entropy alloys," *Intermetallics*, vol. 18, no. 9, pp. 1758–1765, Sep. 2010.
- [56] N. N. Guo, L. Wang, L. S. Luo, X. Z. Li, Y. Q. Su, J. J. Guo, and H. Z. Fu, "Microstructure and mechanical properties of refractory MoNbHfZrTi high-entropy alloy," *Mater. Des.*, vol. 81, pp. 87–94, Sep. 2015.
- [57] O. N. Senkov, S. V. Senkova, D. B. Miracle, and C. Woodward, "Mechanical properties of low-density, refractory multi-principal element alloys of the Cr–Nb–Ti–V–Zr system," *Mater. Sci. Eng. A*, vol. 565, pp. 51–62, Mar. 2013.
- [58] O. N. Senkov, J. M. Scott, S. V. Senkova, D. B. Miracle, and C. F. Woodward, "Microstructure and room temperature properties of a high-entropy TaNbHfZrTi alloy," *J. Alloys Compd.*, vol. 509, no. 20, pp. 6043–6048, May 2011.
- [59] C.-C. Juan, M.-H. Tsai, C.-W. Tsai, C.-M. Lin, W.-R. Wang, C.-C. Yang, S.-K. Chen, S.-J. Lin, and J.-W. Yeh, "Enhanced mechanical properties of HfMoTaTiZr and HfMoNbTaTiZr refractory high-entropy alloys," *Intermetallics*, vol. 62, pp. 76–83, Jul. 2015.
- [60] O. N. Senkov, J. M. Scott, S. V. Senkova, F. Meisenkothen, D. B. Miracle, and C. F. Woodward, "Microstructure and elevated temperature properties of a refractory TaNbHfZrTi alloy," *J. Mater. Sci.*, vol. 47, no. 9, pp. 4062–4074, 2012.
- [61] Y. D. Wu, Y. H. Cai, T. Wang, J. J. Si, J. Zhu, Y. D. Wang, and X. D. Hui, "A refractory Hf₂₅Nb₂₅Ti₂₅Zr₂₅ high-entropy alloy with excellent structural stability and tensile properties," *Mater. Lett.*, vol. 130, pp. 277–280, Sep. 2014.
- [62] H. Chen, A. Kauffmann, B. Gorr, D. Schliephake, C. Seemüller, J. N. Wagner, H.-J. Christ, and M. Heilmaier, "Microstructure and mechanical properties at elevated temperatures of a new Al-containing refractory high-entropy alloy Nb-Mo-Cr-Ti-Al," *J. Alloys Compd.*, vol. 661, pp. 206–215, Mar. 2016.
- [63] N. D. Stepanov, D. G. Shaysultanov, G. A. Salishchev, and M. A. Tikhonovsky, "Structure and mechanical properties of a light-weight AlNbTiV high entropy alloy," *Mater. Lett.*, vol. 142, pp. 153–155, Mar. 2015.
- [64] O. N. Senkov, S. V. Senkova, and C. Woodward, "Effect of aluminum on the microstructure and properties of two refractory high-entropy alloys," *Acta Mater.*, vol. 68, pp. 214–228, Apr. 2014.
- [65] Y. Zhang, Y. Liu, Y. Li, X. Chen, and H. Zhang, "Microstructure and mechanical properties of a refractory HfNbTiVSi_{0.5} high-entropy alloy composite," *Mater. Lett.*, vol. 174, pp. 82–85, Jul. 2016.
- [66] E. M. Savitskii, *Physical Metallurgy of Refractory Metals and Alloys*. Springer US, 2012.
- [67] X. Li, F. Tian, S. Schönecker, J. Zhao, and L. Vitos, "Ab initio-predicted micro-mechanical performance of refractory high-entropy alloys," *Sci. Rep.*, vol. 5, p. 12334, Jul. 2015.
- [68] L. Qi and D. C. Chrzan, "Tuning Ideal Tensile Strengths and Intrinsic Ductility of bcc Refractory Alloys," *Phys. Rev. Lett.*, vol. 112, no. 11, p. 115503, Mar. 2014.
- [69] Y.-J. Hu, S.-L. Shang, Y. Wang, K. A. Darling, B. G. Butler, L. J. Kecskes, and Z.-K. Liu, "Effects of alloying elements and temperature on the elastic properties of W-based

- alloys by first-principles calculations," *J. Alloys Compd.*, vol. 671, pp. 267–275, Jun. 2016.
- [70] G. V Samsonov, "Handbook of the Physicochemical Properties of the Elements," G. V Samsonov, Ed. Boston, MA: Springer US, 1968, pp. 387–446.
- [71] J. L. Murray, "The Hf–Ti (Hafnium-Titanium) system," *Bull. Alloy Phase Diagrams*, vol. 2, no. 2, pp. 181–185, 1981.
- [72] "ISO 6507-1:2005 Metallic materials -- Vickers hardness test -- Part 1: Test method." Geneva, Switzerland, 2005.
- [73] D. C. Joy, "scanning electron microscope (SEM)," *Encyclopædia Britannica Online*, 2016. [Online]. Available: <http://global.britannica.com/technology/scanning-electron-microscope>. [Accessed: 16-May-2016].
- [74] Allegheny Technologies Inc., "ATI 38-644," *www.ATImetals.com*, 2011. [Online]. Available: https://www.atimetals.com/Documents/ati_38-644_tds_en_v1.pdf. [Accessed: 18-May-2016].
- [75] Allegheny Technologies Inc., "ATI 64-MIL," *www.ATImetals.com*, 2011. [Online]. Available: https://www.atimetals.com/Documents/ati_64mil_tds_en_v1.pdf. [Accessed: 18-May-2016].
- [76] Allegheny Technologies Inc., "Zircadyna 702/705," *www.ATImetals.com*, 2012. .

Alloy/properties	Temperature (°C)	Yield Strength (MPa)	Ultimate Tensile Strength (MPa)	Fracture strain (%)	Density (g/cm ³)	Melting point (K)
Alloy 362/Mo-0.5Ti-0.02C [35]	23	825	895	10	10.2	2883
	1095	345	415	-		
	1650	48	76	-		
ATI 38-644 [74]	25	1100	1200	13	4.82	1875
	93	896	1034	17		
	204	827	1034	16		
	316	900	1075	12		
	427	775	948	18		
	538	413	770	30		
ATI 45Nb [53]	25	532.5	546	10	5.7	2173
	100	400	-	-		
	200	320	-	-		
	300	250	-	-		
	400	200	-	-		
	500	175	-	-		
ATI 64-MIL [75]	25	896	1034	20	4.47	1866
	93	793	896	25		
	204	690	793	23		
	316	655	760	18		
	427	586	690	20		
	538	483	520	38		
C103 [30]	20	296	420	27.5	8.85	2623
	538	200	310	20		
	649	186	317	16		
	760	172	320	17		
	871	162	310	18.5		
	1093	138	186	45		
	1371	72	90	70		
	1482	59	65	70		
MHC* [34]	23	880	890	-	9.1	2892
	200	780	810	-		
	400	670	720	-		
	600	600	660	-		
	800	570	620	-		
	1000	490	510	-		
	1200	440	570	-		
	1400	350	380	-		
	1600	110	160	-		

Alloy/properties	Temperature (°C)	Yield Strength (MPa)	Ultimate Tensile Strength (MPa)	Fracture strain (%)	Density (g/cm ³)	Melting point (K)
Mo-0.5Ti-0.1Zr (TZM)*[34]	23	780	825	10	10.16	2893
	200	680	710	-		
	400	570	620	-		
	600	500	550	-		
	800	480	810	-		
	1000	410	470	-		
	1200	380	400	-		
	1400	280	300	-		
	1600	75	110	-		
Mo-47.5 Re [50]	25	845	1180	22	13.5	2723
	800	415	620	-		
	1200	210	240	-		
Nb-5Hf (NC-184) [31]	25	228	348	25.2	8.7*	2737
	1095	127	176	14.4		
Nb-5Hf + 0.08O₂ (NC-250)[31]	25	332	438	24.3	8.7*	2737
	1095	326	339	6.2		
	1205	245	248	9.2		
T-111/Ta-8%W-2%Hf [40]	25	565	590	20	16.83*	3284
	40	560	580	20		
	200	400	450	20		
	425	300	410	16		
	985	275	410	13		
	1090	250	410	18		
	1150	225	375	17		
	1200	175	330	22		
	1310	150	260	36		
	1475	150	225	31		
	1650	100	100	46		
1920	100	100	35			
Ta-10%W[45]	20	460	550	25	16.8	3308
	200	400	515	-		
	750	275	380	-		
	1000	205	305	-		
Ta-2.5%W[44]	21.1	245	345	20	16.7	3269
	98.9	210	331	15		
	199	189	290	10		
	249	176	276	10		
Ta-7.5%W[45]	20	940	1100	6.5	16.8	3297
TZC/Mo-1Ti-0.3Zr-0.15C[34]	23	725	995	22	10.1	2873
	1095	-	640	-		
	1650	-	415	-		

Alloy/properties	Temperature (°C)	Yield Strength (MPa)	Ultimate Tensile Strength (MPa)	Fracture strain (%)	Density (g/cm ³)	Melting point (K)
Zircadyne® 702 [76]	20	321.1	468.1	28.9	6.51	2125
	93	267.5	364	31.5		
	149	195.8	303.7	42.5		
	204	139.3	229.6	49		
	260	128.9	200.6	49		
	316	97.2	197.9	40.1		
	371	82	156.5	44.1		
Zircadyne® 705 [76]	20	506.1	615	18.8	6.64	2112
	93	390.7	494.7	30.5		
	149	272.3	388.9	31.7		
	204	261.8	369.3	33		
	260	195.8	326.1	28.9		
	316	190.2	299.7	29		
	371	173	281	27.8		
Al_{0.4}Hf_{0.6}NbTaTiZr [64]	20	1841	2269	10	9.05	2397
	800	796	834	50		
	1000	298	455	50		
	1200	89	135	50		
AlMo_{0.5}NbTa_{0.5}TiZr [64]	20	2000	2368	10	7.4	1982
	800	1597	1810	11		
	1000	745	772	50		
	1200	250	272	50		
AlNbTiV [63]	20	1020	1318	5	5.59	1920
	600	810	1050	12		
	800	685	-	50		
	1000	158	-	50		
CrNbTiVZr [57]	20	1298	-	3	6.57	2232
	600	1230	-	10		
	800	615	-	50		
	1000	259	-	50		
CrNbTiZr [57]	20	1260	-	6	6.67	2262
	600	1035	-	50		
	800	300	-	50		
	1000	115	-	50		
HfMoNbTaTiZr [59]	20	1512	-	12	9.97	2582
	800	1007	-	23		
	1000	814	-	30		
	1200	556	-	30		
HfMoTaTiZr [59]	20	1600	-	4	10.24	2548
	800	1045	-	19		
	1000	855	-	30		
	1200	404	-	30		

Alloy/properties	Temperature (°C)	Yield Strength (MPa)	Ultimate Tensile Strength (MPa)	Fracture strain (%)	Density (g/cm ³)	Melting point (K)
HfNbTaTiZr [58]	20	928	-	50	9.94	2523
	800	535				
	1000	295				
	1200	92				
HfNbTiVSi_{0.5} [65]	20	1399	-	10.9	8.6	2266
	800	875	-	50		
	1000	1000	-	50		
HfNbTiZr [61]	20	896	969	14.9	8.22	2058
MoNbHfZrTi, as-cast [56]	20	1719	1803	10.12	8.64*	2444
	800	825	1095	60		
	900	728	938	60		
	1000	625	654	60		
	1100	397	399	60		
	1200	187	192	60		
Nb₂₅Mo₂₅Ta₂₅W₂₅ [54]	20	1058	1211	1.5	13.75*	3177
	600	561	-	-		
	800	552	-	-		
	1000	548	1008	16		
	1200	506	-	12		
	1400	421	467	9		
	1600	405	600	27		
NbMoCrTiAl [62]	20	-	1010	-	6.17*	2089
	400	1080	1100	2		
	600	1060	1170	2.5		
	800	860	1000	2		
	1000	594	630	15		
	1200	105	116	24		
NbTiV₂Zr [57]	20	918	-	50	6.32	2245
	600	571	-	50		
	800	240	-	50		
	1000	72	-	50		
NbTiVZr [57]	20	1105	-	50	6.52	2258
	600	834	-	50		
	800	187	-	50		
	1000	58	-	50		
V₂₀Nb₂₀Mo₂₀Ta₂₀W₂₀ [54]	20	1246	1270	1.7	12.36*	2946
	600	862	1597	13		
	800	846	1536	17		
	1000	842	1454	19		
	1200	735	943	7.5		
	1400	656	707	-		
	1600	477	479	-		

* Calculated values using rule of mixture, otherwise unspecified by source